(2)

AL-TR-89-027

AD-

AD-A214 937

Final Report
for the period
September 1988 to
June 1989

Design Manual For Microgravity Two-Phase Flow And Heat Transfer (U)

October 1989

Authors:
C.J. Crowley
M.G. Izenson

Creare Inc.
P.O. Box 71, Etna Road
Hanover, NH 03755

F04611-88-C-0050

Approved for Public Release

Prepared for the: **Air Force Astronautics Laboratory**

Air Force Space Technology Center
Space Division, Air Force Systems Command
Edwards Air Force Base,
California 93523-5000

SECURITY CLASSIFICATION OF THIS PAGE

REPORT DOCUMENTATION PAGE

Form Approved OMB No. 0704-0188

1a. REPORT SECURITY CLASSIFICATION: UNCLASSIFIED	1b. RESTRICTIVE MARKINGS
2a. SECURITY CLASSIFICATION AUTHORITY	3. DISTRIBUTION/AVAILABILITY OF REPORT: Approved for Public Release; Distribution is Unlimited
2b. DECLASSIFICATION/DOWNGRADING SCHEDULE	
4. PERFORMING ORGANIZATION REPORT NUMBER(S): TM-1309	5. MONITORING ORGANIZATION REPORT NUMBER(S): AL-TR-89-027
6a. NAME OF PERFORMING ORGANIZATION: CREARE INC. / 6b. OFFICE SYMBOL (If applicable): ---	7a. NAME OF MONITORING ORGANIZATION: ASTRONAUTICS LABORATORY (AFSC)
6c. ADDRESS (City, State, and ZIP Code): P.O. BOX 71, ETNA ROAD, HANOVER, NH 03755	7b. ADDRESS (City, State, and ZIP Code): AL/VSSP, EDWARDS AFB, CA 93523-5000
8a. NAME OF FUNDING/SPONSORING ORGANIZATION / 8b. OFFICE SYMBOL (If applicable)	9. PROCUREMENT INSTRUMENT IDENTIFICATION NUMBER: F04611-88-C-0050
8c. ADDRESS (City, State, and ZIP Code)	10. SOURCE OF FUNDING NUMBERS: PROGRAM ELEMENT NO. 65502F; PROJECT NO. 2864; TASK NO. 00; WORK UNIT ACCESSION NO. 2Z

11. TITLE (Include Security Classification)

DESIGN MANUAL FOR MICROGRAVITY TWO-PHASE FLOW AND HEAT TRANSFER (U)

12. PERSONAL AUTHOR(S)

CROWLEY, CHRISTOPHER J. and IZENSON, MICHAEL G.

13a. TYPE OF REPORT	13b. TIME COVERED	14. DATE OF REPORT (Year, Month, Day)	15. PAGE COUNT
FINAL	FROM 8809 TO 8906	8910	140

16. SUPPLEMENTARY NOTATION

17. COSATI CODES		
FIELD	GROUP	SUB-GROUP
20	04	--
20	13	--

18. SUBJECT TERMS (Continue on reverse if necessary and identify by block number)

FLUID FLOW, HEAT TRANSFER, SPACE TECHNOLOGY, SPACECRAFT COMPONENTS, THERMODYNAMICS, TWO PHASE FLOW.

19. ABSTRACT (Continue on reverse if necessary and identify by block number)

This report documents two-phase fluid flow and heat transfer methods for microgravity environments. The applications of the work are thermal management, propulsion, and fluid storage and transfer systems for spacecraft. In the near future, these systems will include two-phase, vapor-liquid flows. This Design Manual is intended for use by designers of these systems. Design methods are presented for predicting two-phase flow regimes and pressure drops in pipe flows from earth gravity to microgravity conditions. Forced convection boiling heat transfer methods for pipes with uniform heat flux are included. Also included are methods for analyzing high-vapor-shear condensation in pipes. The analysis methods are mechanistic; that is, based upon fundamental physical principles which should apply to heat transfer liquids with Pr≈1 and scale with pipe size and fluid properties. This Manual incorporates simplified methods (easy-to-use design charts), detailed descriptions of the analysis methods, comparisons with existing microgravity data, and recommended approaches to quantify the range of (ove

20. DISTRIBUTION/AVAILABILITY OF ABSTRACT: ☐ UNCLASSIFIED/UNLIMITED ☒ SAME AS RPT. ☐ DTIC USERS	21. ABSTRACT SECURITY CLASSIFICATION: UNCLASSIFIED
22a. NAME OF RESPONSIBLE INDIVIDUAL: LT. ERIC T. KOUBA	22b. TELEPHONE (Include Area Code): 805-275-5929 / 22c. OFFICE SYMBOL: VSSP

DD Form 1473, JUN 86 — Previous editions are obsolete. — SECURITY CLASSIFICATION OF THIS PAGE

19. ABSTRACT

uncertainty in design calculations.

Accession For	
NTIS GRA&I	☑
DTIC TAB	☐
Unannounced	☐
Justification	
By	
Distribution/	
Availability Codes	
Dist	Avail and/or Special
A-1	

EXECUTIVE SUMMARY

This Phase I Small Business Innovative Research (SBIR) contract produced a Design Manual, a guidebook intended for use by designers of two–phase fluid flow and heat transfer systems for space applications. Design guides are available for one gravity applications of two–phase systems, but none of these are currently applicable to microgravity thermal management systems. This contract produced two documents: a Final Report (AL–TR–89–026) and a Design Manual (AL–TR–89–027). This Design Manual will assist in the confident design of two–phase system components. It provides for quick scoping calculations and more detailed component calculations. Although not covered under this contract, these design methods can be integrated with existing computer codes for transient, system–level performance predictions of thermal management systems. The Design Manual will save considerable time and effort in the development of modelling tools by the Air Force. As part of this contract, recommended areas for follow–on mechanistic model design analysis were identified. These efforts would expand on the topics already presented in the Design Manual and permit the analysis of an entire thermal management system.

Future Air Force space missions will require power levels and heat transport rates at one to two orders of magnitude larger than present systems (10 to 100 kW). Since two–phase systems are a candidate approach to meeting heat transport capabilities for those higher power levels, future thermal management systems will involve vapor–liquid flows. As the missions are specified and two–phase systems come to the drawing board, a framework of design methods common to the designers (primarily the Air Force, NASA and the aerospace industry) will be valuable. In this Design Manual, the plethora of multiphase flow literature, which can easily overwhelm an analyst who is a novice to two–phase flows, is distilled into practical design methods which can be conveniently used. This Design Manual is intended to be a working document illustrating selected topics of basic two–phase flow regime, pressure drop, and heat transfer methods across the range from earth gravity to microgravity conditions.

The focus and organization of this document is at the component level. Typical two–phase transport systems will involve components such as transport lines (pipes), evaporators, condensers, pumps, separators, and radiators. Separate sections of this Design Manual will present design methods for pipes, evaporators and condensers at a level consistent with a Phase I SBIR contract. Alternate approaches can be used in the design of each of these types of components, and methods which are of general application to different approaches are presented in the subsections.

The sections of this Design Manual present the methods at two levels:

- Preliminary sizing calculations can be performed for the components using simple calculations and dimensionless maps presented in the text, and
- Detailed equations are presented so that the methods can be incorporated into design software for detailed component analysis or in system analysis codes.

Each section includes information which:

A. Describes the background and discusses the limitations of the use of the methods presented,

B. Presents the design information (including maps or graphs) for simple, scoping design calculations,

C. Describes in detail the analysis methods (which would be used to develop detailed, computerized analysis routines), and

D. Validates the design methods against available microgravity data.

The scoping design information for each topic is also useful because the dimensionless parameters illustrate the governing physics and the relationships between the key design parameters.

This document considers steady–state modelling of the two–phase flow. Transient two–phase flows can be addressed by implementing these methods into transient analysis codes. The methods incorporated in this Design Manual are all based upon mechanistic analysis methods to the extent possible. There are several advantages to the mechanistic analysis approach used here versus approaches based upon empirical correlations. Use of mechanistic methods:

- Ensures that the design methods scale appropriately with size, pressure (gas density), and fluid properties.
- Uncertainties in the design methods can be quantified by specifying ranges for key modelling parameters.
- The methods can be readily improved and refined as new experiments are performed to verify the models, without disturbing the basic framework of the models.*

The ability to quantify uncertainties in modelling the component behavior is particularly useful in the system design context. The key uncertainties in the system operation can be identified. Therefore, good designs can be made and the range of uncertainty, potential risk, or margin in the design can be identified in order to minimize the risk.

By analogy with analysis codes used for reactor safety calculations by the nuclear industry, the component design methods presented here are suitable for incorporation into system codes which can be used for steady–state or transient analysis of space thermal management systems. For example, the analysis methods are compatible with the ATHENA computer code presently being used by the Air Force for preliminary system design and with the SINDA '85/FLUINT code being used by NASA to design thermal management systems for the Space Station.

*Two–phase, microgravity research is being performed by a number of investigators. The methods presented in this Design Manual have immediate application in the design of the experiments and the interpretation of the data produced by these experiments.

In this Design Manual, the four topics included are:

(1) Flow regimes in adiabatic pipes, unifying methods to determine flow regimes at earth gravity and microgravity,

(2) Pressure drops in adiabatic pipes, using two–phase flow models for four flow regimes of interest (bubbly, slug, annular, and stratified) where the methods are simple, easy–to–use, and sufficiently accurate for design purposes (compared with alternate, detailed analysis methods),

(3) Condensation heat transfer in a condenser controlled by the shear between the vapor and liquid phases (in a pipe of uniform, circular cross–section), and

(4) Boiling heat transfer in an evaporator dominated by forced convection heat transfer (in a pipe of uniform, circular cross–section).

The documentation for each topic includes comparisons of the methods with available microgravity data. Thus, the manual also serves as a summary and review of available microgravity research results.

TABLE OF CONTENTS

LIST OF FIGURES

LIST OF TABLES

NOMENCLATURE

Symbol	Description	Units
a	magnitude of acceleration vector	(m/s^2)
A	cross-sectional area of flow channel or radiator surface	(m^2)
A_g^*	dimensionless cross-section occupied by gas phase in stratified flow	
A_l^*	dimensionless cross-section occupied by liquid phase in stratified flow	
Bo	Bond number, $aD^2(\rho_l - \rho_g)/\sigma$	
c_{pl}	heat capacity of liquid phase	(J/kg-K)
C_g	coefficient in friction factor model for gas phase	
C_l	coefficient in friction factor model for liquid phase	
C_o	bubble distribution coefficient in drift-flux model	
$(dP/dz)_a$	pressure gradient due to acceleration (phase change)	(Pa/m)
$(dP/dz)_f$	frictional pressure gradient	(Pa/m)
$(dP/dz)_g$	pressure gradient due to body forces	(Pa/m)
$(dP/dz)_t$	total pressure gradient	(Pa/m)
D	diameter of pipe	(m)
D_g^*	dimensionless hydraulic diameter for gas phase in stratified flow	
D_h	hydraulic diameter in heated (evaporator) tube	(m)
D_l^*	dimensionless hydraulic diameter for liquid phase in stratified flow	
E_f	fraction of wall heat flux to fluid heating	
E_{fc}	fraction due to forced convection of total heat transfer in saturated boiling	
f_i	friction factor at gas-liquid interface	
f_{wg}	wall friction factor for single-phase gas	
f_{wl}	wall friction factor for single-phase liquid	
F	multiplier for Reynolds number in saturated boiling model	
F_g	Froude number for gas phase, $j_g\rho_g^{0.5}/[aD(\rho_l - \rho_g)]^{0.5}$	
G	mass flux flowing in condenser or evaporator	$(kg/m^2\text{-}s)$
G_c	mass flux of vapor during condensation	$(kg/m^2\text{-}s)$
h	enthalpy	(J/kg)
h_{av}	average heat transfer coefficient in the slug flow regime	$(W/m^2\text{-}K)$
h_b	heat transfer coefficient for conduction across liquid film in the slug flow regime	$(W/m^2\text{-}K)$
h_f	heat transfer coefficient in liquid film in the slug flow region of the condenser	$(W/m^2\text{-}K)$
h_l	liquid level in pipe for stratified flow regime	(m)
h^*	dimensionless liquid level in stratified pipe flow	
h_{fc}	heat transfer coefficient in forced convection	$(W/m^2\text{-}K)$
h_{fg}	latent heat of vaporization of liquid	(J/kg)
h_{nb}	heat transfer coefficient in nucleate boiling	$(W/m^2\text{-}K)$
h_{nb}'	coefficient in nucleate boiling model	$(W/m^2\text{-}K^2)$
h_{tp}	total two-phase heat transfer coefficient	$(W/m^2\text{-}K)$
H	heated perimeter in evaporator tube	(m)
I	value of integral for two-phase condenser heat transfer, $I = 4R_cL^*$	

Symbol	Description	Units
I_{sp}	value of integral for single-phase heat transfer in subcooled region of condenser	
j	total volumetric flux or mixture velocity ($j_g + j_l$)	(m/s)
j_g	gas phase volumetric flux (Q_g/A) or superficial velocity	(m/s)
j_l	liquid phase volumetric flux (Q_l/A) or superficial velocity	(m/s)
Ja	Jakob number, $c_{pl}(T_{sat} - T_f)/h_{fg}$	
k	coefficient for drift velocity in drift-flux model or coefficient for turbulence in slug-to-bubbly flow regime transition model	
k_l	thermal conductivity of liquid phase	(W/m-K)
k_w	thermal conductivity of solid wall material	(W/m-K)
K_g	Kutateladze number for gas phase, $j_g\rho_g{}^{0.5}/[g\sigma(\rho_l - \rho_g)]^{0.25}$	
L	length (of evaporator or condenser)	(m)
L*	dimensionless length of evaporator (L/D_h)	
L_b	length of a Taylor bubble in the slug flow regime	(m)
L_{sc}	length of subcooled region in the evaporator	(m)
L_{sp}	length of single-phase (subcooled) region in the condenser	(m)
L_t	length of gas bubble plus liquid slug	(m)
L_{tot}	total length of condenser ($L_{tp} + L_{sp}$)	(m)
L_{tp}	length of two-phase (condensing) region in the condenser	(m)
m	exponent in friction factor model for gas phase	
m_o	fraction of cross-section occupied by liquid film surrounding a bubble in the slug flow regime	
M	ratio of superficial phase velocities, j_l/j_g	
n	exponent in friction factor model for liquid phase	
Nu_{fc}	Nusselt number in forced convection heat transfer	
Nu_{nb}	Nusselt number in nucleate boiling heat transfer	
p	power	(watts)
P	pressure	(N/m^2 or Pa)
Pr_l	Prandtl number, $c_{pl}\mu_l/k_l$	
P_{sat}	saturation pressure	(N/m^2 or Pa)
ΔP_a	pressure drop due to acceleration (phase change)	(Pa)
ΔP_a*	dimensionless pressure drop due to acceleration in two-phase region of evaporator or the condenser	
ΔP_{ac}	pressure drop due to acceleration (phase change) in two-phase region of condenser	(Pa)
ΔP_{ac}*	dimensionless pressure drop due to acceleration in the two-phase region of the condenser	
ΔP_{ae}	pressure drop due to acceleration (phase change) in two-phase region of evaporator	(Pa)
ΔP_{cond}	total pressure drop in condenser ($\Delta P_{tp} + \Delta P_{sp}$)	(Pa)
ΔP_{evap}	total pressure drop in evaporator ($\Delta P_{tp} + \Delta P_{sp}$)	(Pa)
ΔP_f	frictional pressure drop	(Pa)
ΔP_{fc}	frictional pressure drop in two-phase region of condenser	(Pa)
ΔP_{fc}*	dimensionless frictional pressure drop in two-phase region of condenser	
ΔP_{fe}	frictional pressure drop in two-phase region of evaporator	(Pa)
ΔP_{fe}*	dimensionless frictional pressure drop in two-phase region of evaporator	

Symbol	Description	Units
ΔP_{gc}	pressure drop due to body forces in two-phase region of condenser	(Pa)
ΔP_{gc}^*	dimensionless pressure drop due to body forces in two-phase region of condenser	
ΔP_g	pressure drop due to body forces	(Pa)
ΔP_{ge}	pressure drop due to body forces in two-phase region of evaporator	(Pa)
ΔP_{ge}^*	dimensionless pressure drop due to body forces in two-phase region of evaporator	
ΔP_{sp}	pressure drop in single-phase region of evaporator or condenser	(Pa)
ΔP_{tp}	total pressure drop in two-phase region of evaporator or condenser	(Pa)
ΔP_{sat}	difference between saturation pressures at fluid and heated wall temperatures	(N/m^2 or Pa)
q_{sp}	total heat transferred in the single-phase regime	(W)
q''	wall heat flux	(W/m^2)
q''_{fc}	portion of wall heat flux attributed to forced convection boiling	(W/m^2)
q''_{max}	maximum wall heat flux in the evaporator	(W/m^2)
q''_{sub}	portion of wall heat flux attributed to subcooled boiling	(W/m^2)
r_b	radius of bubble at the onset of nucleate boiling	(m)
r_{crit}	radius of vapor bubble at ONB	(m)
R_c	thermodynamic ratio in high vapor shear condenser	
R_{ev}	thermodynamic ratio in forced convection evaporator	
Re_b	effective Reynolds number in nucleate boiling	
Re_f	Reynolds number for liquid phase, based on inlet velocity, GD/μ_l	
Re_g	Reynolds number for gas phase, based on actual velocity, $\rho_g D u_g/\mu_g$	
Re_{gs}	Reynolds number for gas phase, based on superficial velocity $\rho_g D j_g/\mu_g$	
Re_{ls}	Reynolds number for liquid phase, based on superficial velocity, $\rho_l D j_l/\mu_l$	
Re_{tp}	two-phase Reynolds number, based on mixture velocity, $\rho_m D j/\bar{\mu}$	
S	suppression factor in saturated boiling model	
S_g^*	dimensionless perimeter in contact with gas phase for stratified flow	
S_i^*	dimensionless contact length between gas and liquid phases for stratified flow	
S_l^*	dimensionless perimeter in contact with liquid phase for stratified flow	
St	Stanton number, $Nu/Re_f Pr_l$	
t_w	thickness of condenser wall	(m)
T_f	fluid temperature	(K)
T_o	temperature of heat sink for radiation	(K)
T_r	radiator temperature for condenser	(K)
T_{sat}	saturation temperature	(K)
T_{sub}	temperature of subcooled liquid at the condenser exit	(K)

Symbol	Description	Units
T_w	wall temperature in evaporator	(K)
T_{wonb}	wall temperature in evaporator at ONB transition	(K)
T_2	temperature on secondary (coolant) side of condenser	(K)
ΔT_f	change in fluid temperature due to heat input	(K)
ΔT_{sat}	difference between saturation and fluid temperatures ($T_{sat} - T_f$)	(K)
ΔT_{sub}	difference between wall and saturation temperatures ($T_w - T_{sat}$)	(K)
u_{bo}	velocity of a vapor bubble in the condenser	(m/s)
u_f	actual velocity of liquid phase ($j_l/(1-\alpha)$),	(m/s)
u_{fo}	actual velocity of liquid phase at condenser inlet	(m/s)
u_g	actual velocity of vapor phase (j_g/α),	(m/s)
u_{go}	actual velocity of vapor phase at condenser inlet	(m/s)
U	overall heat transfer coefficient in single-phase flow	(W/m^2-K)
U_g^*	ratio of total pipe area to area occupied by gas phase	
U_l^*	ratio of total pipe area to area occupied by liquid phase	
v_{fg}	difference between liquid and gas phase specific volume ($v_g - v_l$)	(m^3/kg)
v_g	gas phase specific volume	(m^3/kg)
v_l	liquid phase specific volume	(m^3/kg)
w	mass flow rate	(kg/s)
We_j	Weber number, based on mixture velocity, $\rho_g Dj^2/\sigma$	
x	quality (fraction of two-phase mass flow which is vapor)	
x_o	quality at evaporator outlet or condenser inlet	
x_s	quality at transition from annular to slug flow	
z	arbitrary position of length coordinate	(m)
z_{sp}	distance from beginning of single-phase region in the condenser	(m)
z^*	dimensionless length increment, $z^* = z/D$	
X	Martinelli parameter	
X_{tt}	Martinelli parameter assuming turbulent gas and liquid phases	
Y	dimensionless acceleration vector parameter	

Greek

α	void fraction (fraction of two-phase volumetric flow which is vapor)	
α_c	critical void fraction defining a flow regime transition	
β	ratio of calculated to input heat flux in evaporator	
δ	thickness of liquid film in condenser	(m)
δ_o	thickness of liquid film at condenser inlet	(m)
ε	emissivity of radiator surface	
λ	dimensionless fluid property parameter, $\mu_l^2/D\rho_l\sigma$	
ρ_g	gas phase density	(kg/m^3)
ρ_l	liquid phase density	(kg/m^3)
ρ_m	density of two-phase mixture	(kg/m^3)
ρ^*	ratio of phase densities, ρ_l/ρ_g	
ϕ^2	two-phase multiplier	

Symbol	Description	Units
ϕ_{go}^2	two-phase multiplier, ratio of two-phase to single-phase gas pressure gradient	
σ	surface tension	(N/m)
σ_o	Stefan-Boltzmann constant	(W/m^2-K^4)
μ_g	gas phase viscosity	(kg/m-s)
μ_l	liquid phase viscosity	(kg/m-s)
$\overline{\mu}$	average viscosity of two-phase mixture	(kg/m-s)
τ	wall shear stress	(Pa)
τ_i	shear stress at gas-liquid interface	(Pa)
θ	angle between acceleration vector and flow direction 0° = colinear (downflow on earth) 90° = perpendicular (horizontal on earth) 180° = opposing (upflow on earth)	(°)

Subscripts

fdb	fully developed boiling
onb	onset of nucleate boiling

1 TRANSPORT LINES: Cylindrical Pipes with Wetted Walls

Most thermal transport systems for spacecraft will include two–phase flow in the transport line between the evaporator and condenser components or in the radiator components. Some systems will permit two–phase flow at the evaporator exit. Others will have single–phase flow at the evaporator exit, but will have two–phase flow in the transport line, because pressure drops and heat losses from the transport line will lead to condensate formation between the evaporator and the condenser.

The purpose of this section of the Design Manual is to provide methods for determining the two–phase flow regime and for calculating the pressure drop and void fraction in straight segments of piping without phase change. Knowledge of the flow regime is crucial to the calculation of the pressure drop and void fraction. Void fraction is especially important when calculating transient system behavior. The basic data which must be supplied by the designer are the fluid properties, the pipe size, the acceleration (magnitude and direction), and the volumetric flow rate of the gas and the liquid phases.

The methods in this section apply to adiabatic flow in pipes of uniform, circular cross–section. Alternate geometries such as square, rectangular, or triangular channels, which may be used to enhance heat transfer, must be treated separately.

This section assumes that the liquid phase will wet the material of the wall. If the liquid does not wet the wall surface (such as mercury in a glass tube for example), then the flow regimes and pressure drop models may be different than described here. This situation may be treated later.

1.1 Flow Regimes

This section deals with the determination of the flow regime. A key feature of the design methods recommended and used here is that the methods are applicable to a wide range of acceleration levels, including earth gravity and microgravity, and all "inclinations". The upper limit on the acceleration level would be the point where fluid properties vary significantly across the flow channel due to hydrostatic pressures. Once the flow regime is selected from four possible choices, the pressure drop specific to that regime can then be calculated (see Section 1.2).

Section 1.1.1 provides a brief introduction to the concept of flow regimes. It also identifies the information which the designer must have in hand in order to determine the flow regime and the pressure drop.

Section 1.1.2 presents dimensionless design maps for the flow regime determination. This section is set up so that the user does not need to know the details of the theory. The designer approaches the flow regime calculations with knowledge of the phase flow rates, physical geometry, and fluid conditions. Simple flow regime maps are then used where the designer can calculate a few dimensionless parameters, plot a coordinate on a map, and determine the flow regime.

Section 1.1.3 presents the basic equations behind each of three flow regime boundaries which determine the four flow regimes. The equations are presented in sufficient detail that the designer could recreate the dimensionless design maps presented here or generate design maps in dimensional coordinates (such as phase velocities) if desired. Examples of dimensional design maps are provided.

Finally, Section 1.1.4 compares the flow regime maps for the recommended design methods against selected data from microgravity experiments.

1.1.1 Introduction

Figure 1.1 illustrates the four primary flow patterns of interest for two–phase flow in pipes. The patterns include:

- Stratified,
- Slug,
- Annular, and
- Bubbly.

These patterns are referred to as "flow regimes."

In the stratified regime the gas and liquid phases are segregated by body forces due to gravity. Liquid flows near the bottom of the pipe and the gas flows near the top. This regime does not occur in a "vertical" pipe on the ground. (On a spacecraft, the acceleration vector would have to have a component perpendicular to the pipe for this flow regime to occur.) In the slug flow regime, the vapor forms long bubbles so that the vapor phase is not contiguous in the axial (flow) direction but is separated by liquid slugs. The vapor bubbles may be several pipe diameters in length and may be either asymmetrical or symmetrical with respect to the central axis of the pipe. In the annular flow regime, the vapor flows as a continuous gas core, and the liquid flows as a thin film on the wall of the pipe. In the bubbly flow regime, the vapor flows as discrete bubbles within the liquid phase.

The key to determining the flow regime is to first identify the dominant forces acting on the fluid. Balances between the dominant forces are then used to describe the boundaries (the transitions) between the four flow patterns described above. Three flow regime transitions are needed to bound the four regimes:

- Slug to stratified,
- Slug to bubbly, and
- Slug to annular.

These three transitions depend upon different balances of forces, as described in the subsequent discussions.

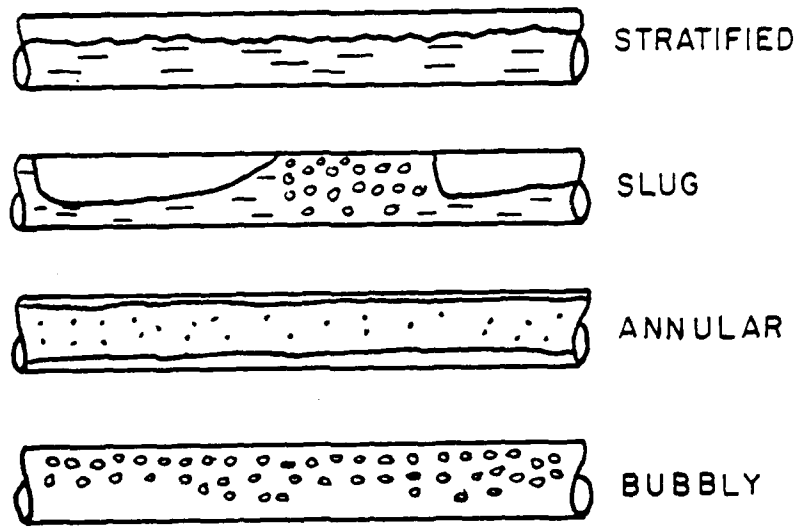

Figure 1.1. ILLUSTRATING FLOW PATTERNS (REGIMES) OF INTEREST

For this Design Manual, the model used for each of these flow regime transitions is mechanistic. In contrast to empirical correlations, the mechanistic approach considers the governing physics for each transition, therefore the mechanistic models should scale well with all acceleration magnitudes (g–levels) and vectors. There are three basic forces and two basic force balances to consider in the determination of the flow regimes:

- Balances of buoyancy and inertia forces, and
- Balances of surface tension and inertia forces.

References which consider the balances of buoyancy and inertia forces include Taitel and Dukler (1976), Barnea (1986), and Dukler (1988). References which consider the balances of surface tension and inertia forces include Lee (1987) and Kachnik et al. (1987).

There is a tendency in current literature to draw a distinction between flow regime models for earth gravity and for microgravity. Based upon the experimental evidence presented thus far, the models developed for earth–gravity conditions reduce satisfactorily to the appropriate limits for microgravity conditions without resorting to separate models. Examples are given for selected flow regime transitions by Reddy Karri (1988) and Revankar (1989). In this Design Manual, it will be shown that all of the significant regime transitions at earth gravity reduce to microgravity conditions, hence a single set of flow regime transitions can be used at all acceleration levels and orientations. Table 1.1 summarizes the models recommended for the Design Manual.

The recommended models have been extensively compared against experimental data at earth gravity in various flow orientations ranging from vertical upward to vertical downward. It will be shown that the models for each orientation reduce to the same model under microgravity conditions and compare well with the available microgravity data.

Table 1.1. RECOMMENDED MODELS FOR FLOW REGIME TRANSITIONS

TRANSITION	RECOMMENDED MODEL	APPROACH	KEY PARAMETER FOR UNCERTAINTY	BASELINE VALUE OF KEY PARAMETER	RANGE OF UNCERTAINTY FOR KEY PARAMETER
SLUG–TO–STRATIFIED	TAITEL–DUKLER (1976)	BALANCE $\left[\frac{\text{gas inertia}}{\text{buoyancy}}\right]_c$	INTERFACIAL SHEAR $\left[f_i/f_{wg}\right]$	10	1 to 10
SLUG–TO–BUBBLY					
(a) TURBULENCE	BARNEA (1986)	BALANCE $\left[\frac{\text{gas inertia}}{\text{buoyancy}}\right]_c$	TURBULENCE COEFFICIENT (k)	0.14	0.725 to 3.7
(b) MAXIMUM VOID FRACTION	TAITEL ET AL (1980)	MAXIMUM PACKING OF VAPOR BUBBLES	CRITICAL VOID FRACTION (α_c)	0.45	0.40 to 0.52
			BUBBLE DISTRIBUTION	1.2	1.0 to 1.2
SLUG–TO–ANNULAR	BARNEA (1986)	"NEUTRAL STABILITY" or "PHYSICAL BLOCKAGE"	INTERFACIAL SHEAR $\left[f_i/f_{wg}\right]$	$[1 + 75(1-\alpha)]$	1 to $[1 + 75(1-\alpha)]$

1.1.2 Dimensionless Design Maps

This section illustrates how the flow regime can be quickly determined from known conditions. The information required in order to determine the flow regime includes:

Fluid Properties

ρ_l Liquid phase density
ρ_g Gas phase density
μ_l Liquid phase viscosity
μ_g Gas phase viscosity
σ Surface tension

Geometry

D Pipe diameter

Acceleration

a Magnitude of acceleration
θ Direction (angle between acceleration vector and the flow direction)

Flow Rates

j_l Liquid phase volumetric flux (Q_l/A)
j_g Gas phase volumetric flux (Q_g/A)

Each of the three flow regime transitions can be represented on dimensionless design maps. The dimensionless coordinates for these regime maps can be determined from the information listed above.

The order of examining the transitions is important to the determination of the flow regime, since certain regimes supersede others. The order should be:

- Slug–to–Stratified Flow Regime Transition,
- Slug–to–Bubbly Flow Regime Transition, and
- Slug–to–Annular Flow Regime Transition.

Figure 1.2 illustrates the logic for the flow regime selection. The dimensionless design maps for flow regimes are presented and discussed in that order below.

Slug–to–Stratified Flow Regime Transition. To determine first whether or not the flow regime is stratified, the proposed design point is mapped on a dimensionless plot of gas Froude number F_g versus the Martinelli parameter X as shown in Figures 1.3a and 1.3b. The definitions of these dimensionless parameters used in the maps are:

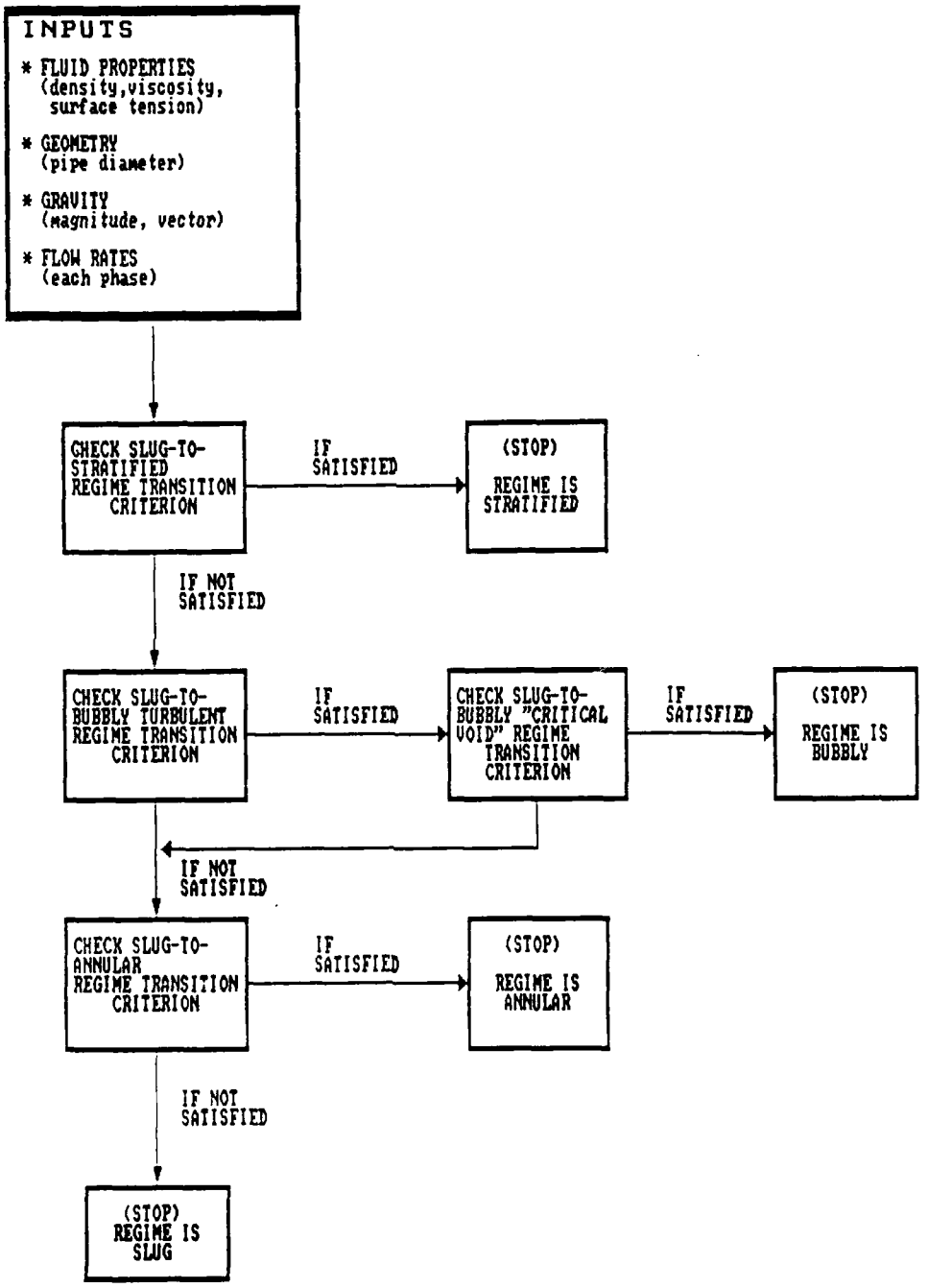

Figure 1.2. LOGIC FOR FLOW REGIME DETERMINATION

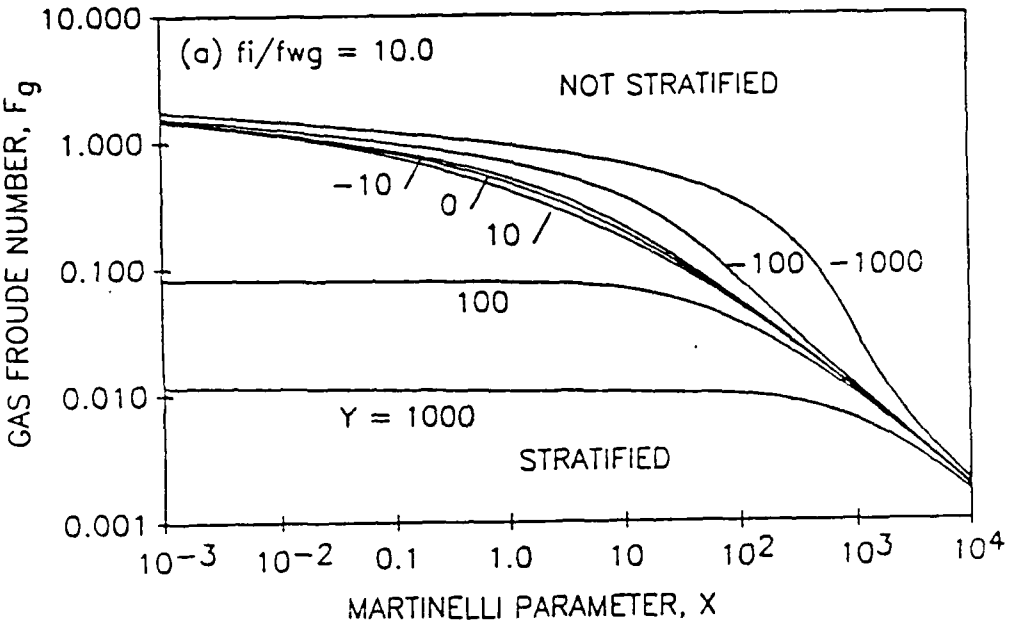

a) Rough vapor/liquid interface

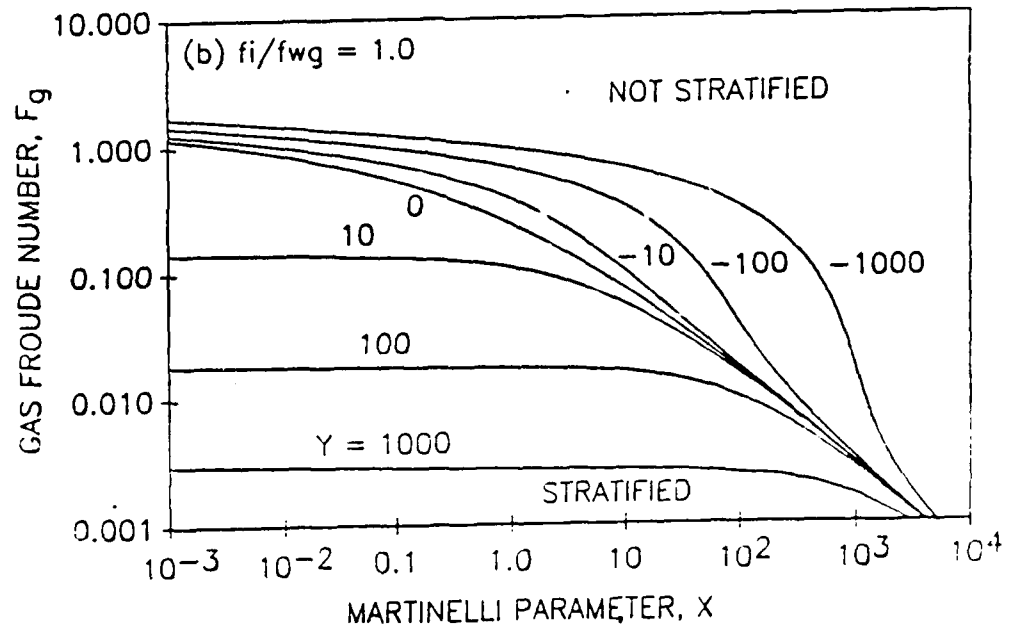

b) Smooth vapor/liquid interface

Figure 1.3. DIMENSIONLESS DESIGN MAP FOR SLUG-TO-STRATIFIED FLOW REGIME TRANSITION (TURBULENT FLOW)

$$F_g = \frac{\rho_g^{0.5} j_g}{[aD(\rho_l - \rho_g)]^{0.5}} \qquad (1\text{–}1)$$

$$X = \left[\frac{\left[\frac{4C_l}{D}\right]\left[\frac{\rho_l D j_l}{\mu_l}\right]^{-n}\left[\frac{\rho_l j_l^2}{2}\right]}{\left[\frac{4C_g}{D}\right]\left[\frac{\rho_g D j_g}{\mu_g}\right]^{-m}\left[\frac{\rho_g j_g^2}{2}\right]} \right]^{0.5} \qquad (1\text{–}2)$$

$$Y = -\left[\frac{a(\rho_l - \rho_g)\cos\theta}{\left[\frac{4C_g}{D}\right]\left[\frac{\rho_g D j_g}{\mu_g}\right]^{-m}\left[\frac{\rho_g j_g^2}{2}\right]} \right] \qquad (1\text{–}3)$$

where

F_g	is the dimensionless Froude number for the gas phase,
X	is the dimensionless Martinelli parameter,
Y	is the dimensionless pipe inclination parameter
a	is the magnitude of the acceleration (m/s^2),
ρ_l	is the gas phase density (kg/m^3),
ρ_g	is the liquid phase density (kg/m^3),
j_l	is the superficial velocity of the liquid phase (m/s),
j_g	is the superficial velocity of the gas phase (m/s),
D	is the pipe diameter (m), and
θ	is the angle betweer the flow direction and the acceleration vector (°) (e.g. 0° is colinear, 90° is perpendicular, and 180° is opposing, corresponding to downflow, horizontal, and upflow on the ground).

Table 1.2 indicates how to determine the values of the friction factor coefficients C_l, C_g, n and m to use in Equations 1–2 and 1–3.

The procedure in using Figures 1.3a and 1.3b is to first calculate the three dimensionless quantities in Equations 1–1, 1–2, and 1–3. These quantities depend upon the superficial phase velocities (or volumetric flow rates) j_l and j_g of each phase and the fluid properties. The desired operating point is plotted on the design map by the coordinates (X, F_g). Then the line of constant Y for the proposed design conditions is located. If the design point falls below the line for the value of Y (Equation 1–3), then the flow regime is stratified. If the design point falls above the line for the value of Y, then the slug–to–bubbly flow regime transition is assessed as described below. Note also that if the acceleration level is very small, for example at microgravity conditions where $a \cong 10^{-6}g$, then $Y \cong 0$.

The difference between Figures 1.3a and 1.3b represents the range of uncertainty in modelling the regime transition. (The uncertainty specifically lies in the interfacial friction between the gas and liquid phases, as described in Section 1.1.3.) The proposed operating point should be located on each of these figures. If both figures indicate that the flow is stratified, then the flow is probably stratified. If Figure 1.3a indicates that the flow is stratified and Figure 1.3b does not, then the flow regime may be uncertain.

Table 1.2. SUMMARY OF PARAMETER VALUES FOR FRICTION FACTOR CALCULATION				
PHASE	**REGIME**	**CRITERION**	C_g	**n**
VAPOR	LAMINAR	$Re_{gs} = \left[\frac{\rho_g D j_g}{\mu_g}\right] < 1500$	16	1.0
	TURBULENT	$Re_{gs} \geq 1500$	0.046	0.2
PHASE	**REGIME**	**CRITERION**	C_l	**n**
LIQUID	LAMINAR	$Re_{ls} = \left[\frac{\rho_l D j_l}{\mu_l}\right] < 1500$	16	1.0
	TURBULENT	$Re_{ls} \geq 1500$	0.046	0.2

Slug–to–Bubbly Flow Regime Transition. The transition from the slug to the bubbly flow regime should be examined as the second step. The slug–to–bubbly flow regime transition consists of two parts:

- A transition based upon fluid turbulence, and
- A transition based upon a critical void fraction,

and both of these criteria need to be checked to determine the flow regime.

Figure 1.4 is the dimensionless design map for the transition based upon turbulence. To determine the flow regime a dimensionless Weber number

$$We_j = \left[\frac{\rho_l D j^2}{\sigma}\right] = \left[\frac{\rho_l D (j_g + j_l)^2}{\sigma}\right] \qquad (1\text{–}4)$$

and a dimensionless Bond number

$$Bo = \left[\frac{aD^2(\rho_l - \rho_g)}{\sigma}\right] \qquad (1\text{–}5)$$

are calculated for the proposed design conditions, where

ρ_l is the liquid phase density (kg/m^3)
ρ_g is the gas phase density (kg/m^3)
D is the pipe diameter (m),
σ is the surface tension (N/m),
j_g is the superficial velocity of the gas phase (m/s), and
j_l is the superficial velocity of the liquid phase (m/s).

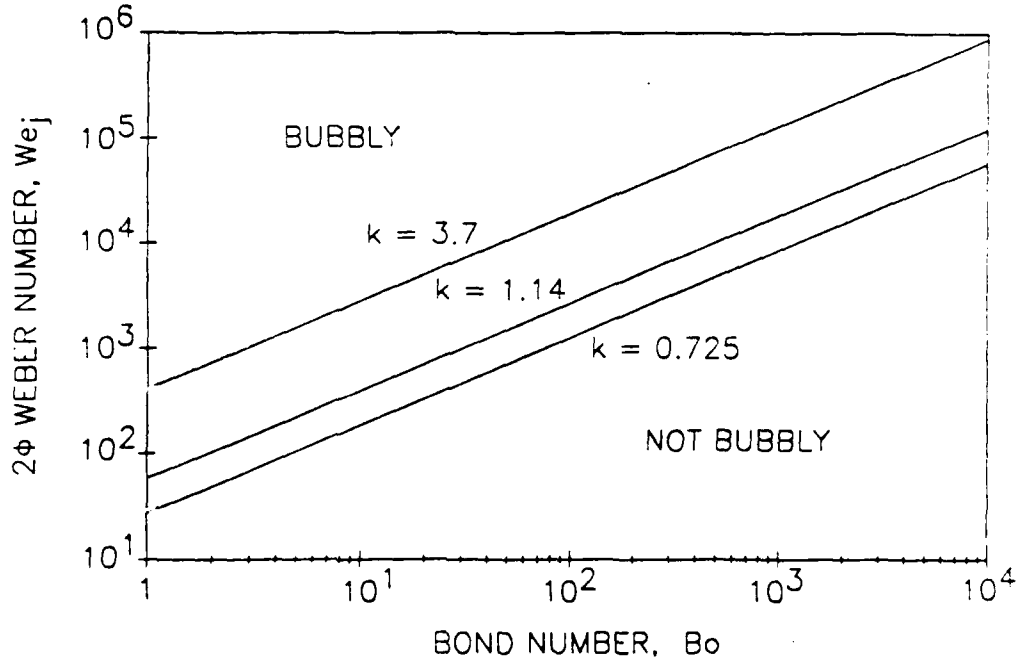

Figure 1.4. DIMENSIONLESS DESIGN MAP FOR SLUG–TO–BUBBLY FLOW REGIME TRANSITION (TURBULENCE CRITERION)

The point with coordinates (Bo, We_j) is then located on Figure 1.4. If the point is above the transition line in the figure, then the regime *may* be bubbly, but the second (void fraction) transition criterion must be checked first. The three lines in Figure 1.4 illustrate the range of uncertainty for the slug–to–bubbly flow regime transition. If the point is below all three transition lines, then the slug–to–annular flow regime transition must be checked, as described below.

Figure 1.5 illustrates the second slug–to–bubbly flow regime transition criterion, based upon a critical void fraction. For this transition, the dimensionless parameters are:

$$M = (j_l/j_g) \tag{1-6}$$

$$K_g = \frac{\rho_g^{0.5} j_g}{[a\sigma(\rho_l - \rho_g)]^{0.25}} \tag{1-7}$$

$$\rho^* = (\rho_l/\rho_g) \tag{1-8}$$

where
- M is the dimensionless superficial velocity ratio,
- K_g is the dimensionless gas Froude number,
- ρ^* is the dimensionless density ratio,

and the other parameters are defined above.

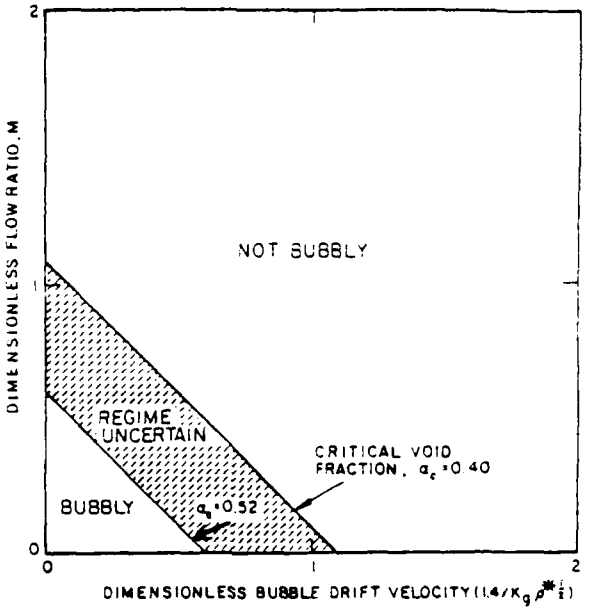

Figure 1.5. DIMENSIONLESS DESIGN MAP FOR SLUG–TO–BUBBLY FLOW REGIME TRANSITION (VOID FRACTION CRITERION)

The proposed design point is plotted in Figure 1.5 at the coordinates $(1.4/K_g \sqrt{\overline{\rho^*}}, M)$. If the design point is below the transition line, then the flow regime is bubbly. If the design point is above this line, then the slug–to–annular flow regime transition needs to be evaluated. In Figure 1.5, the shaded region represents the range of uncertainty in the flow regime determination by this criterion.

Slug–to–Annular Flow Regime Transition. The slug–to–annular flow regime transition involves two of the same dimensionless groups as the stratified–to–slug transition; namely, the parameters X and Y. The proposed design point is plotted on the graph of Figure 1.6, for the coordinates (X,Y). If the location of the design point is below the curve in the figure, then the flow regime is annular. If the location of the design point is above the curve in the figure, then the flow regime is slug. The two lines in the figure illustrate the range of uncertainty for this transition.

It should also be noted that for microgravity conditions where $g \cong 10^{-6}g$ the value of Y is approximately 0, so that only the X coordinate is important. That is, the point can be plotted as (X, 0).

1.1.3 Equations for Flow Regime Transitions

This section describes the detailed analytical equations used for each of the flow regime transitions. Additional design maps in dimensional coordinates can be generated if desired using the equations presented in this section.

Slug–to–Stratified Regime Transition. This flow regime transition involves the simultaneous solution of two equations. One equation is a dimensionless two–phase momentum equation for a separated flow and the other is a dimensionless transition criterion.

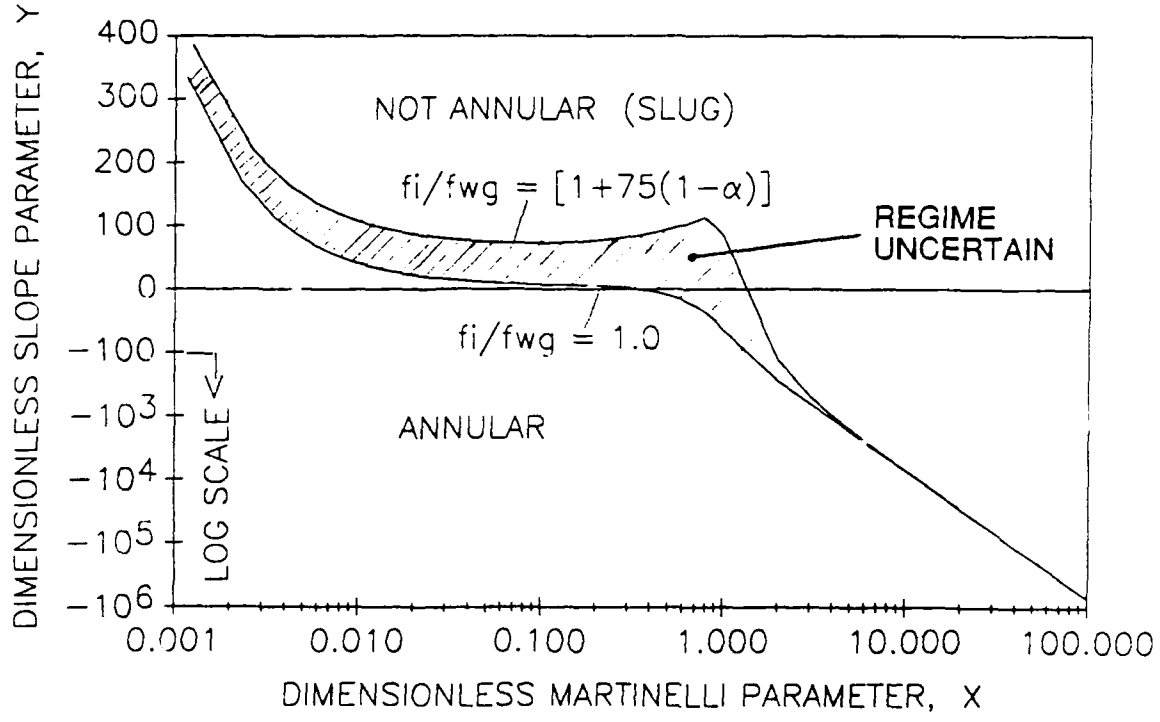

Figure 1.6. DIMENSIONLESS DESIGN MAP FOR SLUG–TO–ANNULAR FLOW REGIME TRANSITION (TURBULENT FLOW)

The dimensionless transition criterion in this model is based upon a balance between gas inertia and buoyancy in the gas and liquid phases. Figure 1.7 illustrates the concept. If the gas flow rate is large enough, the pressure drop created by the flow of the gas over a wave (the Bernoulli effect) is sufficient to lift the waves in a stratified flow to the top of the pipe. A critical gas flow rate is necessary for this condition to occur.

To map this transition in the design method, the dimensionless liquid height h* is varied across the range from 0 to 1. For a given value of the dimensionless liquid height, the criterion for the critical gas velocity is determined by:

$$F_g = [1-h^*]\left[\frac{1}{U_g^*}\right]\left[\frac{A_g^*}{dA_l^*/dh^*}\right]^{0.5} \qquad (1-9)$$

where Table 1.3 defines the other dimensionless geometric parameters which are also based upon the liquid height, h*.

The critical gas velocity at the transition is then determined from the definition of the gas Froude number F_g by:

$$j_g = F_g[aD(\rho_l - \rho_g)/\rho_g]^{0.5} \qquad (1-10)$$

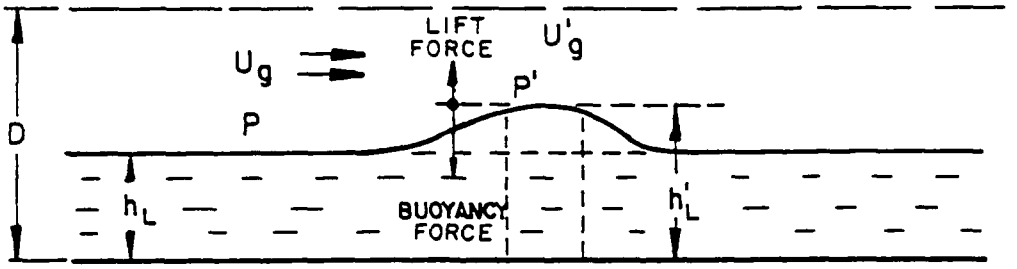

Figure 1.7. ILLUSTRATING FORCE BALANCE FOR SLUG–TO–STRATIFIED FLOW REGIME TRANSITION

Table 1.3. DIMENSIONLESS GEOMETRY PARAMETERS FOR SLUG–TO–STRATIFIED FLOW REGIME TRANSITION

$$h^* = h_l / D, \text{ (Figure 1.7)}$$

$$A_l^* = \frac{1}{4}\left\{\pi - \cos^{-1}(2h^* - 1) + (2h^* - 1)[1 - (2h^* - 1)^2]^{\frac{1}{2}}\right\}$$

$$A_g^* = \frac{1}{4}\left\{\cos^{-1}(2h^* - 1) - (2h^* - 1)[1 - (2h^* - 1)^2]^{\frac{1}{2}}\right\}$$

$$S_l^* = [\pi - \cos^{-1}(2h^* - 1)]$$

$$S_g^* = [\cos^{-1}(2h^* - 1)]$$

$$S_i^* = [1 - (2h^* - 1)^2]^{\frac{1}{2}} = (dA_L^*/dh^*)$$

$$U_l^* = \left[\pi/4A_L^*\right] = 1/(1-\alpha)$$

$$U_g^* = \left[\pi/4A_G^*\right] = 1/\alpha$$

$$D_l^* = \frac{4\,A_L^*}{S_L^*}$$

$$D_g^* = \frac{4A_G^*}{\left[S_G^* + S_i^*\right]}$$

where

F_g is the gas Froude number from Equation 1–9,
a is the magnitude of the acceleration (m/s^2),
D is the pipe diameter (m),
ρ_l is the liquid phase density (kg/m^3), and
ρ_g is the gas phase density (kg/m^3).

The critical gas velocity is then used to calculate a Reynolds number for the gas phase by:

$$Re_{gs} = (\rho_g D j_g / \mu_g) \quad (1-11)$$

where

ρ_g is the gas phase density (kg/m^3)
j_g is the superficial velocity of the gas phase (m/s),
D is the pipe diameter (m), and
μ_g is the gas phase viscosity (kg/m–s).

Then a gas phase friction factor

$$f_{wg} = C_g Re_{gs}^{-m} \quad (1-12)$$

is calculated, where, if $Re_{gs} \geq 1500$ then

$$C_g = 0.046 \text{ and} \quad (1-13a)$$

$$m = 0.2 \quad (1-13b)$$

and if $Re_{gs} < 1500$ then

$$C_g = 16 \text{ and} \quad (1-14a)$$

$$m = 1.0. \quad (1-14b)$$

After the friction factor is calculated, a dimensionless parameter defined by:

$$Y = -\left[\frac{a(\rho_l - \rho_g)\cos\theta}{\left[\frac{4 f_{wg}}{D}\right]\left[\frac{\rho_g j_g^2}{2}\right]}\right] \quad (1-15)$$

is calculated, where

θ is the inclination of the acceleration vector relative to the direction of the flow in the pipe (°).

The parameter Y is then used in a dimensionless two–phase momentum equation to determine a dimensionless parameter related to the liquid flow rate:

$$X^2 = \frac{\left[(U_g{*}D_g{*})^{-m}(U_g{*})^2\right]\left[\frac{S_g{*}}{A_g{*}} + \left[\frac{f_i}{f_{wg}}\right]\left[\frac{S_i{*}}{A_l{*}} + \frac{S_i{*}}{A_g{*}}\right]\right] - 4Y}{[U_l{*}D_l{*}]^{-n}(U_l{*})^2(S_l{*}/A_l{*})} \qquad (1\text{–}16)$$

where the dimensionless geometry parameters (starred parameters) are given in Table 1.3 as a function of the dimensionless liquid level and

f_i/f_{wg} is a constant with a recommended value of 10,
n has two possible values (0.2 or 1.0).

Thus, two values of X^2 are calculated, one with each value of n assumed.

The liquid velocity can then be calculated from the definition of the parameter X^2 by:

$$j_l = \left[\frac{X^2\left[\frac{4C_g}{D}\right]\left[\frac{\rho_g D j_g}{\mu_g}\right]^{-m}\left[\frac{\rho_g j_g^2}{2}\right]}{\left[\frac{4C_l}{D}\right]\left[\frac{\rho_l D}{\mu_l}\right]^{-n}\left[\frac{\rho_l}{2}\right]}\right]^{1/(2-n)} \qquad (1\text{–}17)$$

where:

C_l is 0.046 with n = 0.2 and is 16 with n = 1.0

and two values of the superficial liquid velocity are then calculated, one with each set of values for the parameters C_l and n. The superficial liquid velocity at the transition is the minimum of the two values.

Equations 1–9 and 1–16, with the equations in Table 1.3, produce the parameters F_g and X for dimensionless flow regime plots such as Figures 1.3a and 1.3b. This assumes that constant values of Y and f_i/f_{wg} are selected for use in Equation 1–16. The range of recommended values for f_i/f_{wg} is from 1 to 10. The value of 1 represents a smooth gas–liquid interface. The value of 10 represents a rough (wavy) gas–liquid interface.

Equations 1–10 and 1–17 convert the dimensionless parameters into superficial velocities (volumetric fluxes) for each phase. For each value of h* selected for the calculations, a pair of values (j_l, j_g) can be determined. Figures 1.8a, b, and c show the calculated slug–to–stratified regime transition for one set of conditions at earth gravity. The different figures show the results at angles of 180°, 90°, and 20°. Compared with the results where the flow direction and the acceleration vector are 90° apart (corresponding to a horizontal pipe on the ground), the range of the stratified flow regime shrinks as the flow direction and the acceleration vector oppose each other more (corresponding to upflow on the ground). The stratified regime expands as the flow direction and the acceleration vector become colinear (corresponding to downflow on the ground).

Figure 1.9 shows the effect of the magnitude of the acceleration level on the results. The stratified region also diminishes with reduced gravity for flow regime maps in these coordinates. In fact, the stratified flow regime is of little interest at acceleration levels of 10^{-2}g to 10^{-3}g or lower.

Note: Example of map for specific conditions – not for general use

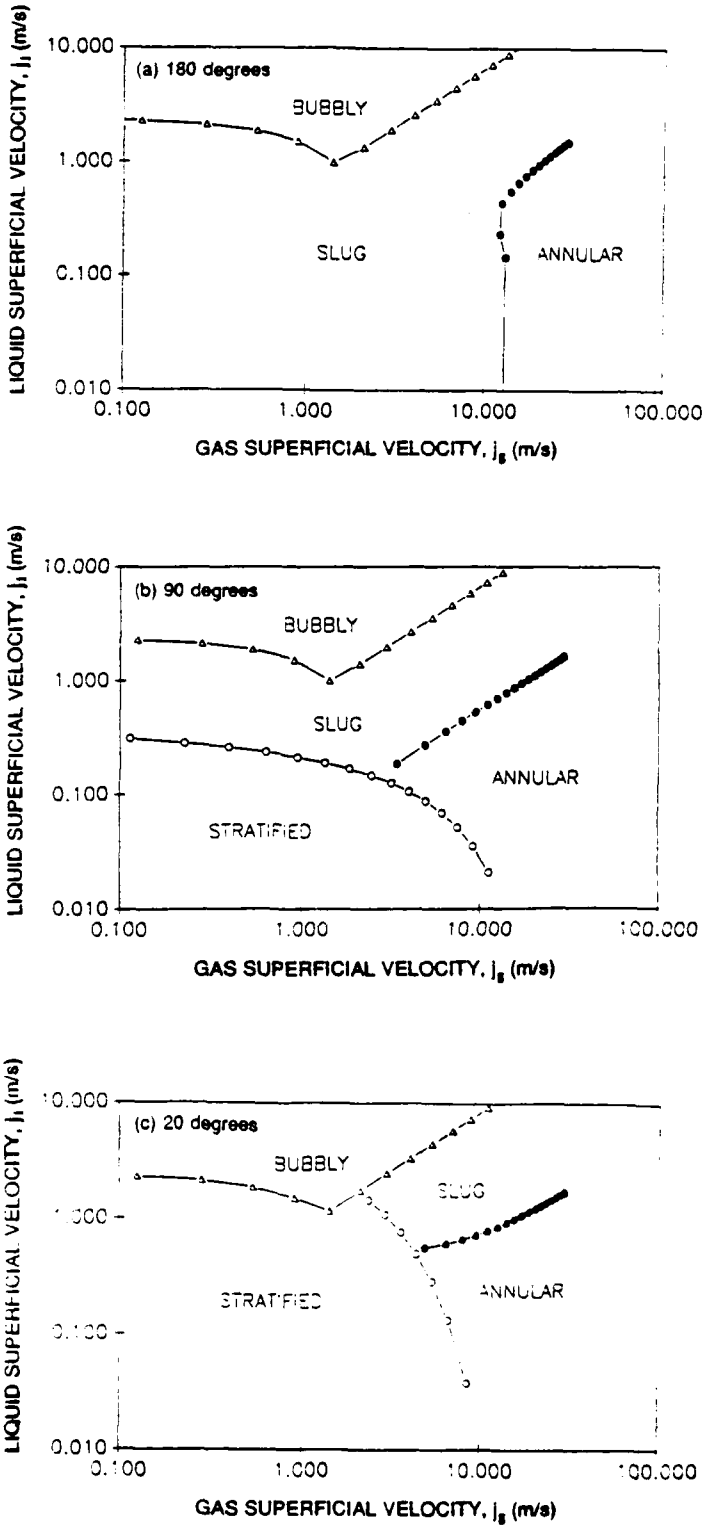

Figure 1.8. EFFECT OF PIPE INCLINATION ON FLOW REGIME MAP AT EARTH GRAVITY (SUPERFICIAL VELOCITY COORDINATES)

Note: Example of map for specific conditions – not for general use

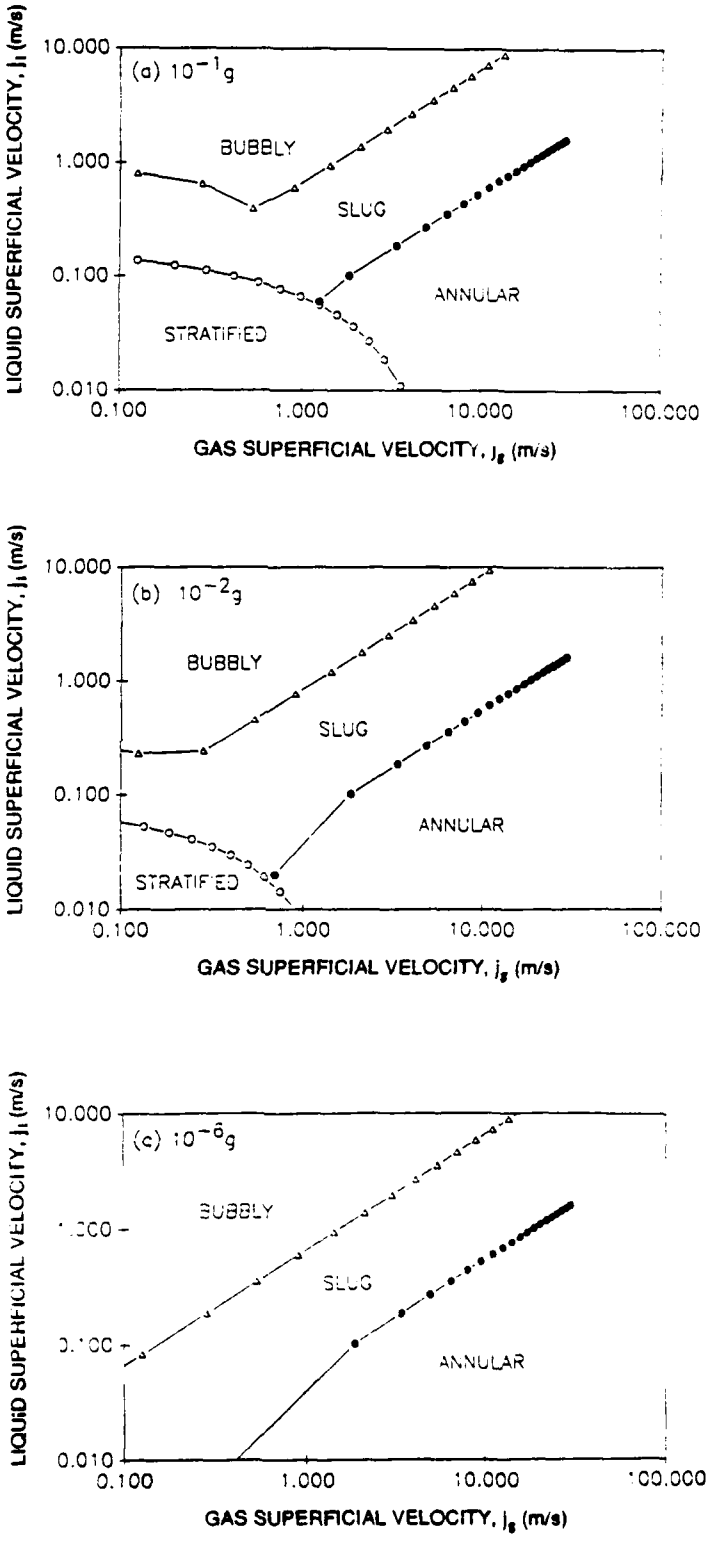

Figure 1.9. EFFECT OF GRAVITY ON FLOW REGIME MAP (SUPERFICIAL VELOCITY COORDINATES)

Slug–to–Bubbly Flow Regime Transition. This flow regime transition involves two parts. The first part considers a balance between the inertia of the two phase flow and buoyancy (Figure 1.10). A limiting criterion in this condition is the maximum packing of bubbles in the pipe – the void fraction can only be so large before the bubbles touch and coalesce into large bubbles in a slug flow pattern.

For the first transition criterion, Barnea (1988) suggests an equation which has the dimensionless form:

$$We_j = \left[\frac{1.2k}{f_{w_l}{}^{0.4}}\right]^{1.67} Bo^{0.835} \qquad (1\text{–}18)$$

where

f_{w_l} is a friction factor with a value of $\cong$ 0.005, and
k is a constant in the range of 0.725 to 3.7. (Taitel and Dukler (1982) recommend a value of k = 1.14).

Figure 1.4 plots this dimensionless equation for the flow regime transition. The range of uncertainty in the value of k from 0.725 to 3.7 is shown in the design map.

Using the definition of the two–phase Weber number in Equation 1–4, it can be rewritten to solve for the superficial liquid velocity

$$j_l = \left[\frac{We_j \sigma}{\rho_l D}\right]^{0.5} - j_g \qquad (1\text{–}19)$$

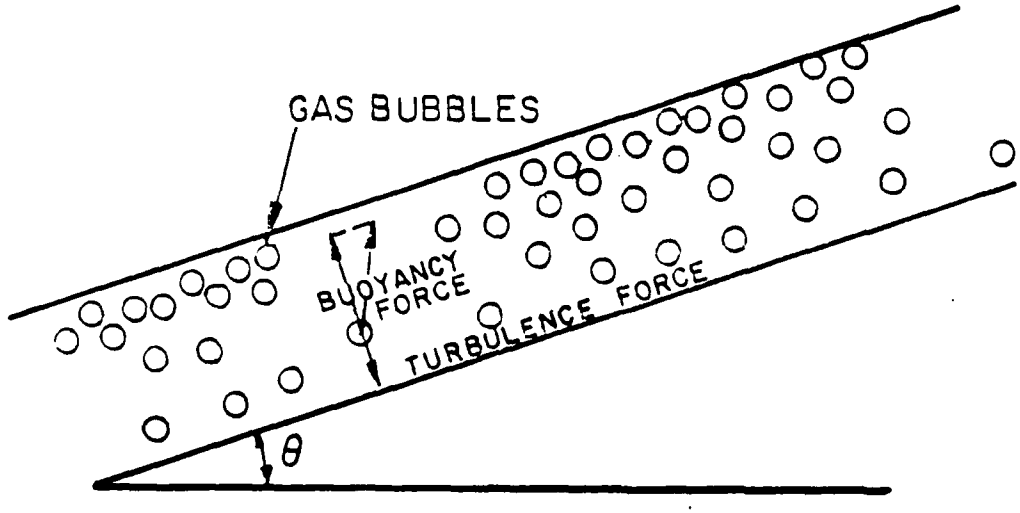

Figure 1.10. ILLUSTRATING FORCE BALANCE FOR SLUG–TO–BUBBLY FLOW REGIME TRANSITION

Equation 1–19 can be used to map the transition as (j_l, j_g) pairs by selecting a range of values of j_g and calculating the corresponding j_l values, using the Weber number from Equation 1–18.

The second criterion for the slug–to–bubbly transition comes from a basic drift–flux equation (Zuber–Findlay, 1965) for bubbly flow

$$\frac{j_g}{\alpha_c} = C_o(j_g + j_l) + 1.41\left[\frac{a\sigma(\rho_l - \rho_g)}{\rho_l^2}\right]^{0.25} \qquad (1–20)$$

where

α_c is a critical value of the void fraction for maximum packing of the bubbles. Dukler (1988) recommends a value of $\alpha_c = 0.45$, though other recommended values range from 0.4 to 0.52 (Taitel–Dukler, 1976).

C_o is a constant typically near 1.2.

Equation 1–20 can be written in dimensionless form as

$$\left[\frac{j_l}{j_g}\right] = \left[\frac{1}{C_o\alpha_c} - 1\right] - \frac{1.41}{K_g}\left[\frac{\rho_g}{\rho_l}\right]^{0.5} \qquad (1–21)$$

The design map in Figure 1.5 plots the dimensionless regime transition of Equation 1–21 using the parameters defined by Equations 1–6 to 1–8. The design map uses the recommended value $C_o = 1.2$ and shows the uncertainty due to the variation in the critical void fraction from 0.4 to 0.52.

Equation 1–20 can be written to solve for the superficial liquid velocity as

$$j_l = \left[\frac{1}{C_o\alpha_c} - 1\right]j_g - \left[\frac{1.41}{C_o}\right]\left[\frac{a\sigma(\rho_l - \rho_g)}{\rho_l^2}\right]^{0.25} \qquad (1–22)$$

Similarly to Equation 1–19, values of (j_l, j_g) pairs can be determined by varying j_g across an appropriate range of values.

The transition from slug to bubbly flow regimes is mapped by selecting the pair of coordinates with the higher value of j_l for a given value of j_g. Said another way, for the flow regime map, the transition criterion with a higher liquid velocity at a given gas velocity (Equation 1–19 or 1–22) takes precedence in the flow regime transition.

Figures 1.8 and 1.9 also plot the slug–to–bubbly flow regime on regime maps in superficial velocity coordinates. Figures 1.8a, b, and c show that pipe inclination has very little effect on the transition. This is confirmed by data at earth gravity conditions (Barnea, 1986). Figure 1.9 shows that as the magnitude of the acceleration is reduced, the portion of the transition criterion related to turbulence (Equation 1–19) disappears and the portion of the transition related to void fraction (Equation 1–22) remains.

Slug–to–Annular Flow Regime Transition. This regime transition, proposed by Barnea (1986), also consists of two parts. Both describe blockage of an annular core, but by different mechanisms. As Barnea explains, the first mechanism ("neutral stability") is an instability of the annular flow configuration, and the second occurs when the liquid film is large enough to cause blockage as a result of flow in the liquid film.

The first part of the transition involves the simultaneous solution of two equations. In dimensionless form, the two equations are:

$$Y = \left[\frac{(f_i/f_{wg})}{\alpha^{2.5}(1-\alpha)}\right] - \left[\frac{1}{(1-\alpha)^3}\right]X^2 \qquad (1\text{–}23)$$

$$Y = \frac{[2 - 1.5(1-\alpha)]}{(1-\alpha)^3[1 - 1.5(1-\alpha)]}X^2 \qquad (1\text{–}24)$$

Equation 1–23 is the two–phase void fraction equation for the annular flow regime (Wallis, 1969). (See Section 1.2.3.) Equation 1–24 is the transition criterion derived by Barnea (1986).

If the void fraction is varied between values of unity and zero, the Equations 1–23 and 1–24 map out coordinates of (X, Y) as shown by the upper portion of the curve with positive values of Y in the design map of Figure 1.6.

The second transition criterion involves using a critical void fraction $\alpha_c = 0.76$ in Equation 1–23. Coordinates in (X,Y) pairs can be mapped out when this substitution is made. This leads to the lower portion of the transition criterion with negative values of Y in the design map of Figure 1.6.

The parameter (f_i/f_{wg}) in Equation 1–23 represents the interfacial friction between the gas and the liquid phases. For the purpose of these design maps, the value proposed by Wallis (1969) based on tests at earth gravity is used:

$$(f_i/f_{wg}) = [1 + 75(1-\alpha)] \qquad (1\text{–}25)$$

which is also used by Dukler (1988) for microgravity comparisons. Various models for this appear in the literature, but the Wallis (1969) model appears to be a reasonable limit for most data. The minimum value of this parameter would be unity, representing a smooth gas–liquid interface. Figure 1.6 reflects this range of uncertainty in this key parameter.

Once values of the coordinates Y and X are determined from the equations for the transition, they can be readily converted to dimensional form using the definitions of these parameters in Equations 1–3 and 1–2, respectively. Figures 1.8 and 1.9 also show the slug–to–annular transition on flow regime maps in (j_l, j_g) coordinates. The set of plots in Figure 1.8 shows that this transition is approximately linear in a horizontal pipe at earth gravity, but the lower portion of the transition approaches a constant liquid velocity for downward inclinations and approaches a constant gas velocity for upward inclinations. Barnea (1986) shows that this is consistent with experimental flow regime data at earth gravity. Figure 1.9 shows that the transition is approximately the same under microgravity conditions as it is for a horizontal pipe at earth gravity. This is readily apparent because the parameter Y approaches zero in the case of either low inclinations ($\theta = 0$) or low acceleration level ($a = 0$).

Alternate Regime Map Coordinates. Simple transformations can convert the flow regime maps in (j_l, j_g) coordinates as described above to mass flux versus flow quality (G, x) coordinates:

$$G = (\rho_g j_g + \rho_l j_l) \tag{1–26}$$

$$x = \frac{\rho_g j_g}{(\rho_g j_g + \rho_l j_l)} = \left[\frac{\rho_g j_g}{G}\right] \tag{1–27}$$

where

G is the mass flux (kg/m^2–s), and
x is the quality (ratio of vapor mass flow rate to the total mass flow rate).

Figures 1.11 and 1.12 show how the regime maps in Figures 1.8 and 1.9 appear when converted to these coordinates. It is particularly interesting to note that under microgravity conditions (Figure 1.12c), the transitions from slug–to–bubbly and slug–to–annular flow regimes are are seen to be lines at approximately constant flow quality.

1.1.4 Validation with Microgravity Flow Regime Data

As Barnea (1986) points out, the methods and models described here apply well at earth gravity to the full range of pipe inclinations from vertical upward, to horizontal, to vertical downward. Examples of the flow regime comparisons are given in Barnea (1986), Barnea et al. (1982) and Taitel (1980).

The purpose of this section is to illustrate that the same models can be extrapolated to microgravity conditions. At this time, there are four key sets of experimental flow regime data obtained under microgravity conditions. These include:

- Heppner (1975, 1978),
- Lee (1987) (also see Kachnick et al., 1987),
- Dukler et al. (1988), and
- Chen et al. (1988).

All represent experiments on aircraft, where acceleration levels of 10^{-2}g can be achieved for periods of approximately 30 seconds as the aircraft negotiates a parabolic trajectory. Dukler et al. have also included some experimental data from drop tower experiments where the low acceleration levels are for periods of a few seconds. No flow regime data in pipes are available for long–term microgravity conditions.

As discussed by Dukler, the Heppner data provided the initial qualitative concepts for two–phase flow regimes in microgravity. Unfortunately, the reconciliation of the reported flow regimes with recent observations of the flow regimes depends upon information no longer available about those experiments. For that reason, the validation of the models here includes data from the other three experiments only.

Note: Example of map for specific conditions – not for general use

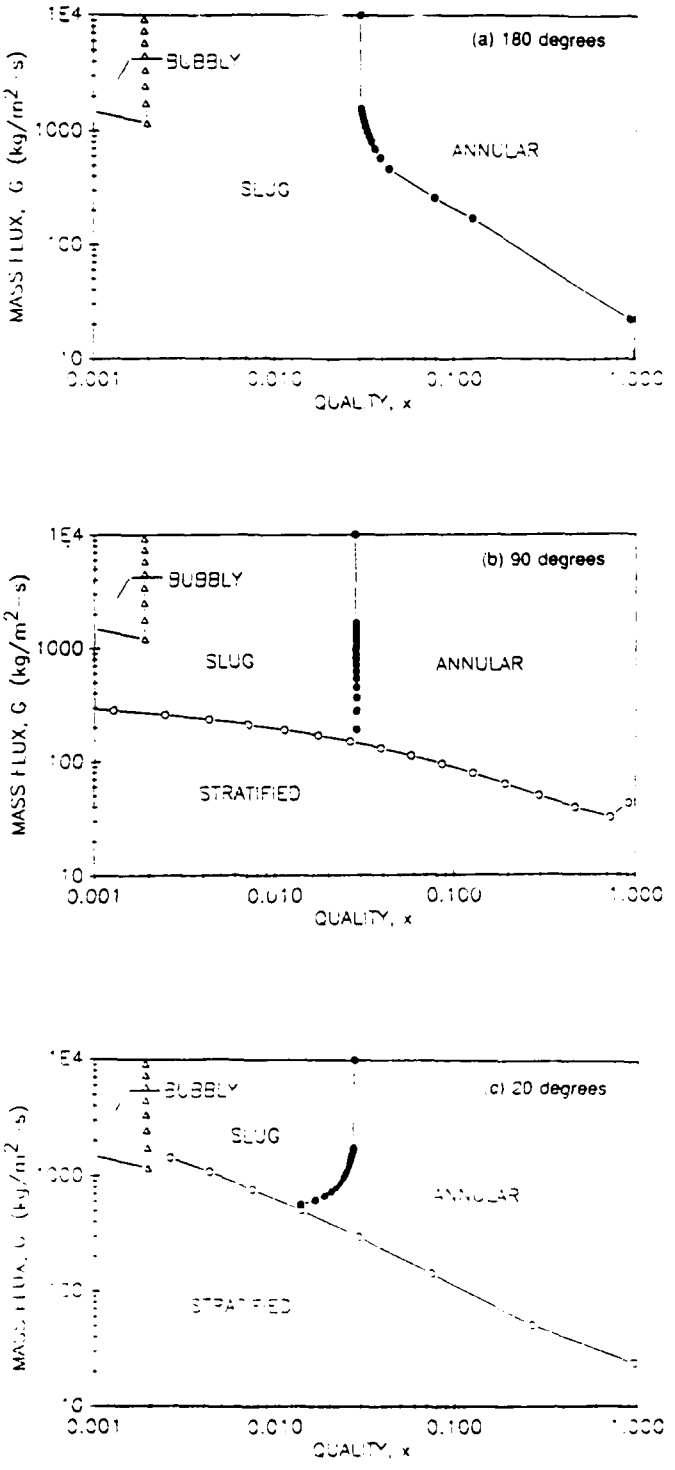

Figure 1.11. EFFECT OF PIPE INCLINATION ON FLOW REGIME MAP AT EARTH GRAVITY (MASS FLUX AND QUALITY COORDINATES)

Note: Example of map for specific conditions – not for general use

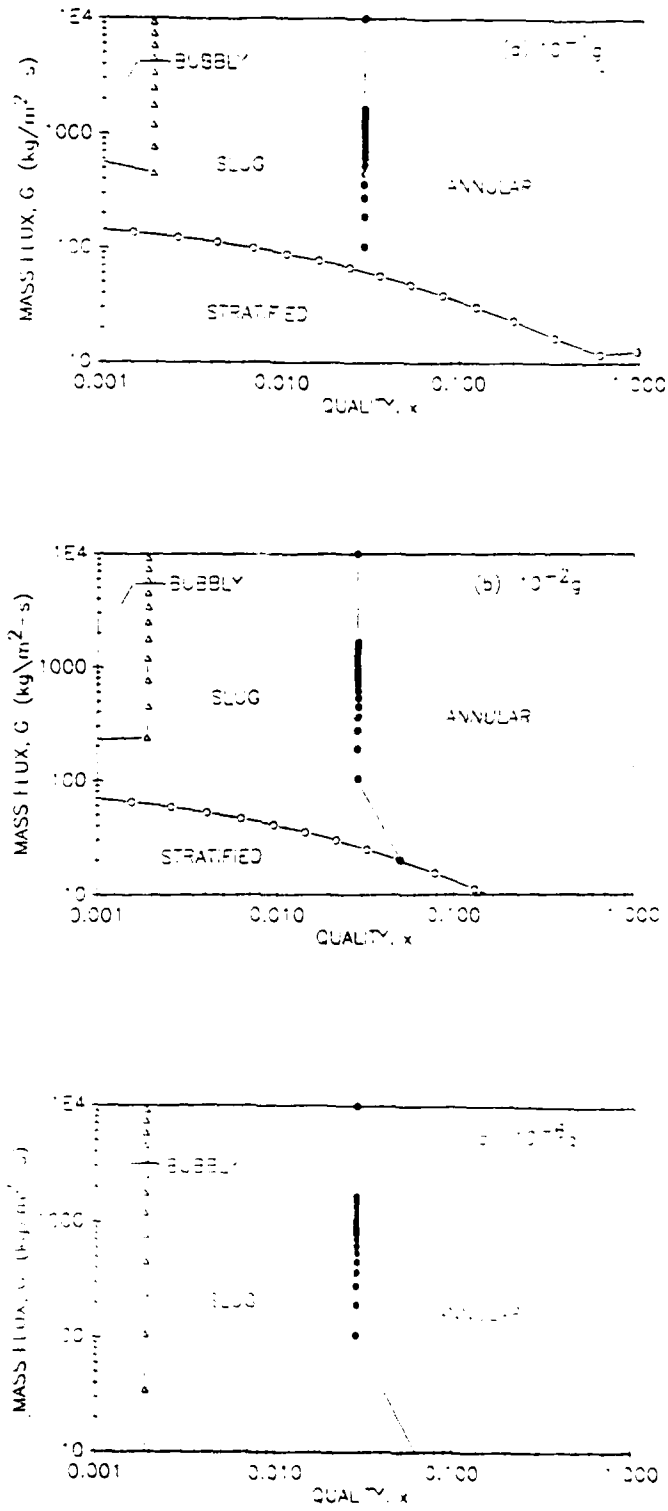

Figure 1.12. EFFECT OF GRAVITY ON FLOW REGIME MAP (MASS FLUX AND QUALITY COORDINATES)

Table 1.4 summarizes the conditions for each of the experiments compared below. Figures 1.13, 1.14, and 1.15 compare the measured flow regime data from these experiments on flow regime maps in velocity coordinates. (Since the dimensionless groups are different for each flow regime transition, it is not possible to plot data from different regimes on a single dimensionless plot.)

The comparisons with the Dukler et al. flow regime data (Figure 1.13) show quite good agreement with the mechanistic analysis methods. It should be noted that reducing the acceleration level in the mechanistic models proposed by Barnea (1986) leads to effectively the same result as the microgravity modelling methods proposed by Dukler et al. (1988). Although the starting point in each approach is different, the end result under low gravity conditions is not significantly different.

The comparisons with the Lee et al. flow regime data (Figure 1.14) also agree well with the mechanistic analysis. This is not unexpected since the test conditions are quite close to those of the Dukler et al. experiments (Table 1.4).

The limited data from the experiments by Chen (at one mass flux with varying quality) show the location of the transition from slug to annular flow regimes (Figure 1.15). Comparison with the locations of the predicted and measured transitions for the previous data (e.g. Figure 1.13) shows that the transition occurs at a liquid–to–gas velocity ratio about 5 times greater in the Chen experiment. The reason is that the density ratio (liquid to gas) is about 28 times larger in the Chen experiments (with Freon R–114 at elevated pressure) than for the other experiments (with air and water at atmospheric pressure). By analysis (Equations 1–23 and 1–2) it can be shown that the transition depends upon the square root of the density ratio. Thus, the limited experimental data confirm the scaling of the low gravity flow regime results with gas density.

With these low gravity comparisons and the previous comparisons of the mechanistic model with data at earth gravity, it is seen that the proposed design method is valid for a wide range of inclinations and gravity (acceleration) levels.

1.2 Pressure Drop

Once the flow regime is selected from the four choices according to the methods described in Section 1.1, or if the flow regime to be analyzed is known in advance, the pressure drop can then be calculated. This section describes the methods used to calculate the pressure drop in the four regimes identified:

- Annular,
- Stratified,
- Slug, and
- Bubbly.

For space systems operating under microgravity conditions, the annular flow regime is likely to be the most common. This is because the annular flow regime occurs at flow qualities above x = 0.05 to 0.1. Flow qualities approaching 1.0 take maximum advantage of the latent heat of vaporization of the liquid, which is of course the purpose in using two–phase systems in the first place. The slug and bubbly flow regimes will be less common during steady–state operation because they occur at low flow flow qualities. Slug and bubbly flows may be encountered at turndown conditions, during startup and shutdown, or in short regions of high–shear condensers and evaporators.

Table 1.4. CONDITIONS FOR MICROGRAVITY FLOW REGIME EXPERIMENTS				
EXPERIMENTER	DUKLER ET AL. (1988)		LEE (1987)	CHEN ET AL (1988)
MODE	LEAR JET	DROP TOWER	KC-135	KC-135
ACCELERATION LEVEL	$\cong 10^{-2}g$	$\cong 10^{-3}g$	$\cong 10^{-2}g$	$\cong 10^{-2}g$
FLUIDS	AIR WATER	AIR WATER	AIR OR N_2 WATER	R-114 (337 K)
PRESSURE	1 atm	1 atm	1 atm	6.3 atm
TUBE DIAMETER (mm)	12.7	9.5	6.0	15.8

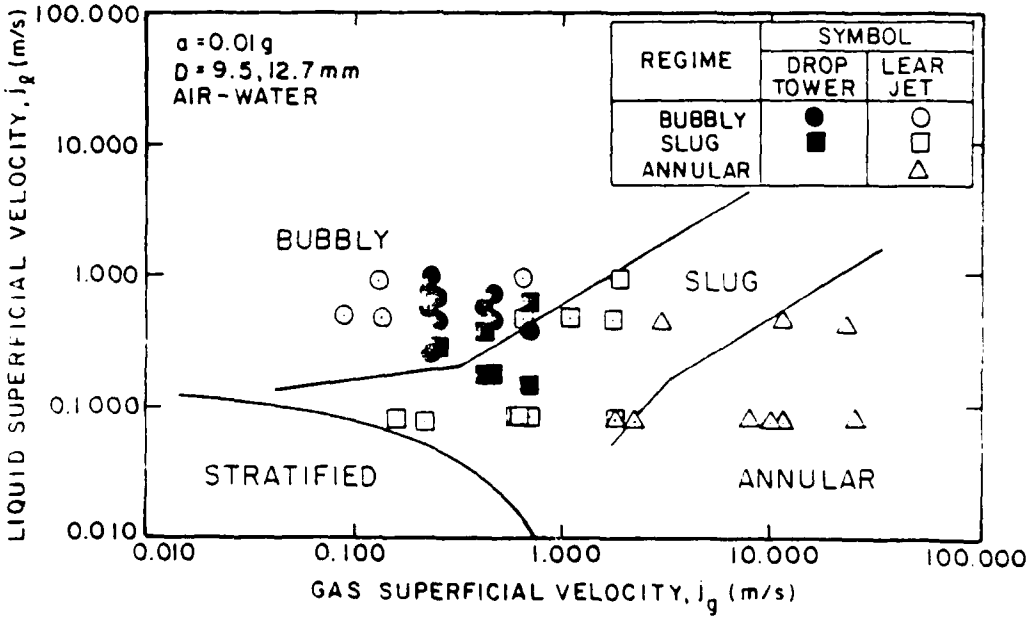

Figure 1.13. FLOW REGIME COMPARISONS FOR DUKLER ET AL. (1988) MICROGRAVITY DATA

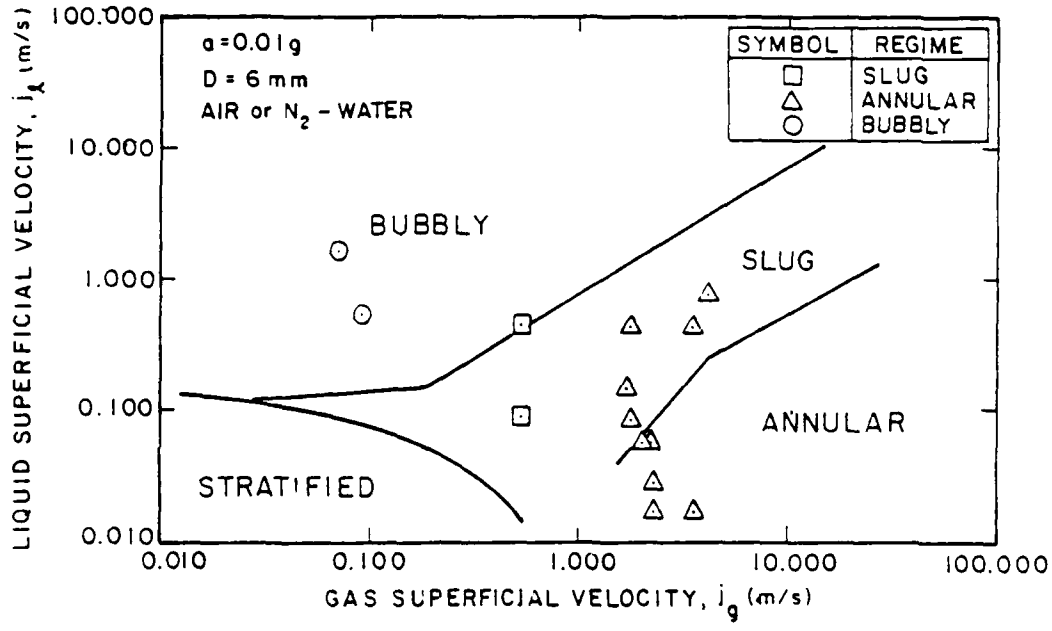

Figure 1.14. FLOW REGIME COMPARISONS FOR LEE (1987) MICROGRAVITY DATA

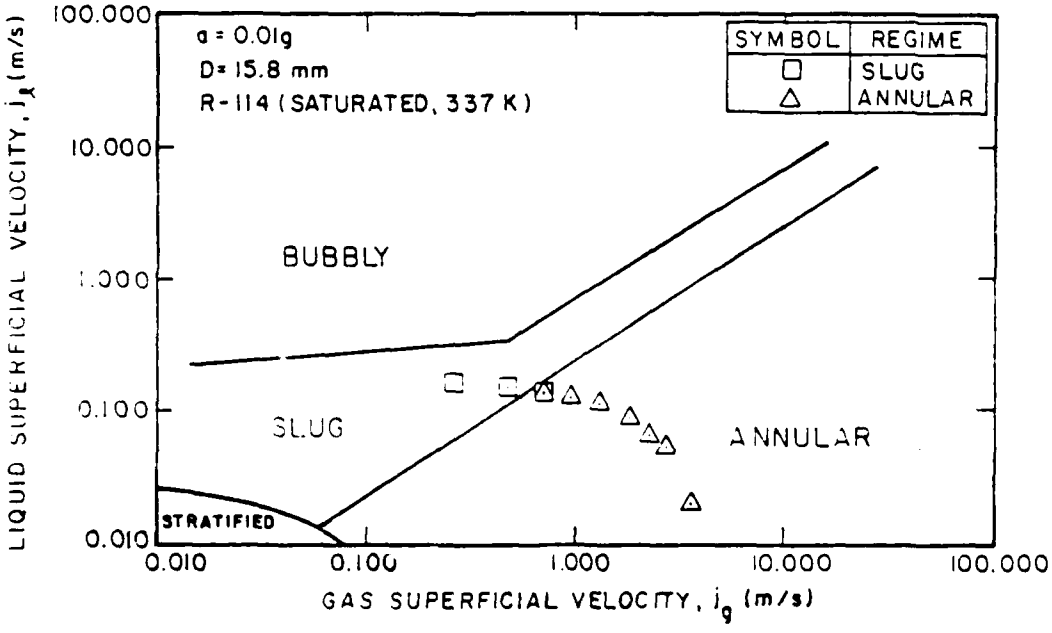

Figure 1.15. FLOW REGIME COMPARISONS FOR CHEN ET AL. (1988) MICROGRAVITY DATA

Section 1.2.1 provides a brief introduction to the recommended models and the approaches for pressure drop calculations in pipes of constant, circular cross–section.

Section 1.2.2 summarizes the information which the designer must have in hand in order to calculate the pressure drop. It also presents dimensionless parameters and graphs which can be used to quickly calculate void fraction and pressure gradient for a specific regime. This section is set up so that the user does not need to know the details of the theory or the equations. The designer approaches the calculations with knowledge of the flow regime, the phase flow rates, physical geometry, and fluid conditions. Simple dimensionless parameters are used to determine a void fraction or a two–phase multiplier on plots. The pressure gradient is then calculated by using this information in explicit equations.

Section 1.2.3 presents the basic equations for the pressure gradient calculations in each of the four flow regimes. The equations are presented in sufficient detail that the designer could recreate the dimensionless design plots presented here or incorporate the calculations into a computer routine.

Finally, Section 1.2.4 compares the pressure gradient calculations for the recommended design methods against limited data available from microgravity experiments.

1.2.1 Introduction

Summary of Recommended Models. Table 1.5 summarizes the main features of the recommended Design Manual models for pressure gradient. The model used for each of the flow regimes is mechanistic. In contrast to empirical correlations, which abound in the two–phase flow literature, the mechanistic approach considers the governing physics in the momentum balances, therefore the mechanistic models should scale well over a range of acceleration magnitudes (g–levels) and vectors.

These are not the only mechanistic modelling approaches in the literature. Generally, alternate mechanistic models can be derived at various levels of detail for each of the four flow regimes. However, the models recommended here are sufficient for design purposes.

The recommended models have been extensively compared against experimental data at earth gravity in various flow orientations ranging from vertical upward to vertical downward. In the absence of gravity, the hydrostatic component of the pressure gradient becomes negligible and the frictional component dominates, so the models reduce to the appropriate limits under microgravity conditions.

Brief Review of Modelling Approaches for Two–Phase Flow. Table 1.5 shows that the mechanistic models for the slug and the bubbly flow regimes are based upon a "drift–flux" approach and that the models for the annular and stratified flow regimes are based upon a "separated" approach. For the designer unfamiliar with the modelling of two–phase flows, the following paragraphs briefly review the basic modelling approaches which include:

- Homogeneous,
- Drift–flux, and
- Separated (or two–fluid).

Table 1.5. RECOMMENDED MODELS FOR PRESSURE DROP CALCULATIONS

FLOW REGIME	RECOMMENDED MODEL	APPROACH	KEY PARAMETER FOR UNCERTAINTY	BASELINE VALUE OF KEY PARAMETER	RANGE OF UNCERTAINTY FOR KEY PARAMETER
ANNULAR	HEWITT (1982) WALLIS (1969)	SEPARATED FLUIDS	INTERFACIAL FRICTION (f_i / f_{wg})	$1 + 75(1-\alpha)$	1 to $[1 + 75(1-\alpha)]$
STRATIFIED	TAITEL-DUKLER (1976)	SEPARATED FLUIDS	INTERFACIAL FRICTION (f_i / f_{wg})	10	1 to 10
SLUG	WALLIS (1969)	DRIFT-FLUX	DISTRIBUTION PARAMETER (C_o)	1.3	1.0 to 1.3
BUBBLY	WALLIS (1969)	DRIFT-FLUX	DISTRIBUTION PARAMETER (C_o)	1.2	1.0 to 1.2

For more detailed information, the reference texts on two-phase flow modelling by Wallis (1969) and Collier (1986) are recommended reading.

In the homogeneous modelling approach, both the liquid and vapor phases are assumed to have equal velocities. The two-phase flow is treated as if it is a single-phase flow, with mass, momentum and energy conservation equations using effective (or average) properties. The techniques of solution draw upon standard procedures, and the formulations resemble familiar ones from gas dynamics for example. The key is to define suitable average properties for the two-phase mixture. Applying this method is most appropriate when the flow is relatively uniform and well-mixed. Examples include emulsions or a dispersion of small bubbles. This approach is also useful for providing quick calculations for flow conditions which remain to be analyzed in detail. This approach is the basis for several large computer programs for steady-state and transient thermal/hydraulics (e.g. RELAP4/MOD5 and SINDA/FLUINT).

The gas and liquid phases need not necessarily move at the same velocity. The drift-flux model is a way of modifying the homogeneous approach to account for relative motion between the phases. It is less complicated than the separated flow model (see below) and can often be deduced from the separated flow model by deriving the relative motion from a force balance or similar simplifying assumption. It has found most practical use where the relative motion is due to a body force field, such as gravity. That is why it is used for the slug and bubbly flow regimes here. Equations describing the relative motions between the phases in slug and bubbly flow regimes have been well studied. Thermal/hydraulic computer codes such as RELAP4/MOD7, RETRAN, TRAC-PD2 and COBRA/TRAC use this approach in one-dimensional components.

In the separated (or two-fluid) approach the phases are treated as interwoven continua, flowing side by side and interacting with each other. Separate conservation laws (mass, momentum, and energy) are written for each phase, thus doubling the number of equations compared with the homogeneous approach. The variables describing the motion of each phase, such as velocity and pressure, are averaged over some volume or surface larger than the size of the individual entities (e.g. bubbles) but smaller than the size of the physical system.

The two–fluid model has the virtue of providing a self–consistent framework for conservation laws that, because of greater flexibility, can represent many more phenomena than homogeneous or drift–flux models. However, knowledge of the interaction terms in the equations (which are often empirical), closure laws (if they exist) and conditions for numerical convergence are still at an elementary level. Fortunately, empirical interaction terms have been derived which work well for the annular and stratified flow regimes for flow in pipes. Reasonable limits to the interaction terms can be defined in order to define the range of the uncertainty in calculating the pressure gradient and void fraction. The thermal/hydraulic codes RELAP5, ATHENA and TRAC–PF1 are examples of computer programs which use this modelling approach.

1.2.2 Dimensionless Design Calculations

This section illustrates how quick estimates of the void fraction and the pressure gradient can be performed. In addition to the flow regime, the information required in order to calculate these quantities includes:

Fluid Properties

ρ_l	Liquid phase density
ρ_g	Gas phase density
μ_l	Liquid phase viscosity
μ_g	Gas phase viscosity
σ	Surface tension

Geometry

D	Pipe diameter

Acceleration

a	Magnitude of acceleration
θ	Direction (angle between acceleration vector and the flow direction)

Flow Rates

j_l	Liquid phase volumetric flux (Q_l/A)
j_g	Gas phase volumetric flux (Q_g/A)
j	The total volumetric flux ($j_g + j_l$), and
G	The total mass flux ($\rho_g j_g + \rho_l j_l$)

See the section below for the annular, stratified, slug, or bubbly flow regime as appropriate.

Annular Flow Regime. The procedure to calculate the pressure gradient in the annular flow regime is:

- Calculate the dimensionless parameters (in Equations 1–28, 1–29, and 1–30),
- Obtain the void fraction (see Figure 1.16 or 1.18),
- Obtain the two–phase multiplier for the frictional portion of the pressure gradient (see Figure 1.17 or 1.19), and
- Calculate the total pressure gradient (Equation 1–32).

The dimensionless parameters for the annular flow regime are:

$$X = \left[\frac{\left[\frac{4C_l}{D}\right]\left[\frac{\rho_l D j_l}{\mu_l}\right]^{-n}\left[\frac{\rho_l j_l^2}{2}\right]}{\left[\frac{4C_g}{D}\right]\left[\frac{\rho_g D j_g}{\mu_g}\right]^{-m}\left[\frac{\rho_g j_g^2}{2}\right]} \right]^{0.5} \qquad (1–28)$$

$$Y = -\left[\frac{a(\rho_l - \rho_g)\cos\theta}{\left[\frac{4C_g}{D}\right]\left[\frac{\rho_g D j_g}{\mu_g}\right]^{-m}\left[\frac{\rho_g j_g^2}{2}\right]} \right] \qquad (1–29)$$

$$\rho^* = (\rho_l/\rho_g) \qquad (1–30)$$

where

X	is the dimensionless Martinelli parameter,
Y	is the dimensionless pipe inclination parameter,
ρ^*	is the dimensionless liquid/gas density ratio,
a	is the magnitude of the acceleration (m/s^2),
ρ_l	is the gas phase density (kg/m^3),
ρ_g	is the liquid phase density (kg/m^3),
j_l	is the superficial velocity of the liquid phase (m/s),
j_g	is the superficial velocity of the gas phase (m/s),
D	is the pipe diameter (m), and
θ	is the angle between the flow direction and the acceleration vector (°) (e.g. 0° is colinear, 90° is perpendicular, and 180° is opposing, corresponding to downflow, horizontal, and upflow on the ground).

Table 1.2 indicates how to determine the values of the friction factor coefficients C_l, C_g, n and m to use in Equations 1–28 and 1–29.

The dimensionless parameters in Equations 1–28 and 1–29 are the same as those calculated for the slug–to–annular flow regime, Equations 1–2 and 1–3 (in Section 1.1.2). Therefore if these parameters have been previously calculated as part of the flow regime determination, then they do not need to be recalculated here.

Figure 1.16 shows the liquid fraction $(1-\alpha)$ for the annular flow regime. The void fraction (one minus the liquid fraction) can be estimated using only the dimensionless parameters X and Y. Note that the line represented by Y = 0 would apply to microgravity conditions. (Generally, the absolute value of Y will be within the range ±10 for $a \leq 10^{-2}g$.)

A two–phase multiplier can be determined for the annular flow regime by using Figure 1.17. This two–phase multiplier is defined as the ratio of the frictional pressure gradient in the annular flow regime to the equivalent pressure gradient as if single–phase (vapor) flowed in the pipe. That is,

$$\phi_{go}^2 = \left[\frac{(dP/dz)_f}{f_{wg}\left[\frac{\rho_g j_g^2}{2}\right]}\right] \qquad (1-31)$$

where: $(dP/dz)_f$ is the frictional pressure gradient in two–phase flow,
f_{wg} is the single–phase friction factor for the gas phase alone,

and the other parameters are defined above.

Once the frictional two–phase multiplier is determined, the total pressure gradient can be calculated by:

$$(dP/dz)_t = -\phi_{go}^2\left[\frac{4f_{wg}}{D}\right]\left[\frac{\rho_g j_g^2}{2}\right] + a[(1-\alpha)\rho_l + \alpha\rho_g]\cos\theta \qquad (1-32)$$

This is the basic pressure gradient equation for a separated (two–fluid) flow. In Equation 1–32, the first term on the right hand side is the frictional component, and the second term is the hydrostatic (body force) component. The friction factor in this equation can be evaluated from a smooth–pipe model such as the Blasius equation:

$$f_{wg} = \begin{cases} 16/Re_g & \text{for laminar flow, } Re_g < 1500 \\ 0.046/Re_g^{0.2} & \text{for turbulent flow, } Re_g > 1500 \end{cases} \qquad (1-33)$$

or any other appropriate model. For example, the Colebrook friction factor equation found in standard fluid flow textbooks could be used if the value of the pipe roughness would have a significant effect on the friction factor. Note that if the g–level is near zero (microgravity) or the vector angle is 90° (horizontal pipe), then the hydrostatic term in Equation 1–32 becomes negligible and the pressure gradient is due only to the frictional term.

The equations and figures above give a best estimate for the void fraction and pressure gradient in the annular flow regime. Using Figures 1–18 and 1–19 in place of Figures 1–16 and 1–17 allows the uncertainty to be assessed. (The uncertainty specifically lies in the interfacial friction between the gas and liquid phases, as described in Section 1.2.3.) The variation in the void fraction obtained using Figure 1–16 versus 1–18 and in pressure gradient values from Figure 1–17 versus 1–19 represents the range of the uncertainty.

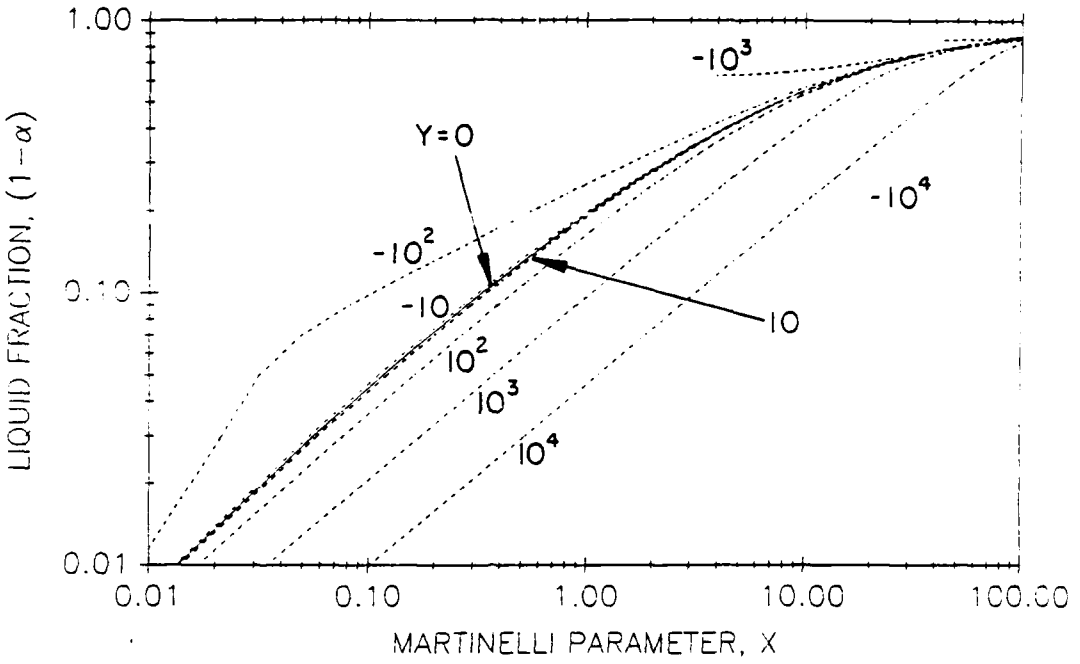

Figure 1.16. BEST-ESTIMATE VOID FRACTION FOR THE ANNULAR FLOW REGIME (WALLIS MODEL, $f_i/f_{wg} = [1 + 75(1-\alpha)]$)

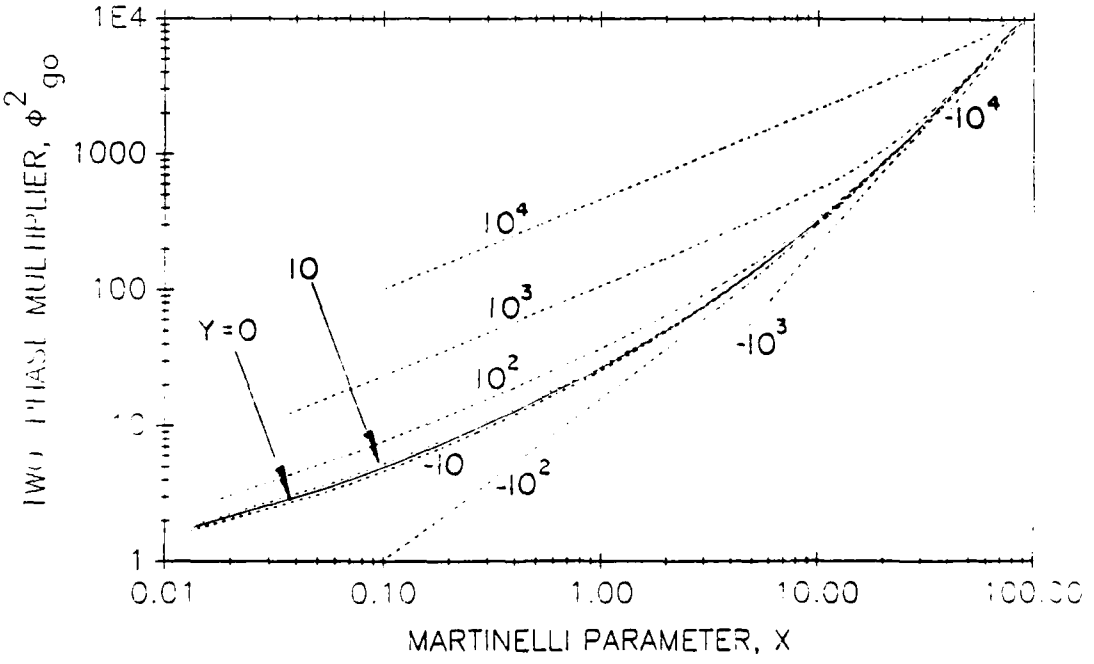

Figure 1.17. BEST-ESTIMATE TWO-PHASE MULTIPLIER FOR THE ANNULAR FLOW REGIME (WALLIS MODEL $f_i/f_{wg} = [1 + 75(1-\alpha)]$)

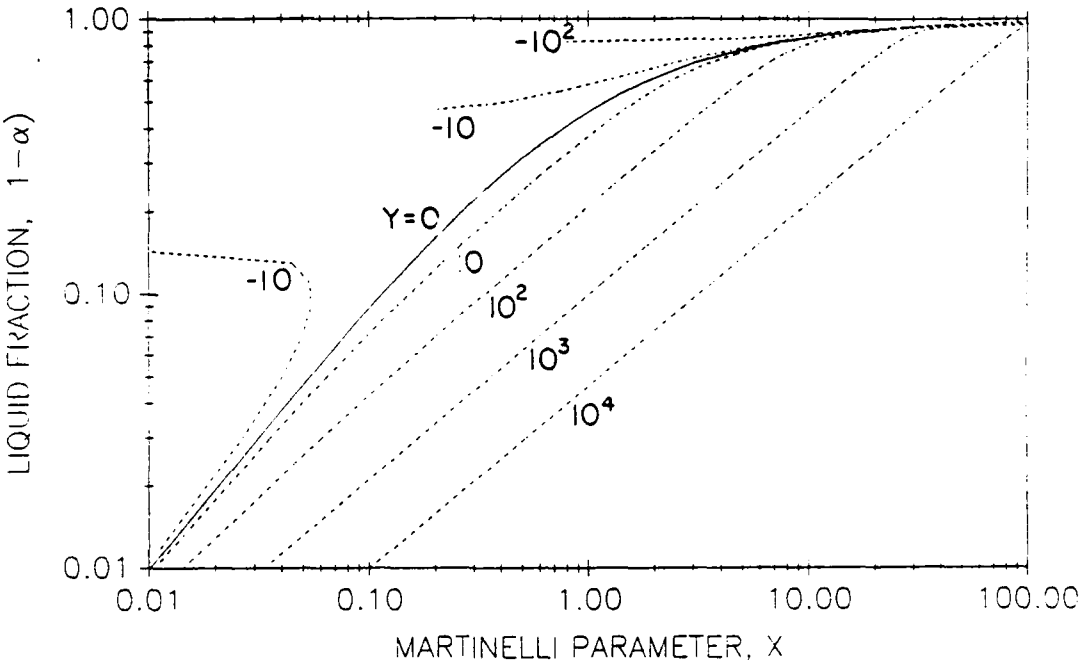

Figure 1.18. LIMITING VOID FRACTION FOR THE ANNULAR FLOW REGIME (*SMOOTH INTERFACE*; $f_i/f_{wg} = 1$)

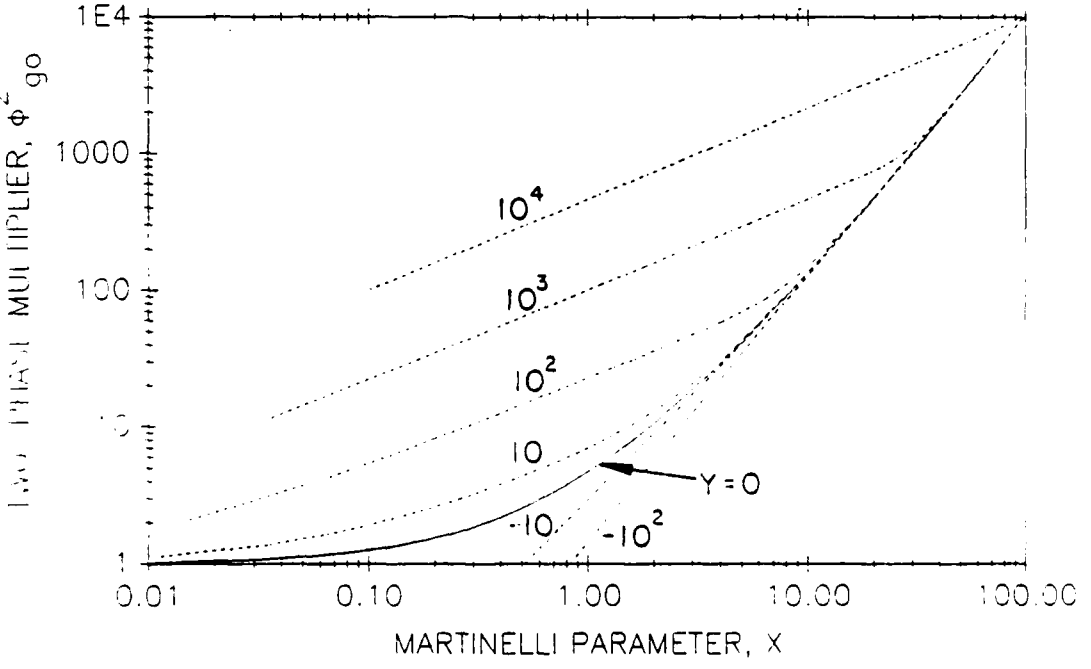

Figure 1.19. LIMITING TWO-PHASE MULTIPLIER FOR THE ANNULAR FLOW REGIME (SMOOTH INTERFACE; $f_i/f_{wg} = 1$)

Stratified Flow Regime. The procedure for calculating the void fraction and the pressure gradient in the stratified flow regime is the same as for the annular flow regime, only the figures used to estimate the void fraction and the two–phase multiplier are different. The procedure to calculate the pressure gradient in the stratified flow regime is:

- Calculate the dimensionless parameters (in Equations 1–28, 1–29, and 1–30),
- Obtain the void fraction (see Figure 1.20 or 1.22),
- Obtain the frictional two–phase multiplier (see Figure 1.21 or 1.23), and
- Calculate the total pressure gradient (Equation 1–32).

Figure 1.20 shows that the void fraction α in the stratified flow regime can be estimated using the dimensionless parameters X and Y, just as it was for the annular flow regime. Note that the line represented by Y = 0 is appropriate for microgravity conditions.

Figure 1.21 plots the two–phase multiplier for the frictional portion of the pressure gradient in the stratified flow regime. Once the two–phase multiplier is determined, Equation 1–32 can again be used to determine the actual pressure gradient in the stratified flow regime.

Using Figures 1.22 and 1.23 instead of Figures 1.20 and 1.21 allows the uncertainty in modelling the void fraction and the pressure gradient to be assessed. (The uncertainty specifically lies in the interfacial friction between the gas and liquid phases, as described in Section 1.2.3.) The uncertainty in the void fraction is given by the difference in values obtained with Figures 1.20 and 1.22. The uncertainty in the pressure gradient is given by using the values obtained from Figures 1.21 and 1.23.

Slug Flow Regime. The procedure to calculate the pressure gradient in the slug flow regime is:

- Calculate the dimensionless velocity ratio (Equation 1–34),
- Obtain the void fraction (see Figure 1–24 or 1–25), and
- Calculate the pressure gradient (Equation 1–35).

The dimensionless velocity parameter required for the slug flow regime is the ratio:

$$M = (j_f/j_g) \qquad (1–34)$$

Figure 1.24 shows that the void fraction can be estimated using this parameter. The drift–flux relationship shown here is simplified – as discussed in Section 1.2.3 – but should provide adequate estimates, especially for microgravity conditions.

Once the void fraction is determined, the total pressure gradient can be readily evaluated from the simple equation:

$$(dP/dz)_t = -\left[\frac{2f_w \rho_f j^2}{D}\right](1-\alpha) + a[(1-\alpha)\rho_f + \alpha\rho_g]\cos\theta \qquad (1–35)$$

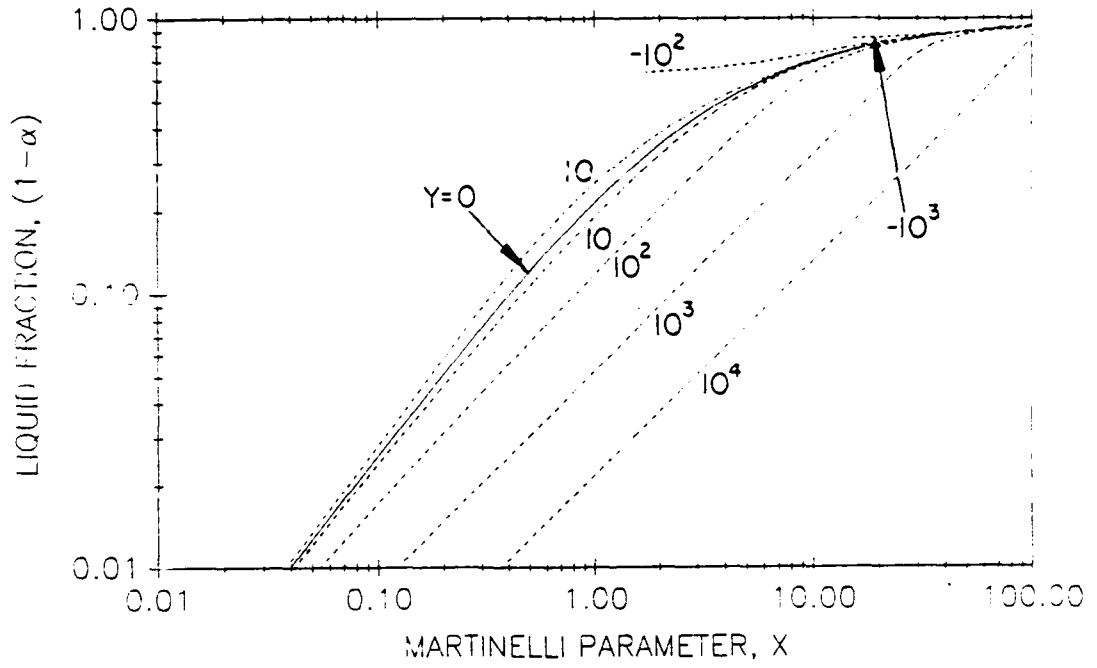

Figure 1.20. BEST-ESTIMATE VOID FRACTION FOR THE STRATIFIED FLOW REGIME (f_i/f_{wg} = 10)

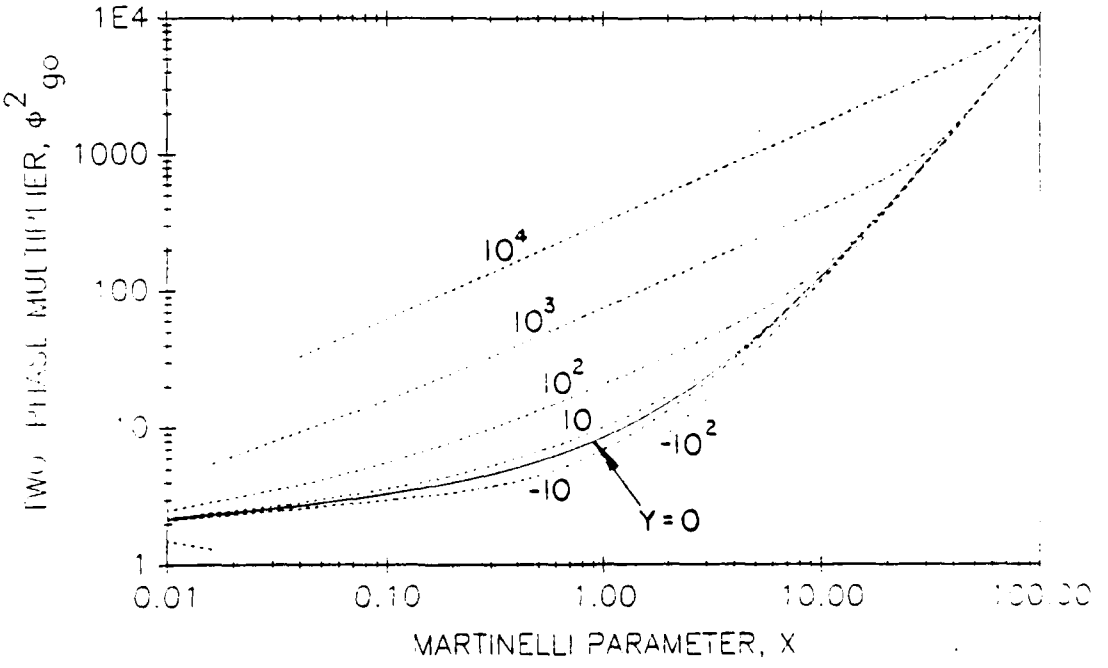

Figure 1.21. BEST-ESTIMATE TWO-PHASE MULTIPLIER FOR THE STRATIFIED FLOW REGIME (f_i/f_{wg} = 10)

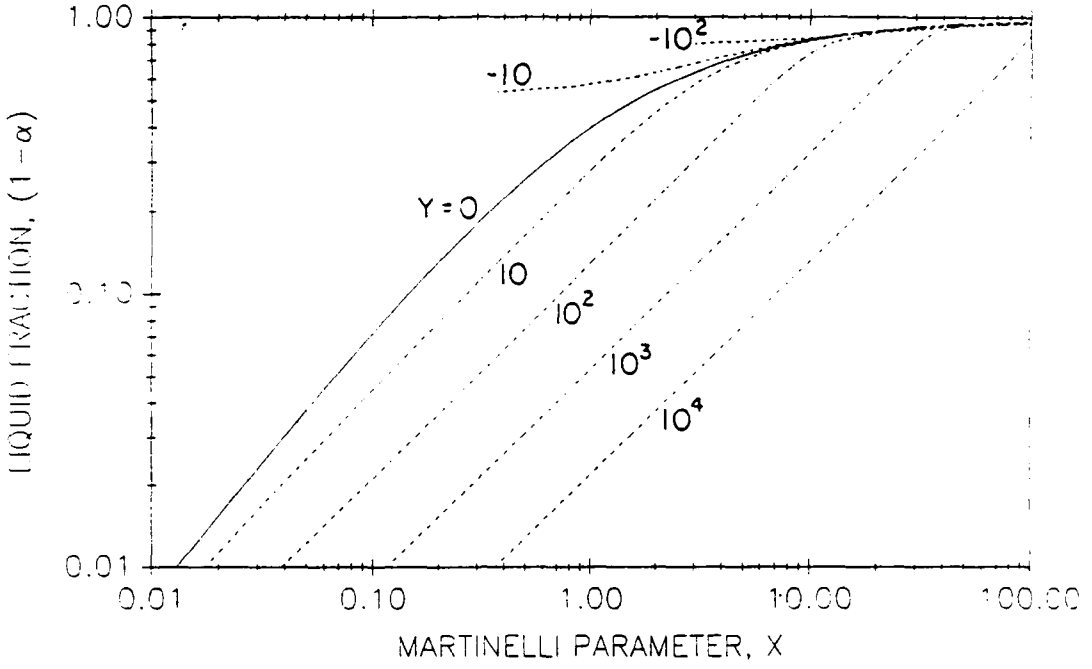

Figure 1.22. LIMITING VOID FRACTION FOR THE STRATIFIED FLOW REGIME ($f_i/f_{wg} = 1$)

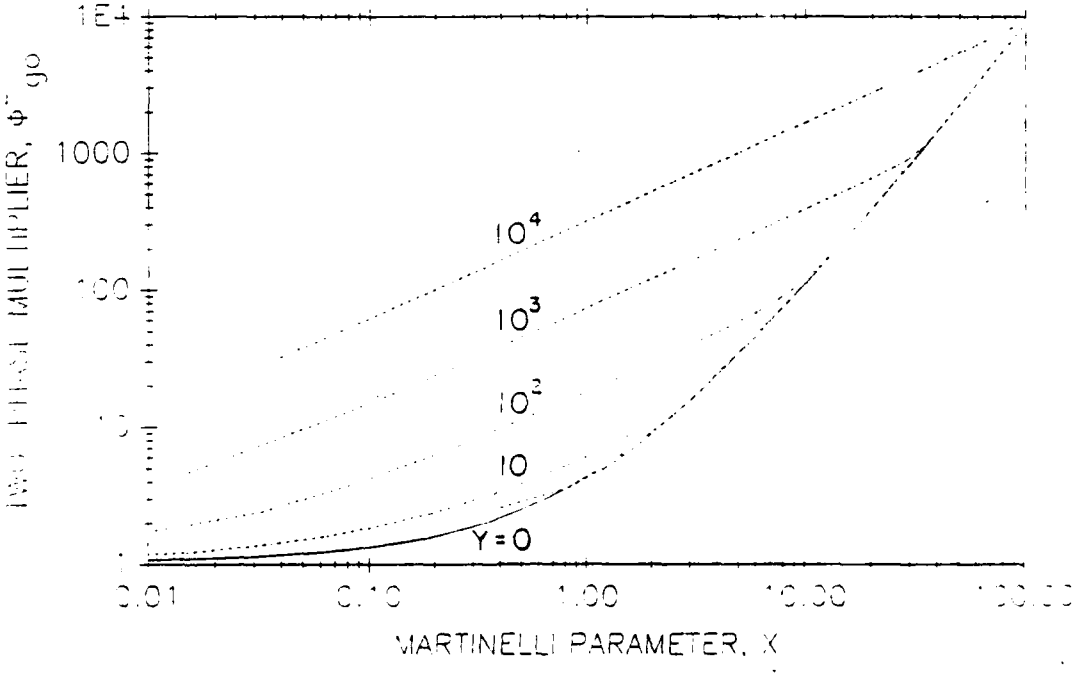

Figure 1.23. LIMITING TWO-PHASE MULTIPLIER FOR THE STRATIFIED FLOW REGIME ($f_i/f_{wg} = 1$)

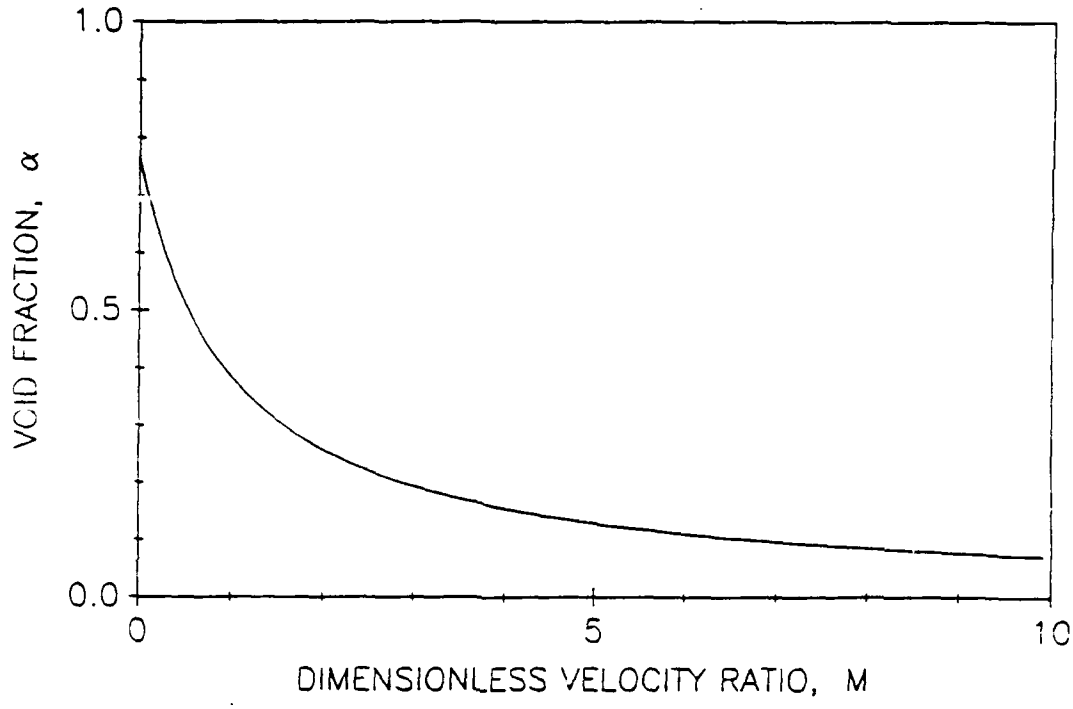

Figure 1.24. BEST-ESTIMATE VOID FRACTION FOR THE SLUG FLOW REGIME (C_o = 1.3)

The first term on the right hand side of this equation is the frictional component of the pressure gradient, and the second term is the hydrostatic component. Note that if the magnitude of the acceleration becomes small, as it would under microgravity conditions, then only the frictional component remains.

Using Figure 1.25 instead of Figure 1.24 allows the uncertainty in modelling the void fraction and the pressure gradient to be assessed. (The uncertainty specifically lies in the velocity difference between the gas and liquid phases, as described in Section 1.2.3.) Figure 1.25 represents a limiting case of homogeneous flow (see Section 1.2.1). The variation in the void fraction and pressure gradient values obtained from using Figure 1.25 in place of Figure 1.24 illustrates the range of the uncertainty. Void fraction values will be higher and hence the pressure gradient lower using the homogeneous approach. The magnitude of the effect is about 30% on the void fraction and 30% on both pressure gradient components.

Bubbly Flow Regime. The procedure to calculate the pressure gradient in the bubbly flow regime is:

- Calculate the dimensionless velocity ratio (Equation 1–34),
- Obtain the void fraction (see Figure 1.26 or 1.25), and
- Calculate the pressure gradient (Equation 1–36),

which is very similar to the procedure in the slug flow regime.

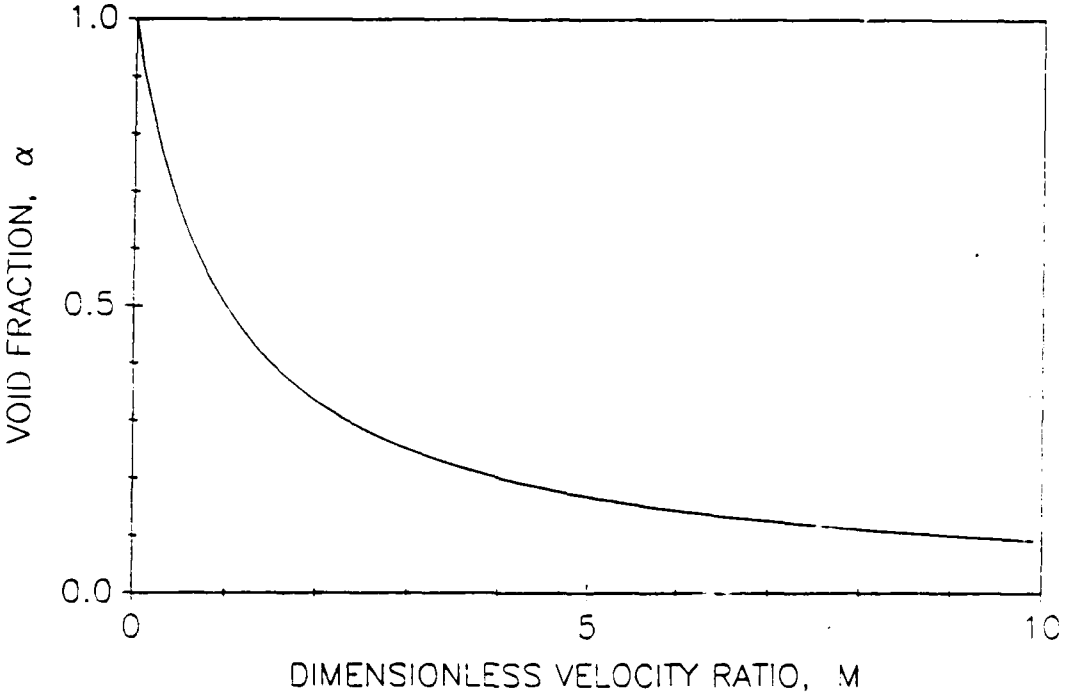

Figure 1.25. *LIMITING (HOMOGENEOUS) VOID FRACTION FOR THE SLUG OR BUBBLY FLOW* **REGIME (C_o = 1.0)**

Figure 1.26 shows that the void fraction can be estimated using the dimensionless velocity ratio M. The dimensionless velocity ratio required for the bubbly flow regime is the same as for the slug flow regime (Equation 1–34). The drift–flux relationship shown in this figure is simplified – as discussed in Section 1.2.3 – but should provide adequate estimates, especially for microgravity conditions.

Once the void fraction is determined the total pressure gradient can be calculated from

$$(dP/dz)_t = -\left[\frac{2f_{w\,l}Gj}{D}\right] + a[(1-\alpha)\rho_l + \alpha\rho_g]\cos\theta \qquad (1\text{–}36)$$

As before, the first term on the right hand side of this equation is the frictional component of the pressure gradient, and the second term is the hydrostatic component.

Using Figure 1.25 instead of Figure 1.26 allows the uncertainty in modelling the void fraction and the pressure gradient to be assessed. (The uncertainty specifically lies in the velocity difference between the gas and liquid phases, as described in Section 1.2.3.) Figure 1.25 represents the limiting case of homogeneous flow (see Section 1.2.1). The variation in the void fraction and pressure gradient values obtained from using Figure 1.25 in place of Figure 1.26 illustrates the range of the uncertainty. The magnitude of the effect is about 20% in the void fraction. This does not affect the frictional component of the pressure gradient at all, but does affect the hydrostatic component by 20%.

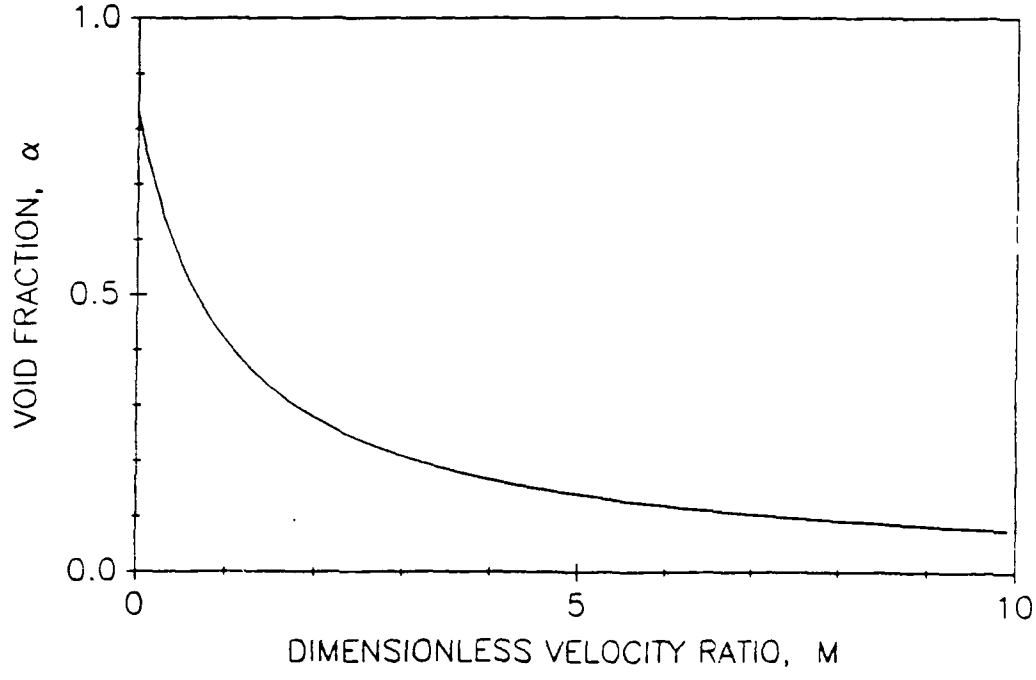

Figure 1.26. BEST–ESTIMATE VOID FRACTION FOR THE BUBBLY FLOW REGIME (C_o = 1.2)

1.2.3 Equations for Pressure Drop Calculations

This section presents the exact analytical equations used to calculate the void fraction and the pressure gradient in each of the four flow regimes. Additional design maps with alternate values of the key modelling parameters can be generated if desired using the equations presented in this section.

Annular Flow Regime. Derivation of the basic model for the annular flow regime is discussed in the references by Wallis (1969) and Hewitt (1982). In the separated fluid approach used in this regime, individual momentum equations are written for balances on the gas and liquid phases. These two momentum equations are then subtracted (to eliminate the pressure gradient) and, using the definitions of the dimensionless parameters X and Y, the following equation

$$X^2 = \left[\frac{(f_f/f_{wg})(1-\alpha)^2}{\alpha^{2.5}}\right] - (1-\alpha)^3\, Y \qquad (1\text{–}37)$$

is obtained to relate the void fraction α and the dimensionless parameters X and Y.

The parameter (f_i/f_{wg}) in Equation 1–37 represents the interfacial friction between the gas and the liquid phases. For the purposes of this Design Manual, the empirical relationship proposed by Wallis (1969)·

$$(f_i/f_{wg}) = [1 + 75(1 - \alpha)] \qquad (1–38)$$

is recommended. This relationship is also used by Dukler (1988) in his analysis of flow regimes in microgravity. Figure 1.16, the void fraction map for the annular flow regime, has been generated using Equation 1–38 in Equation 1–37. Various models for this relationship appear in the literature for the annular flow regime, but the Wallis (1969) model appears to be a reasonable limit for most data.

The interfacial friction is the key modelling parameter in the annular flow regime. The major uncertainties in the modelling are represented by it. The minimum value of this parameter would be unity ($f_i/f_{wg} = 1$), representing a smooth interface between the gas and the liquid phases. Figure 1.18 is based on this limiting value of the key parameter. Minimum values of the void fraction are obtained using this limit.

The "separated model" equation for the total pressure gradient in the annular flow regime is:

$$(dP/dz)_t = -\left[\frac{2 f_{w\,l}\rho_l j_l^2}{D(1 - \alpha)^2}\right] + a[(1 - \alpha)\rho_l - \alpha\rho_g]\cos\theta \qquad (1–39)$$

which is obtained by adding the momentum equations for each phase in order to eliminate the interfacial friction factor ratio. The first term on the right hand side of this equation represents the frictional portion of the pressure gradient. This equation could be evaluated directly from known information once the void fraction is calculated.

For convenience in this Manual, a two–phase multiplier for the frictional portion of the pressure gradient is defined as

$$\phi_{go}^2 = \frac{X^2}{(1 - \alpha)^2} \qquad (1–40)$$

Since the void fraction is related to the parameters X and Y by Equation 1–37, the two–phase multiplier can be plotted as a function of the same parameters. Figures 1.17 and 1.19 have been prepared using the Wallis model $[1 + 75(1 - \alpha)]$ and the limiting value of 1.0 for the interfacial friction, respectively. The pressure gradient is then evaluated using Equation 1–32.

More complicated models could be written for the annular flow regime, involving liquid droplet entrainment and deposition. For most cases of interest to thermal management systems, liquid droplet entrainment should not be significant. The effect of liquid droplet entrainment on the pressure gradient is relatively small in any event.

Stratified Flow Regime. The approach to the model for the stratified flow regime is similar to that used for the annular regime. Taitel and Dukler (1976) first developed this approach for the stratified flow regime, although the form used was first proposed by Lockhart

and Martinelli in the 1950s. Separate momentum equations are written for the gas and liquid phases as before. The main difference compared with the annular flow model is in the geometric parameters which describe the interfaces between the wall and the fluids and between the liquid and vapor phases. The void fraction relationship for the stratified flow regime is:

$$X^2 = \frac{[(U_g^* D_g^*)^{-m}(U_g^*)^2]\left[\frac{S_g^*}{A_g^*} + \left[\frac{f_i}{f_{wg}}\right]\left[\frac{S_i^*}{A_l^*} + \frac{S_i^*}{A_g^*}\right]\right] - 4Y}{[U_l^* D_l^*]^{-n}(U_l^*)^2(S_l^*/A_l^*)} \qquad (1\text{–}41)$$

Where the dimensionless parameters X and Y have the usual definitions. The "starred" parameters in Equation 1–41 are the geometric parameters for the stratified flow regime. Table 1.3 summarizes these parameters as a function of the dimensionless liquid level and shows how they are related to the void fraction.

The values of the parameters n and m are determined from the Reynolds numbers for the liquid and gas phases. Table 1.2 provides the equations necessary to determine these values.

Just as in the annular flow regime, the parameter (f_i/f_{wg}) represents the interfacial friction, the key modelling parameter. Various empirical correlations have been proposed for this relationship in the stratified flow regime. In this Design Manual a constant value of $(f_i/f_{wg}) = 10$ is recommended. This selection is based upon extensive work by the authors reviewing alternative modelling approaches and specific models representing the interfacial shear in stratified flows at high gas densities.

The void fraction relationship in Figure 1.20 represents Equation 1–41 using the recommended value for the interfacial friction. Values of $n = m = 0.2$ have also been used (assuming turbulent flow in both phases). Other void fraction relationships for the stratified flow regime could be derived using alternative models for the interfacial friction. Figure 1.22 is for the limiting case of a smooth gas–liquid interface. This limit gives the minimum void fraction. It is also the limit used by Taitel and Dukler in the original derivation of this model; the model has been modified here to accommodate alternative interfacial friction models.

The dimensional equation for the total pressure gradient in the stratified flow regime is:

$$(dP/dz)_t = -\left[\frac{2f_{wl}\rho_l j_l^2}{\pi D}\right](U_l^*)^2(S_l^*) - \left[\frac{2f_{wg}\rho_g j_g^2}{\pi D}\right](U_g^*)^2(S_g^*) \qquad (1\text{–}42)$$

$$+ a[(1-\alpha)\rho_l + \alpha\rho_g]\cos\theta$$

which is obtained by adding the momentum equations for each phase in order to eliminate the interfacial shear ratio. The first two terms on the right hand side of this equation represent the frictional portion of the pressure gradient. This equation could be evaluated directly from known information once the void fraction is calculated.

For convenience, a two–phase multiplier for the frictional portion of the pressure gradient can be defined. For the stratified flow regime, this multiplier has the form:

$$\phi_{go}^2 = \left[\frac{1}{\pi}\right]\left[X^2(U_l^*)^2(S_l^*) + (U_g^*)^2(S_g^*)\right] \qquad (1–43)$$

Since the dimensionless geometric parameters U_l^*, U_g^*, S_l^*, and S_g^* are related to the void fraction, which in turn is a function of the parameters X and Y by Equation 1–41, this allows the two–phase multiplier to be plotted as a function of the X and Y parameters, just as for the annular flow regime. Figures 1.21 and 1.23 have been prepared using the recommended interfacial shear model $(f_i/f_{wg}) = 10$ and the limiting value of unity for the interfacial friction, respectively.

Defining the two–phase multipliers for the annular and the stratified flow regimes in the manner shown allows a comparison of the void fractions and the pressure drops in the two regimes. Comparison of Figures 1.16 and 1.20 shows that the void fraction tends to be somewhat greater in the stratified flow regime. Comparison of Figures 1.17 and 1.21 shows that the two–phase multiplier, and hence the frictional pressure gradient, tends to be significantly greater in the annular flow regime. (This is due to the increased interfacial area in the annular flow regime.)

More complicated models could be written for the stratified flow regime, involving liquid droplet entrainment and deposition. For most cases of interest to thermal management systems, liquid droplet entrainment would not be significant. The effect of liquid droplet entrainment on the pressure gradient is relatively small in any event.

Slug Flow Regime. The model for void fraction in the slug flow regime is based upon a drift–flux approach, which requires an empirical relationship between the void fraction and the flow rates of each phase. The basic modelling approach for the pressure gradient is a homogeneous one, as suggested by Wallis (1969).

The drift--flux equation recommended for the slug flow regime has the form:

$$\frac{j_g}{\alpha} = C_o(j_g + j_l) + k\left[\frac{aD(\rho_l - \rho_g)}{\rho_l}\right]^{0.5} \qquad (1–44)$$

where

C_o is a constant typically near 1.3, and
k is a constant whose value is given in Table 1.6, and

the other parameters have been defined previously. The values in Table 1.6 have been selected based upon our review of almost two dozen experiments.

Equation 1–44 can be rearranged in the form

$$\left[\frac{j_l}{j_g}\right] = \left[\frac{1}{C_o\alpha_c} - 1\right] - k\left[\frac{\rho_g}{\rho_l}\right]^{0.5}\frac{[aD(\rho_l - \rho_g)]^{0.5}}{j_g\rho_g{}^{0.5}} \qquad (1–45)$$

Using the definitions of the dimensionless parameters M, ρ^*, and F_g (Equations 1–6, 1–7, and 1–1), Equation 1–45 can be written in dimensionless form as

$$M = \left[\frac{1}{C_o\alpha} - 1\right] - \frac{k}{F_g}\left[\frac{1}{\rho^*}\right]^{0.5} \qquad (1\text{–}46)$$

or rearranging the equation to solve for the void fraction

$$\alpha = \frac{1}{C_o(1 + M) + (k/F_g\rho^{*0.5})} \qquad (1\text{–}47)$$

Figure 1.24 plots the void fraction relationship in Equation 1–47 using the recommended value $C_o = 1.3$ with the approximation that $k = 0$ under all conditions. The contribution of the term with the constant k in Equation 1–47 is generally small, so the approximation with $k = 0$ is valid. The approximation should be very good for microgravity conditions because this term also becomes negligible when the magnitude of the acceleration approaches zero.

The key uncertainty in the drift–flux relationship of Equation 1–47 is the value of the parameter C_o. The limiting case of $C_o = 1.0$ with $k = 0$ represents a homogeneous flow, i.e. no drift–flux. This is the relationship plotted in Figure 1.25. This limit maximizes the void fraction in the slug flow regime.

The basic homogeneous form of the equation for pressure gradient is:

$$(dP/dz)_t = -\left[\frac{2f_{w\,l}\rho_m j^2}{D}\right] + a[(1 - \alpha)\rho_l + \alpha\rho_g]\cos\theta \qquad (1\text{–}48)$$

where ρ_m is the homogeneous mixture density.

Table 1.6. DRIFT–FLUX PARAMETERS FOR THE SLUG FLOW REGIME

ANGLE θ BETWEEN FLOW DIRECTION AND ACCELERATION VECTOR (°)	DISTRIBUTION PARAMETER C_o	k
$90° \le \theta \le 180°$	1.3	0.35
$\theta = 90°$	1.3	0
$0° < \theta \le 90°$	1.0	− 0.35

Since the gas density is generally much smaller than the liquid density, the simple approximation

$$\rho_m \equiv (1-\alpha)\rho_l \tag{1–49}$$

can be used to obtain a slightly simpler form of the equation, which is

$$(dP/dz)_t = -\left[\frac{2f_{wl}\rho_l j^2}{D}\right](1-\alpha) + a[(1-\alpha)\rho_l + \alpha\rho_g]\cos\theta \tag{1–50}$$

This is the pressure gradient equation solved in the slug flow regime.

More complicated models could be written for the slug flow regime also. These models would involve asymmetric gas bubbles or corrections for long gas bubbles. Models with as many as 17 parameters have been developed (Fernandes, 1982). For microgravity flow conditions, these detailed models are believed to be unnecessary.

Bubbly Flow Regime. The drift–flux approach is also used to calculate the void fraction in the bubbly flow regime. Similarly to the slug flow regime, the equation for the pressure gradient is a homogeneous one, as suggested by Wallis (1969). The empirical drift–flux model used with the pressure gradient equation is based on extensive research.

The drift–flux equation recommended for the bubbly flow regime has the form

$$\frac{j_g}{\alpha} = C_o(j_g + j_l) + k\left[\frac{a\sigma(\rho_l - \rho_g)}{\rho_l^2}\right]^{0.25} \tag{1–51}$$

where

C_o is a constant typically near 1.2,
k is a constant whose value is given in Table 1.7,

and the other parameters have been defined previously. The values of C_o and k are based upon work by Mishima and Ishii (1984), Harmathy (1960), Zuber and Hench (1962), and Martin (1973) for swarms of bubbles flowing in a liquid.

Equation 1–51 can be rearranged to obtain

$$\left[\frac{j_l}{j_g}\right] = \left[\frac{1}{C_o\alpha} - 1\right] - k\left[\frac{\rho_g}{\rho_l}\right]^{0.5}\frac{[a\sigma(\rho_l - \rho_g)]^{0.25}}{j_g\rho_g^{0.5}} \tag{1–52}$$

Using the dimensionless parameters M, ρ^*, and K_g defined previously (Equations 1–6, 1–7 and 1–8), Equation 1–52 can be written in the dimensionless form

$$M = \left[\frac{1}{C_o\alpha} - 1\right] - \frac{k}{K_g}\left[\frac{1}{\rho^*}\right]^{0.5} \tag{1–53}$$

and rearranging to solve for the void fraction gives

$$\alpha = \frac{1}{C_o(1 + M) + (k/K_g\rho^{*0.5})} \qquad (1-54)$$

Figure 1.26 plots the void fraction relationship in Equation 1–54 using the recommended value $C_o = 1.2$ with the approximation that $k = 0$ under all conditions. For the high phase velocities necessary to cause bubbly flow in pipes, the contribution of the term with the constant k in Equation 1–54 is small, so the approximation with $k = 0$ is valid. The approximation should be very good for microgravity conditions because this term also becomes negligible when the magnitude of the acceleration is very small.

The key uncertainty in the drift–flux relationship of Equation 1–54 is the value of the parameter C_o. The limiting case of $C_o = 1.0$ (with $k = 0$) represents a homogeneous flow, i.e. no drift–flux. This is the relationship plotted in Figure 1.25. This limit maximizes the void fraction in the bubbly (or slug) flow regime.

Equation 1–48 is the homogeneous equation for the total pressure gradient. For the bubbly flow regime, this equation can be modified using the approximation that

$$\rho_m j \equiv (\rho_g j_g + \rho_l j_l) = G \qquad (1-55)$$

in order to obtain the pressure gradient equation in the form

$$(dP/dz)_t = -\left[\frac{2f_{w\,l}Gj}{D}\right] + a[(1-\alpha)\rho_l + \alpha\rho_g]\cos\theta \qquad (1-56)$$

which is the equation solved in the bubbly flow regime.

Table 1.7. DRIFT–FLUX PARAMETERS FOR THE BUBBLY FLOW REGIME

ANGLE θ BETWEEN FLOW DIRECTION AND ACCELERATION VECTOR (°)	DISTRIBUTION PARAMETER C_o	k
$90° \le \theta \le 180°$	1.2	1.4
$\theta = 90°$	1.2	0
$0° < \theta \le 90°$	1.0	0

More complicated models could be written for the bubbly flow regime, involving determining the sizes of vapor bubbles and calculating the interfacial forces on gas bubbles. For bubbly flow under most conditions, the simple drift–flux model is adequate.

1.2.4 Validation with Microgravity Pressure Drop Data

The purpose of this section is to demonstrate that the mechanistic pressure drop models can be used for microgravity conditions. Data obtained under microgravity conditions are presently available from Chen et al. (1989).

Additional experiments are planned by NASA Lewis Research Center (U. of Houston) and the Weapons Laboratory (Creare and Foster–Miller); however, no data have yet been produced by these experiments. All represent experiments on aircraft, where acceleration levels of 10^{-2}g can be achieved for periods of approximately 30 seconds as the aircraft negotiates a parabolic trajectory. No pressure drop data are available for long–term microgravity conditions.

Table 1.4 summarizes the conditions for the Chen experiments with Freon R–114. Experiments were performed at a mass flux of approximately 40 kg/m^2–s in a tube 15.8 mm in diameter and 1830 mm long. Figures 1.27 and 1.28 compare the measured pressure drop data from these experiments with calculations from the models. The measured pressure drops are in the range of 0.07 to 1.5 kPa (0.01 to 0.22 psi). Note that the reported accuracy of the transducer used to make the pressure drop measurements is 0.33 kPa (0.05 psi) so that some of the smaller pressure drops reported have a large uncertainty.

In ground tests, the two–phase test section was primarily in the stratified flow regime. Figure 1.27 shows that the calculated pressure drops in the stratified flow regime are in good agreement with measured pressure drops at the larger, more accurate values. Using the model for the annular flow regime would overpredict the pressure drop by a factor of three or more for the stratified data.

Figure 1.28 shows that the pressure drop data in the annular flow regime are bounded by the models suggested in this Design Manual. Using the Wallis model for interfacial shear (see Figures 1.16 and 1.17), the pressure drop is overpredicted by about 50%. Using the limiting case of a smooth interface (see Figures 1.17 and 1.18) the pressure drop is underpredicted by about a factor of two. Chen et al. suggested a modified interfacial shear relationship to match their experimental data. Figure 1.28 also shows that this model succeeds in matching the data, though the difference between this model and the Wallis model is within the accuracy of the pressure measurements.

With these low gravity comparisons and numerous previous comparisons of the mechanistic models with data at earth gravity, the proposed design method appears to be valid for the annular flow regime in microgravity. Additional microgravity data in the other flow regimes are needed in order to validate the models. The experiments in progress by the University of Houston and the Weapons Laboratory should supply the needed data.

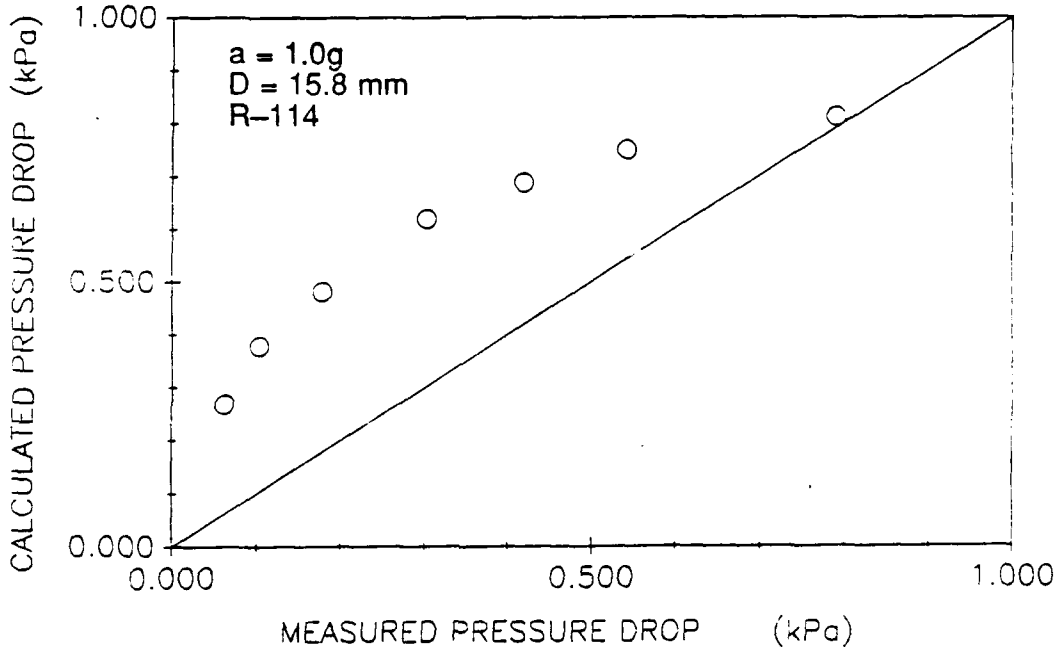

Figure 1.27. COMPARISON BETWEEN GROUND TEST DATA (CHEN ET AL.) AND THE PRESSURE DROP MODEL FOR THE STRATIFIED FLOW REGIME

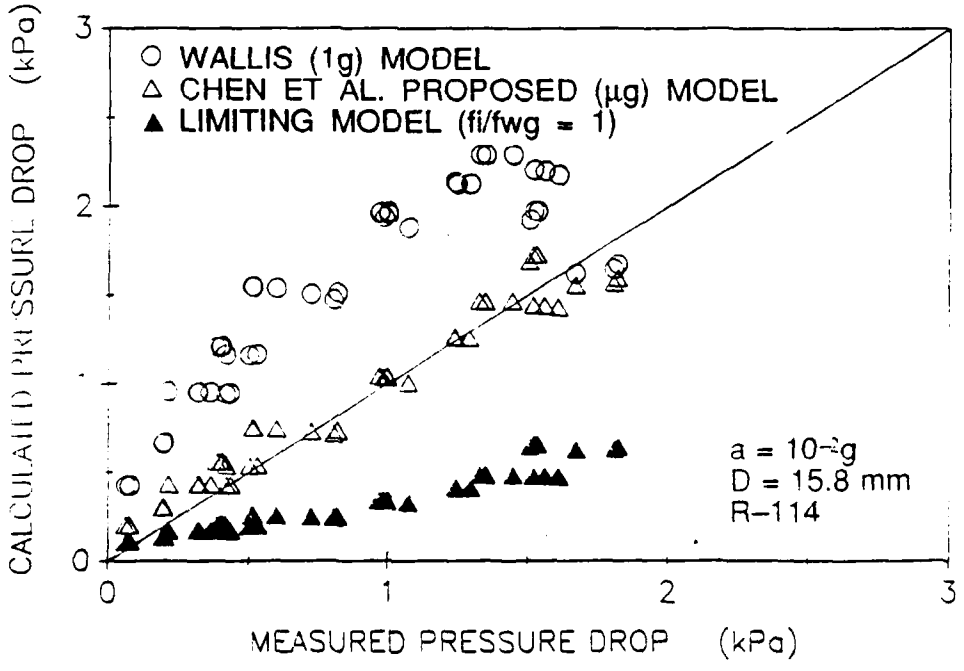

Figure 1.28. COMPARISON BETWEEN MICROGRAVITY TEST DATA (CHEN ET AL.) AND THE PRESSURE DROP MODEL FOR THE ANNULAR FLOW REGIME

1.3 References

Barnea, D., Shoham, O. and Taitel, Y.; *Flow Pattern Transition for Downward Inclined Two Phase Flow: Horizontal to Vertical*; Chemical Engrg. Science, 37(5), 1982, pp. 735–746.

Barnea, D.; *Transition from Annular Flow and From Dispersed Bubble Flow--Unified Models for the Whole Range of Pipe Inclinations*; Int. J. Multiphase Flow, 12(5), 1986, pp. 733–744.

Chen, I.–Y. and Downing, R.S.; *A Reduced Gravity Flight Experiment: Observed Flow Regimes and Pressure Drops of Vapor and Liquid Flow in Adiabatic Piping*; AIChE Symposium Series, Volume 84(26), 1988, pp. 203–216.

Chen, I.–Y., Downing, R.S., Keshock, E. and Al–Sharif, M.M.; *An Experimental Study and Prediction of a Two-Phase Pressure Drop in Microgravity*; Paper 89–0074. Presented at the AIAA 27th Aerospace Science Meeting, Reno, Nevada, January 9–12, 1989.

Collier, J.G.; Convective Boiling and Condensation; McGraw–Hill Book Company, New York, New York, 2nd Ed., 1986.

Dukler, A.E., Fabre, J.A., McQuillen, J.B. and Vernon, R.; *Gas-Liquid Flow at Microgravity Conditions: Flow Patterns and Their Transitions*; Int. J. Multiphase Flow, 14(4), 1988, pp. 389–400.

Fernandes, R.C.; *Hydrodynamic Model for Gas-Liquid Slug Flow in Vertical Tubes*; AIChE J., 29(6), Nov. 1983, pp. 981–989.

Kachnik, L., Lee, D., Best, F. and Faget, N.; *A Microgravity Boiling and Convective Condensation Experiment*; ASME 87–WA/HT–12, Presented at ASME Winter Annual Meeting, Boston, Massachusetts, December 13–18, 1987.

Heppner, D.B., King, C.D. and Littles, J.W.; *Zero-G Experiments in Two-Phase Fluid Flow Regimes*; ASME 75–ENAS–24, 1975.

Heppner, D.B., King, C.D. and Littles, J.W.; *Aircraft Flight Testing of Fluids in Zero Gravity Experiments*; General Dynamics Report CASD NAS–74–054, 1978.

Hewitt, G.R.; Flow Regimes: Chapter 2.1, Handbook of Multiphase Systems, G. Hetsroni, ed., Washington D.C., Hemisphere Publishing Corp., 1982.

Laurinat, J.E., Hanratty, T.J. and Dallman, J.C.; *Pressure Drop and Film Height Measurements for Annular Gas-Liquid Flow*; Int. J. Multiphase Flow, 10(3), June 1984, pp. 341–356.

Lee, D.; *Thermohydraulic and Flow Regime Analysis for Condensing Two Phase Flow in a Microgravity Environment*; PhD Thesis, Texas A&M University, Nuclear Engineering Department, December, 1987.

Mishima, K. and Ishii, M.; *Flow Regime Transition Criteria for Upward Two-Phase Flow in Vertical Tubes*; Int. J. Heat Mass Transfer, 27(5), May 1984, pp. 723–738.

Reddy Karri, S.B. and Mathur, V.K.; *Two-Phase Flow Regime Map Predictions Under Microgravity*; R&D Notes, AIChE J., 34(1), January, 1988.

Revankar, S.T.; *Flow Regime Map for Gas-Liquid Flow in Channel at Microgravity Condition*; Sixth Symposium on Space Nuclear Power Systems, Transactions, Albuquerque, New Mexico, CONF–890103, January 8–12, 1989.

Taitel, Y. and Dukler, A.E.; *A Model for Predicting Flow Regime Transitions in Horizontal and Near Horizontal Gas-Liquid Flow*; AIChE J., 22(1), January, 1976, pp. 47–55.

Taitel, Y. and Dukler, A.E.; *Brief Communication - A Theoretical Approach to the Lockhart-Martinelli Correlation for Stratified Flow*; Int. J. Multiphase Flow, Vol. 2, 1976, pp. 591–595.

Taitel, Y., Barnea, D. and Dukler, A.E.; *Modeling Flow Pattern Transitions for Steady* Upward Gas–Liquid Flow in Vertical Tubes; AIChE J., 26(3), May 1980, pp. 345–354.

Wallis, G.B.; One–Dimensional Two–Phase Flow; McGraw–Hill Book Company, New York, New York, 1969.

Zuber, N. and Findlay, J.A.; *Average Volumetric Concentration in Two-Phase Flow Systems*; J. Heat Transfer, Trans. ASME, 87(4), November, 1965, pp. 453–468.

2 EVAPORATORS: Forced Convection Dominated Tubes

Evaporators are the points of contact between two–phase thermal management systems and spacecraft components (computers, the environment, payloads, power sources, sensors, etc.) which produce heat and therefore require cooling. Heat is absorbed from spacecraft components into the thermal management system by vaporizing the working fluid, hence the name "evaporator." There are two major categories of evaporators for space thermal management systems: those which produce a two–phase mixture of vapor and liquid and those which produce only single–phase vapor. Designs for forced convection evaporators include straight and curved flow channels. In curved tubes ("swirl" flow), heat transfer can be enhanced by centrifugal forces at the expense of larger pressure drops than straight tubes. Devices to produce single–phase vapor generally use capillary–controlled evaporators or evaporate extremely thin liquid films. The goal of microgravity evaporator design is to provide heat removal in a small, light–weight component which operates independently of spacecraft acceleration and which does not require excessive pumping power.

This section provides basic relationships between coolant properties, evaporator geometry, fluid flow, temperature, heat transfer and pressure losses for the evaporator concept with a straight tube of circular cross–section where boiling (vaporization) is dominated by forced–convection. This topic was selected for this Design Manual because it is the most basic approach and is therefore the starting point for understanding alternate concepts. Some of the more exotic two–phase evaporator concepts (such as swirl evaporators) are simple variations on the straight tube concept. Furthermore, the approach described here is used in microgravity evaporator experiments, and data will soon be available for comparison with the design models.

For microgravity applications these evaporators should be designed so that heat transfer is dominated by forced convection. Heat transfer in the evaporator actually has two mechanisms: forced convection and nucleate boiling. Nucleate boiling heat transfer may depend to some extent on the spacecraft acceleration, however this dependence is still poorly understood and no satisfactory test data are yet available. Forced convection, on the other hand, is entirely independent of acceleration. Therefore the approach recommended in this Design Manual is to design the evaporator so that forced convection is the dominant mechanism. An evaporator designed this way operates independently of the spacecraft acceleration regardless of possible acceleration effects on nucleate boiling heat transfer.

First, design maps and calculation methods for heat transfer are presented (Section 2.1). This section instructs the designer how to size the evaporator tube to obtain the desired outlet quality and to operate independently of spacecraft acceleration. Section 2.2 concerns pressure losses in a straight tube evaporator. The designer uses the maps and methods in this section to calculate the pressure drop through the evaporator in order to estimate system pumping power requirements.

Some of the design maps in this Section are less general than in the previous Section on flow regimes and pressure losses. This is because heat transfer is still largely an empirical science. The present state of the art does not provide generalized mechanistic design maps for many of the important phenomena. In such cases the designer must carry out more detailed calculations for specific design cases.

2.1 Heat Transfer

2.1.1 Introduction

This section describes the main phenomena for two–phase heat transfer in an evaporator tube. In general, an evaporator has several possible thermal boundary conditions: If the inlet conditions are constant, then either the temperature of the heated surface and/or the heat flux on the tube wall must be related or specified. Here we assume a constant heat flux to the tube (and a constant inlet temperature) so that the temperature of the heated surface is a dependent variable. Figure 2.1 illustrates this situation. The alternate situation of a fixed wall temperature with heat flux as the dependent variable is not of great interest to spacecraft thermal management systems.

Heat Transfer Regimes. Heat transfer occurs by several mechanisms in the evaporator tube because the fluid quality increases along the tube length. The flow rates of each phase along the tube depend on the heat transfer which, in turn, depends on the flow regime. For the simple case of a constant heat flux input along the length of the tube, the quality can be calculated by a simple energy balance. The major unknown variable in this case is the wall temperature.

Figure 2.2 illustrates all of the two–phase heat transfer regimes. In a forced–convection evaporator the regimes will appear in the order indicated by the figure:

- single–phase liquid,
- subcooled nucleate boiling,
- saturated nucleate boiling, and
- two–phase forced convection heat transfer.

Liquid deficient and single–phase vapor regimes have poor heat transfer and will not appear in a well–designed evaporator, though they are shown in the figure for completeness.

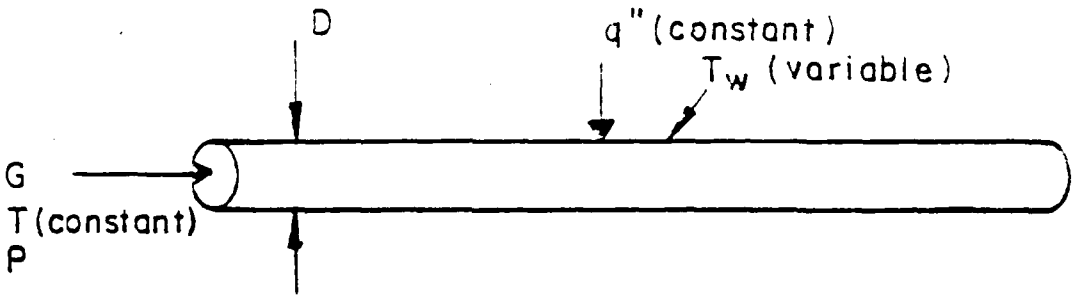

Figure 2.1. EVAPORATOR TUBE DESIGN INPUTS

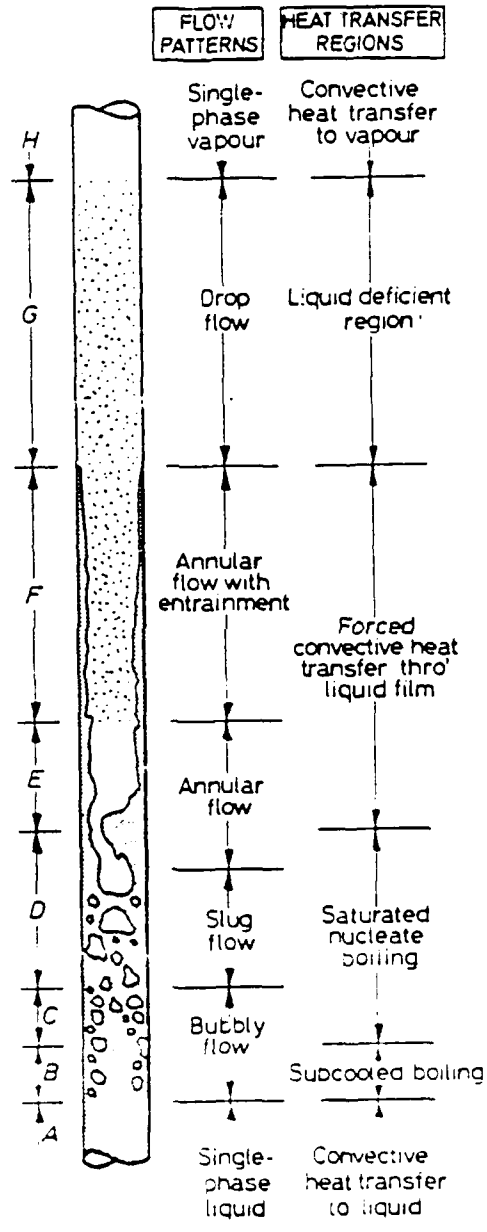

Figure 2.2. HEAT TRANSFER REGIMES IN CONVECTIVE BOILING (COLLIER, 1986)

Single-Phase Liquid. Single–phase heat transfer occurs when subcooled liquid enters the evaporator and the wall temperature is too low to nucleate bubbles. This regime is treated using standard correlations which relate the heat transfer coefficient to fluid properties and the single–phase Reynolds number.

Nucleate Boiling. The two nucleate boiling regimes occur between the single–phase liquid and the two–phase forced convection regimes. The wall temperature must be high enough to nucleate bubbles, and the void fraction must be small enough so that an annular flow pattern is not established. Heat transfer coefficients are very high, however the total amount of heat transfer is usually small since this regime exists over only a short length of the tube. As described in the detailed design section below, there are actually two types of subcooled nucleate boiling, fully developed and partially developed, which differ in the extent of nucleation on the tube wall.

Two-phase Forced Convection. For most cases of practical interest this is the only important heat transfer regime. The major design parameters for an evaporator tube can be estimated by assuming that the entire tube is characterized by this regime. The design maps in Section 2.1.2 use this approach.

In this regime the fluid flows in an annular pattern with a vapor core and a liquid film on the tube wall. Vaporization occurs by two mechanisms: nucleate boiling in the liquid at the wall and evaporation at the vapor/liquid interface. Two–phase forced convection is the dominant mechanism of heat transfer for practical coolants because the void fraction is quite high even at low qualities, implying an annular flow regime over most of the tube length.

In this Design Manual the "saturated nucleate boiling" regime (Figure 2.2) is considered a part of the two–phase forced convection regime because they are treated identically in most cases. This regime of non–annular (bubbly or slug) flow is typically very small and has little effect on the overall design.

A useful concept for describing heat transfer in the two–phase forced convection regime is the *superposition principle*. Heat transfer is treated as the sum of two components. One is due to nucleate boiling at the wall, and the other is due to forced convection heat transfer to the liquid film. Quantitatively, the total heat flux, q", is expressed as a sum:

$$q'' = (h_{fc} + h_{nb})\,\Delta T_{sat} \qquad (2\text{–}1)$$

where h_{fc} is the "forced convection" heat transfer coefficient, h_{nb} is the "nucleate boiling" heat transfer coefficient, and ΔT_{sat} is the temperature difference between the tube wall and the fluid.

The superposition principle is the basis for an important evaporator design criterion. Since forced convection heat transfer is independent of gravity while nucleate boiling heat transfer has an uncertain gravity dependence, a design criterion for evaporators in microgravity is:

$$h_{fc} >> h_{nb} \qquad (2\text{–}2)$$

In this way operation of the evaporator is assured regardless of the spacecraft acceleration.

Typical Behavior. Figure 2.3 shows predicted fluid and wall temperature profiles in one particular forced convection evaporator tube. This temperature plot applies to a 6 mm evaporator tube with a uniform wall heat flux of 2.7 W/cm^2. The coolant is Freon R–114 which enters with a subcooling of 3.3°C and a flow rate of 5.66 g/s. In the single–phase liquid regime, the coolant temperature increases steadily due to the constant heat input. The wall temperature remains a fixed amount above the fluid temperature because the single–phase heat transfer coefficient is constant. In the nucleate boiling regime, the coolant temperature continues to rise but the wall temperature drops because heat transfer is very effective. After the fluid reaches its saturation temperature, the two–phase forced convection regime begins. The wall temperature increases at first, as bubble nucleation is suppressed, but falls along the length of the tube as interaction between the liquid and high velocity vapor act to increase the heat transfer coefficient.

Figure 2.4 shows the predicted quality and void fraction in the same 6 mm evaporator tube. The quality increases linearly over the entire tube length because the heat flux is constant. The void fraction increases much more quickly because the vapor density is much less than the liquid density. Thus the volume fraction of the vapor is larger than its mass fraction.

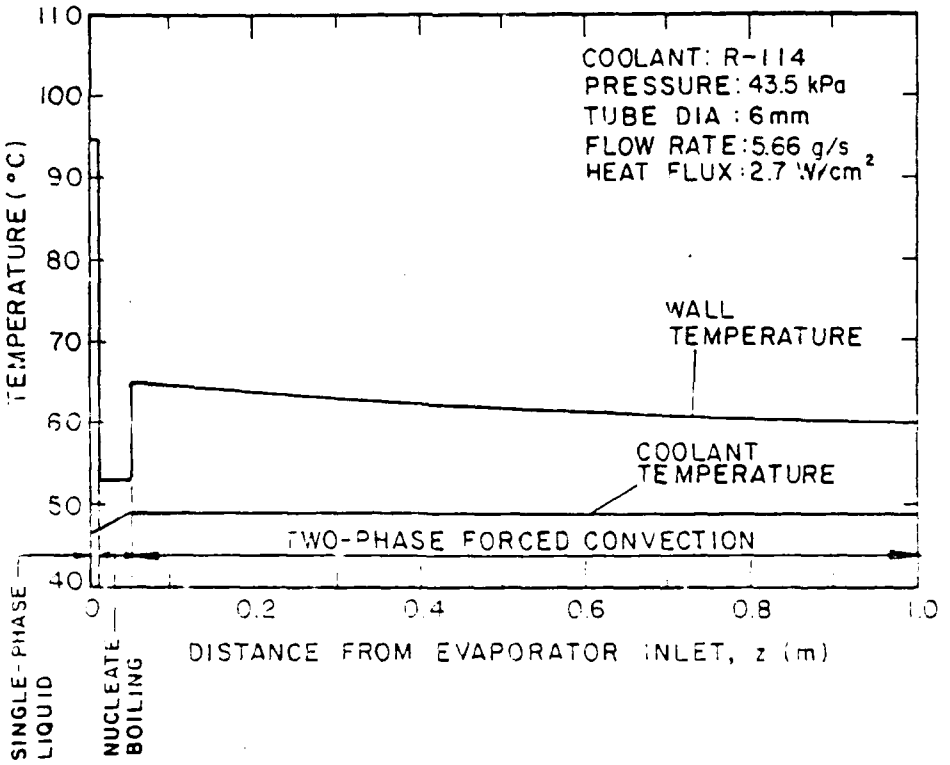

Figure 2.3. TEMPERATURE PROFILES IN A FORCED–CONVECTION EVAPORATOR TUBE

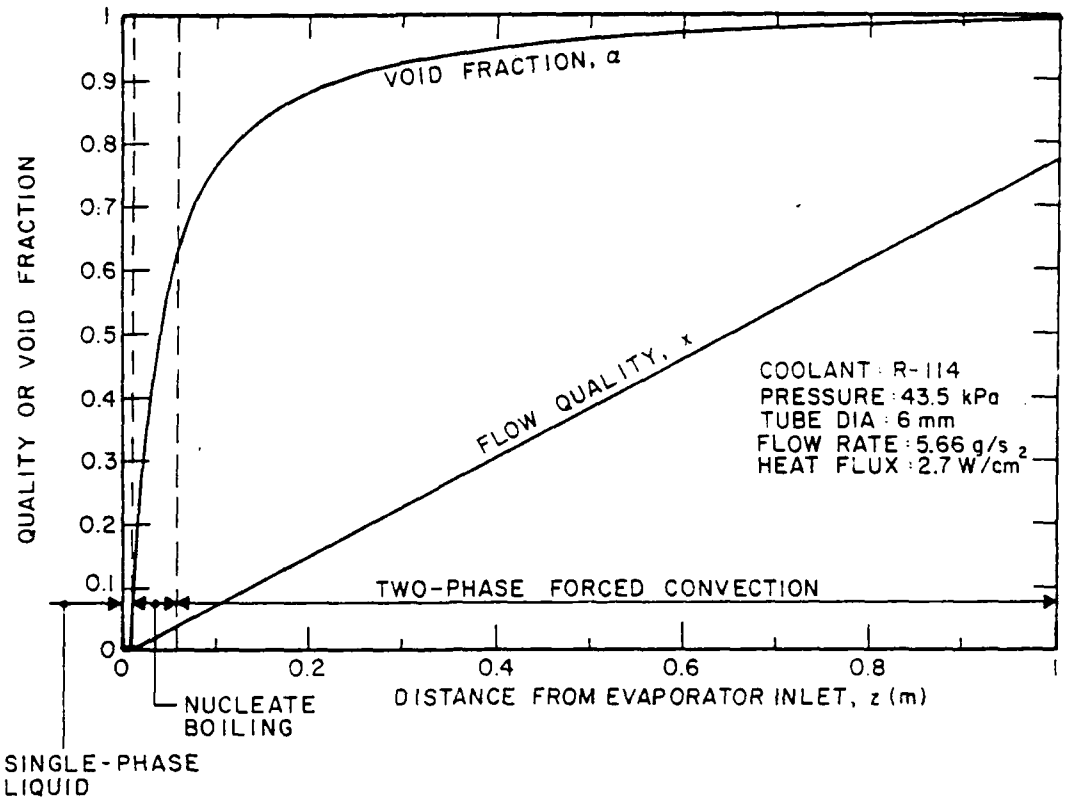

Figure 2.4. QUALITY AND VOID FRACTION IN A FORCED CONVECTION EVAPORATOR

Depending on the heat flux level, some of the heat transfer regimes may not occur in an evaporator tube. At heat fluxes which are high relative to the liquid mass flux, various other regimes may occur, as described by Collier (1986). However, these cases represent poor evaporator designs in which the tube walls dry out and reach very high temperatures. This discussion is limited to well designed evaporators in which two–phase forced convection is the major heat transfer mechanism.

As will be shown in Section 2.2, pressure drops in evaporator tubes are usually quite small compared to the absolute pressure of the coolant. As a result the coolant properties will not change appreciably along the tube.

Readers who wish further background in two–phase heat transfer should consult the text by Collier (1986) or the report by Eastman (1985).

2.1.2 Design Maps and Scoping Calculations

This section presents methods for scoping calculations of the evaporator size and heat transfer. It is assumed that the heat flux and the fluid conditions at the inlet are known and that the primary design goals are to achieve a desired fluid exit quality and to ensure operation independent of spacecraft acceleration. The basic procedure to meet these objectives is:

- Estimate the evaporator tube length,
- Estimate the forced convection fraction, and
- Check the design for maximum heat flux and tube wall temperature.

Two–phase forced convection with annular flow is the dominant regime in an evaporator tube if the inlet subcooling of the fluid is only a few degrees. The following discussion assumes that this regime dominates the evaporator behavior. For detailed design all of the heat transfer regimes must be treated explicitly, and the detailed analysis presented in Section 2.1.3 is recommended.

The information needed in order to perform the scoping calculations includes:

Fluid Properties

ρ_l	density of liquid phase (kg/m^3)
μ_l	viscosity of liquid phase (kg/m–s)
c_{pl}	specific heat of liquid phase (J/kg–K)
σ	surface tension (N/m)
h_{fg}	latent heat of evaporation (J/kg)
μ_g	viscosity of vapor phase (kg/m–s)
ρ_g	density of vapor phase (kg/m^3)

Operating Conditions

T_{sat}	saturation temperature (K)
ΔT_{sub}	inlet subcooling (K)
G	mass flux (kg/m^2–s)
P	evaporator absolute pressure (Pa)
x_o	evaporator outlet quality (–)

Geometry

H	tube heated perimeter (m)
A	cross–sectional flow area (m^2)

Evaporator Tube length. Figure 2.5 is a universal design map (independent of heat transfer regime) which shows the required evaporator tube length in terms of the desired change in fluid quality and an evaporator thermodynamic ratio, R_{ev}, which is proportional to the heat flux divided by the mass flux. A compact evaporator has a large thermodynamic ratio, unfortunately this competes with design requirements for forced–convection dominance and low pressure drops. The optimum R_{ev} comes from a tradeoff between these objectives.

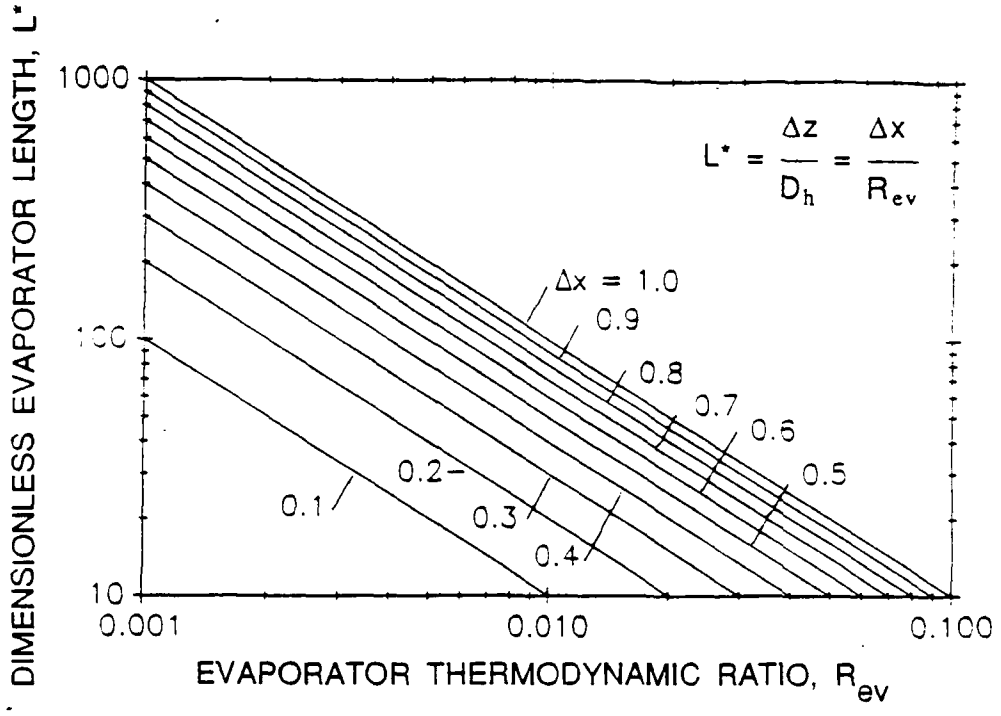

Figure 2.5. EVAPORATOR TUBE LENGTH

The procedure to use this map includes three steps as described below.

1) First, calculate the thermodynamic ratio, R_{ev}, for the evaporator:

$$R_{ev} \equiv \frac{4q''}{G h_{fg}} \qquad (2-3)$$

where:

q'' = the evaporator tube's (uniform) heat flux (W/m^2), and
G and h_{fg} are defined above.

2) Next, determine the change in fluid quality, Δx, which the evaporator is to produce. The inlet subcooling and exit quality, and thus the change in quality within the evaporator, are determined as part of the overall system design. If fluid enters the evaporator with a subcooling, ΔT_{sub}, and is to exit with a quality x_o, then the change in enthalpy is:

$$\Delta h = c_{pf} \Delta T_{sub} + x_o h_{fg} \qquad (2-4)$$

The change in quality in the evaporator is calculated by:

$$\Delta x \equiv \Delta h/h_{fg} \qquad (2\text{–}5)$$

3) Select the line which corresponds to Δx in Figure 2.5 and locate the point with the abscissa R_{ev}. The value of the ordinate at this point is the dimensionless tube length, L*, which will produce the desired exit quality. The required tube length is:

$$L = L^*D_h \qquad (2\text{–}6)$$

where:

L = tube length (m), and
D_h = 4A/H (the hydraulic diameter) (m).

Forced Convection Fraction. The evaporator design should ensure that forced convection is the dominant heat transfer mechanism. The fraction of heat transfer due to forced convection in the two–phase forced convection regime depends on the coolant properties, mass flux, tube hydraulic diameter, heat flux and the quality. Figures 2.6 through 2.9 are dimensionless design maps which allow the designer to estimate the forced convection fraction for any situation. Figures 2.10 and 2.11 show specific design maps for Freon 11 and Freon 114 in a 6 mm diameter tube with a heat flux of 2 W/cm^2. Though the first two maps are more general, they are considerably more difficult to use than the specific maps. Additional specific maps can be generated using the procedures detailed in Section 2.1.3 which follows.

The forced convection fraction for any fluid in any straight tube evaporator can be calculated using Figures 2.6 through 2.9. These figures permit the designer to estimate the forced convection and nucleate boiling heat transfer coefficients (h_{fc} and h_{nb}) as a function of fluid properties and condenser operating conditions. The forced convection fraction, E_{fc}, is simply a ratio of these heat transfer coefficients.

There are 10 steps to calculate the forced convection fraction:

1. Select a representative fluid quality, x.
2. Calculate the Martinelli parameter, X_{tt} (Equation 2–7).
3. Determine the Reynolds number factor, F (Figure 2.6).
4. Calculate the two–phase Reynolds number, Re_{tp} (Equation 2–8).
5. Determine the forced–convection heat transfer coefficient, h_{fc} (Figure 2.7 and Equation 2–9).
6. Determine the suppression factor, S (Figure 2.8).
7. Estimate the wall superheat, ΔT_{sat} (Equations 2–10 and 2–11).
8. Determine the nucleate boiling heat transfer coefficient, h_{nb} (Equation 2–12 or Figure 2.7).
9. Check the heat flux, and iterate (return to Step 8) if necessary (Equation 2–17).
10. Calculate the fraction of the heat transfer due to forced convection, E_{fc} (Equation 2–19).

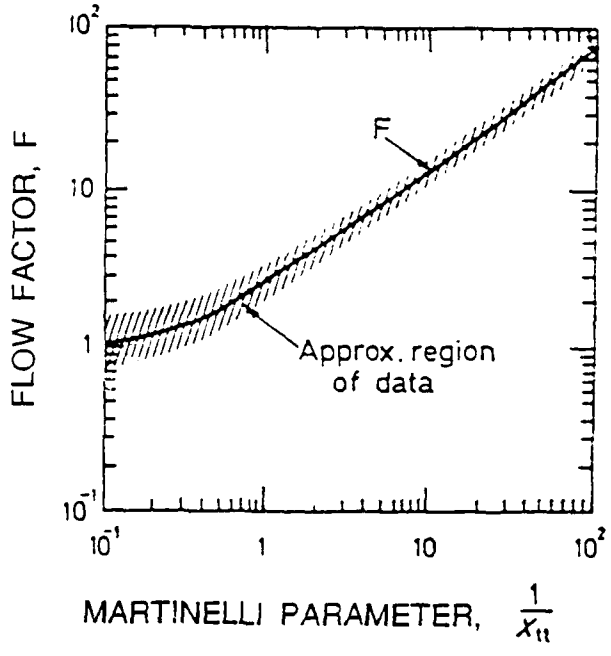

Figure 2.6. REYNOLDS NUMBER FACTOR, F (CHEN, 1963)

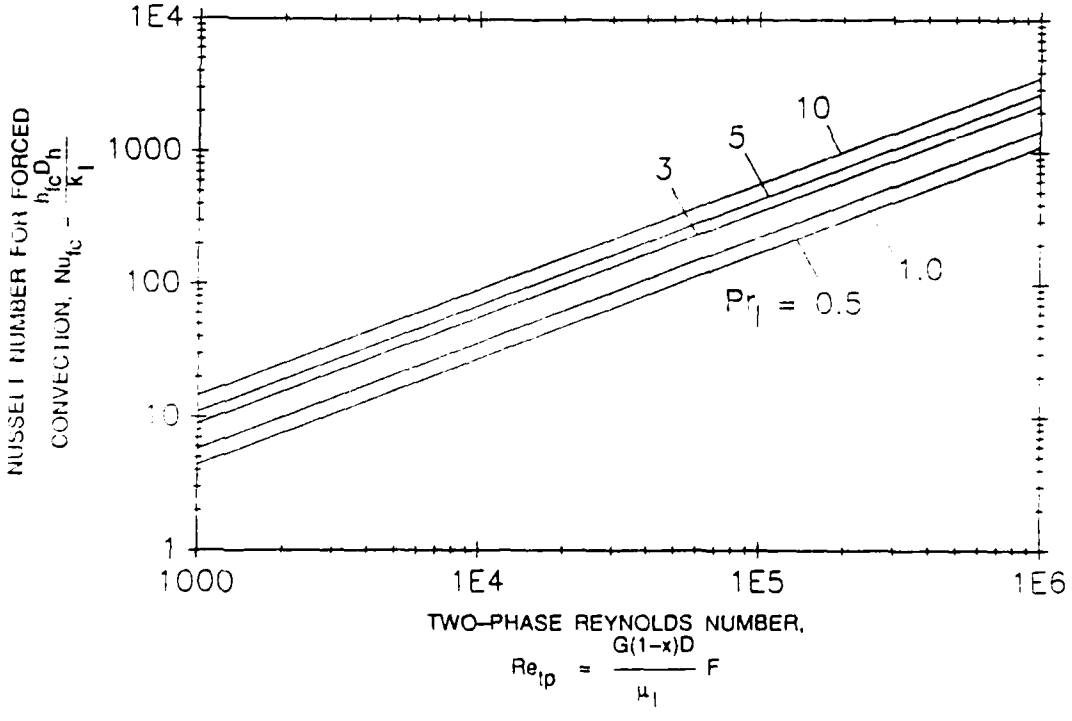

Figure 2.7. DESIGN MAP FOR FORCED CONVECTION HEAT TRANSFER IN TWO-PHASE FORCED CONVECTION

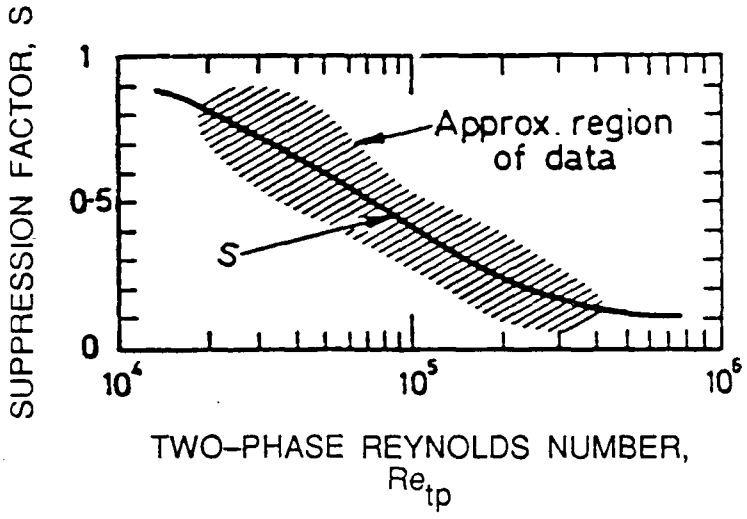

Figure 2.8. SUPPRESSION FACTOR, S (CHEN, 1963)

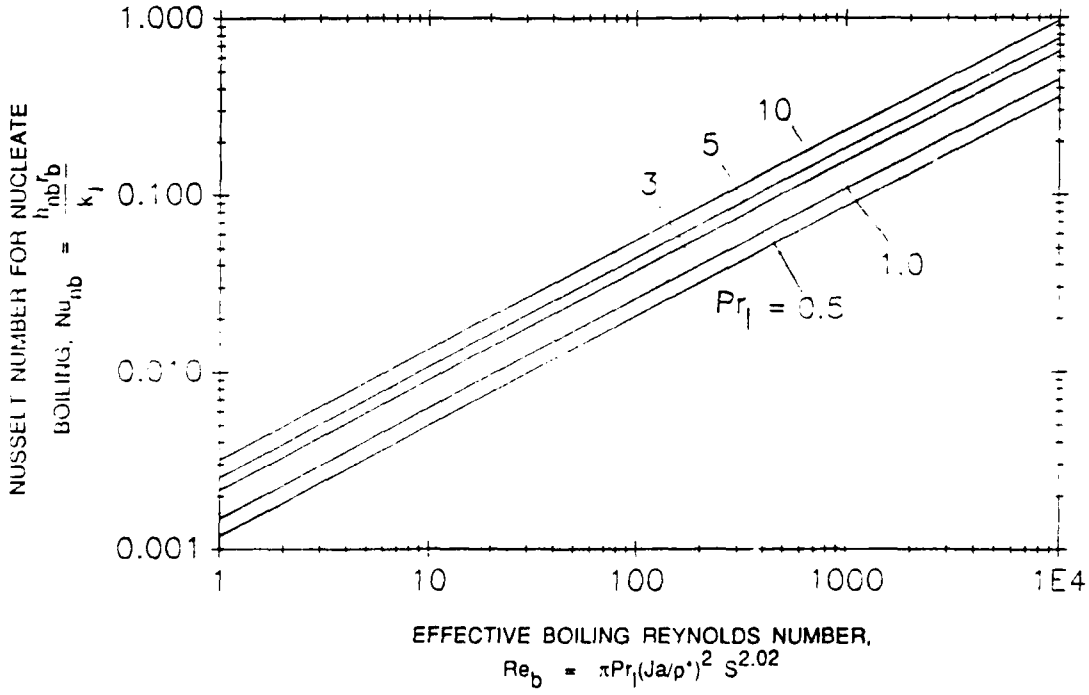

Figure 2.9. DESIGN MAP FOR NUCLEATE BOILING HEAT TRANSFER IN TWO-PHASE FORCED CONVECTION

These steps are described in more detail below.

1) Select a representative fluid quality, x: The average flow quality in the channel will do. This is simply one–half the exit quality.

2) Calculate the Martinelli parameter, X_{tt}:

$$X_{tt} = \left[\frac{1-x}{x}\right]^{0.9}\left[\frac{\rho_g}{\rho_l}\right]^{0.5}\left[\frac{\mu_l}{\mu_g}\right]^{0.1} \qquad (2-7)$$

3) Determine the Reynolds number factor: The F factor may be read directly as a function of $1/X_{tt}$ by referring to Figure 2.6.

4) Calculate the two–phase Reynolds number:

$$Re_{tp} = \frac{G(1-x)D_h}{\mu_l} F^{1.25} \qquad (2-8)$$

5) Determine the forced–convection heat transfer coefficient, h_{fc}. Use Figure 2.7 and read the value of the Nusselt number for forced convection (Nu_{fc}) which corresponds to the two–phase Reynolds number and the liquid Prandtl number ($Pr_l = \mu_l c_{pl}/k_l$). Then calculate the heat transfer coefficient:

$$h_{fc} = \frac{Nu_{fc} k_l}{D_h} \qquad (2-9)$$

6) Determine the suppression factor S: S is a function of Re_{tp} and can be read directly from Figure 2.8.

7) Estimate the wall superheat: The wall superheat can then be estimated by

$$\Delta T_{sat} = \left[(h_{fc}/2h_{nb}')^2 + (q''/h_{nb}')\right]^{0.5} - (h_{fc}/2h_{nb}') \qquad (2-10)$$

where

$$h_{nb}' = 0.00122 \frac{k_l^{0.79} c_{pl}^{0.45} \rho_l^{0.49} h_{fg}^{0.51}}{T_{sat}^{0.75} \sigma^{0.5} \mu_l^{0.29} \rho_g^{0.24} v_{fg}^{0.75}} S \qquad (2-11)$$

(which is approximately $h_{nb}/\Delta T_{sat}$).

8) Determine the nucleate boiling heat transfer coefficient: The easiest way to do this is simply to calculate

$$h_{nb} = h_{nb}' \Delta T_{sat} \qquad (2-12)$$

Alternatively, Figure 2.9 can be used to read the Nusselt number for nucleate boiling, Nu_{nb}. The design map in Figure 2.9 is relatively impractical to use because the heat transfer coefficient is a function of several dimensionless parameters, and Equation 2–12 is recommended instead. Nevertheless, Figure 2.9 is useful because it shows that this procedure scales to any fluid. If this figure is used, the Nu_{nb} is located which corresponds to the liquid Prandtl number and the bubble Reynolds number, Re_b:

$$Re_b = \frac{\pi k_l c_{pl}}{\mu_l}\left[\frac{\rho_g \Delta T_{sat}}{\rho_l h_{fg}}\right]^2 S^{2.02} \qquad (2\text{–}13)$$

The heat transfer coefficient for nucleate boiling is then:

$$h_{nb} = \frac{Nu_{nb} k_l}{r_b} \qquad (2\text{–}14)$$

where r_b is a characteristic bubble radius given by:

$$r_b = \frac{\Delta T_{sat}}{h_{fg}\rho_g}\left[\frac{2\pi k_l \rho_l c_{pl}\sigma}{\Delta P_{sat}}\right]^{\frac{1}{2}}\left[\frac{\rho_l}{\Delta P_{sat}}\right]^{\frac{1}{4}} S^{0.25} \qquad (2\text{–}15)$$

and ΔP_{sat} is the difference in saturation pressures which corresponds to the wall superheat:

$$\Delta P_{sat} = \Delta T_{sat}\frac{h_{fg}}{T_{sat}(v_g - v_l)} \qquad (2\text{–}16)$$

where v_g and v_l are the specific volumes of the gas and liquid phases, respectively.

9) Check the heat flux and iterate if necessary: Verify that the estimated wall superheat is accurate by comparing the known heat flux with the heat flux calculated from ΔT_{sat}, h_{fc} and h_{nb}. Calculate this ratio:

$$\beta = \frac{(h_{fc} + h_{nb})\Delta T_{sat}}{q''} \qquad (2\text{–}17)$$

There are now two possibilities:

a) β is acceptably close to 1.0 – in this case, go on to step 10 to calculate E_{fc}. "Acceptably close" depends upon the level of precision desired in the design. Since the Chen correlation is only accurate to within 10% of the actual heat flux, it is usually acceptable to go on if β lies between 0.9 and 1.10.

b) If β is outside the acceptable range, modify the estimate for ΔT_{sat} and go back to step 8. A good next guess for the superheat is:

$$\Delta T_{sat} \simeq \left[\frac{q''}{h_{fc} + h_{nb}}\right] \qquad (2\text{–}18)$$

10) Calculate the forced convection fraction: The fraction of the heat transfer due to forced convection, E_{fc}, is:

$$E_{fc} = \left[\frac{h_{fc}}{h_{fc} + h_{nb}} \right] \qquad (2\text{–}19)$$

This ratio should be near unity ($E_{fc} \geq 0.9$) for forced convection to dominate.

Figure 2.10 shows the forced convection fraction as a function of flow quality and mass flux for the specific design case of an R–11 evaporator operating at a pressure of 227 kPa, a heat flux of 2 W/cm^2 and with a diameter of 6 mm. Figure 2.11 shows the same information for R–114 at 434 kPa. These design charts are simpler to use than the dimensionless maps; however, to generate such plots, the designer must perform the calculations outlined in Section 2.1.3 which follows.

Maximum Heat Flux. There are two limits which should be checked for evaporator design. One is the maximum heat flux and the other is the wall temperature. To first order, if the fraction E_{fc} is greater than 0.9, operation should be possible.

High heat fluxes tend to increase the importance of nucleate boiling within the two–phase forced convection regime. For a given fluid, mass flux and tube diameter there is a maximum value of the heat flux above which forced convection is no longer the dominant mechanism of heat transfer. For an evaporator tube which is to operate in microgravity this value is a limit to the heat flux which should not be exceeded. There are also heat flux limits due to critical heat flux considerations which are not included in this Design Manual but which may, in some cases, be more restrictive than these.

Figure 2.12 provides the designer with quick checks on potential evaporator designs with Freon. To operate in microgravity, the tube heat flux should be less than the maximum values indicated by Figure 2.12. The design map shown in Figure 2.12 presents limiting heat flux values for R–11 in tubes of various diameters. The mass flux is expressed as a Reynolds number for the flow rate of liquid at the inlet:

$$Re_f \equiv GD_h/\mu_l \qquad (2\text{–}20)$$

The heat flux indicated by Figure 2.12 is the value above which nucleate boiling accounts for over 10% of the heat transfer along the tube length. Note that there is roughly a second–power relationship between the maximum heat flux and the mass flux:

$$q''_{max} \approx G^2 \qquad (2\text{–}21)$$

Figure 2.12 also shows the same calculation for R–114. Section 2.1.3 details how to produce similar design maps for other coolants.

Wall Temperature. The evaporator designer may be faced with temperature limits for the tube material. Figure 2.13 shows the wall temperatures which correspond to the maximum heat fluxes illustrated in the previous design maps. The wall temperature remains fairly constant until a critical value of the heat flux is reached. Beyond this point the wall temperature increases rapidly. Design maps for additional coolants can be prepared using procedures in Section 2.1.3.

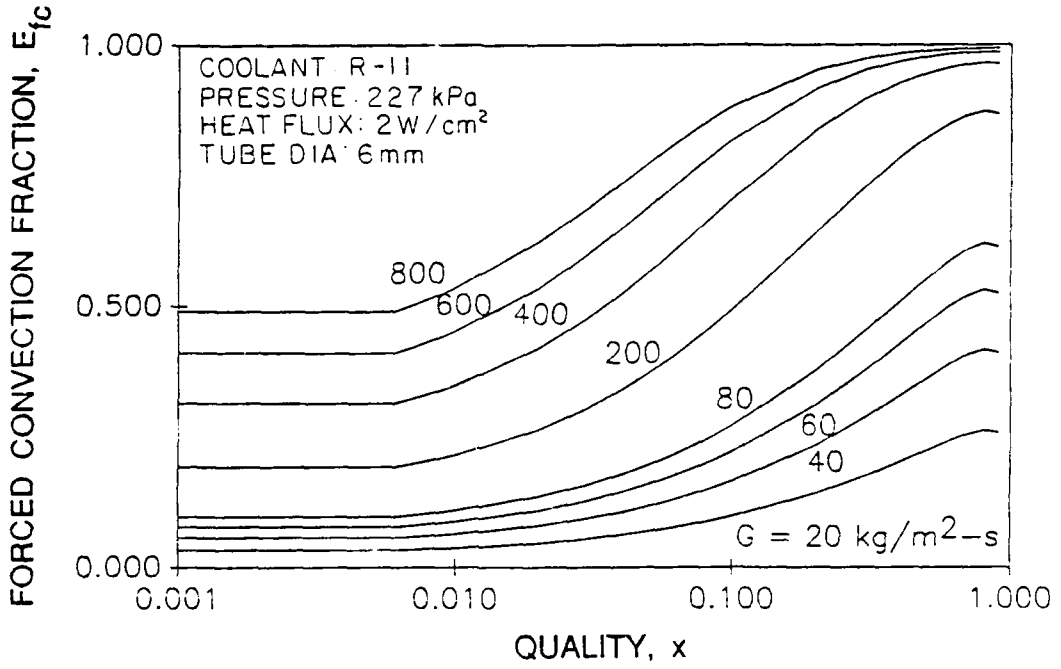

Figure 2.10. FORCED CONVECTION FRACTION FOR R-11 IN A 6 mm EVAPORATOR TUBE

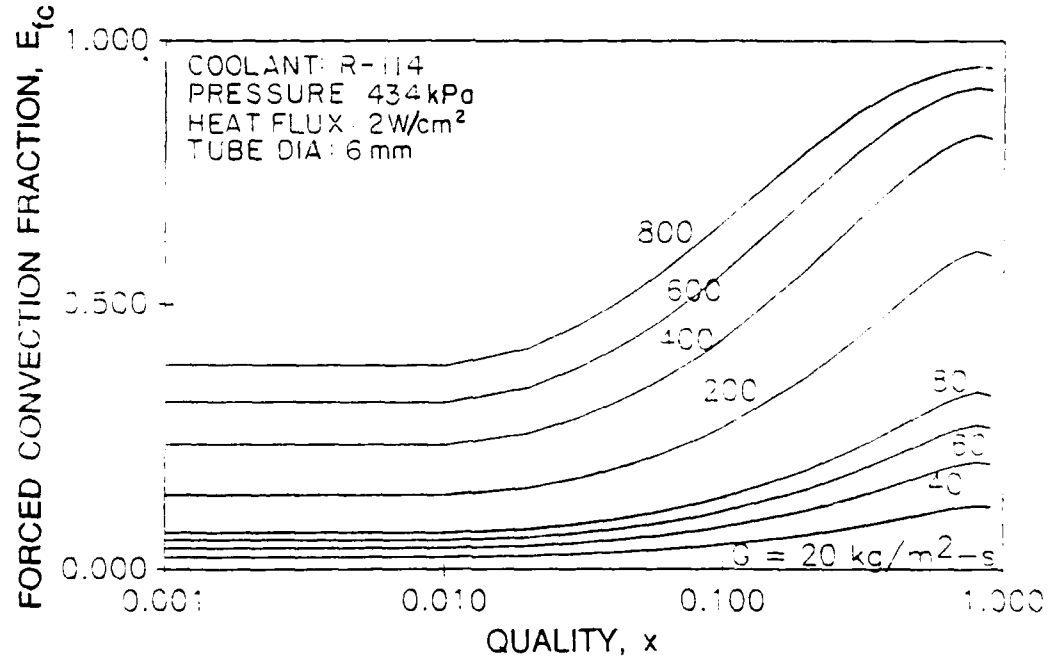

Figure 2.11. FORCED CONVECTION FRACTION FOR R-114 IN A 6 mm EVAPORATOR TUBE

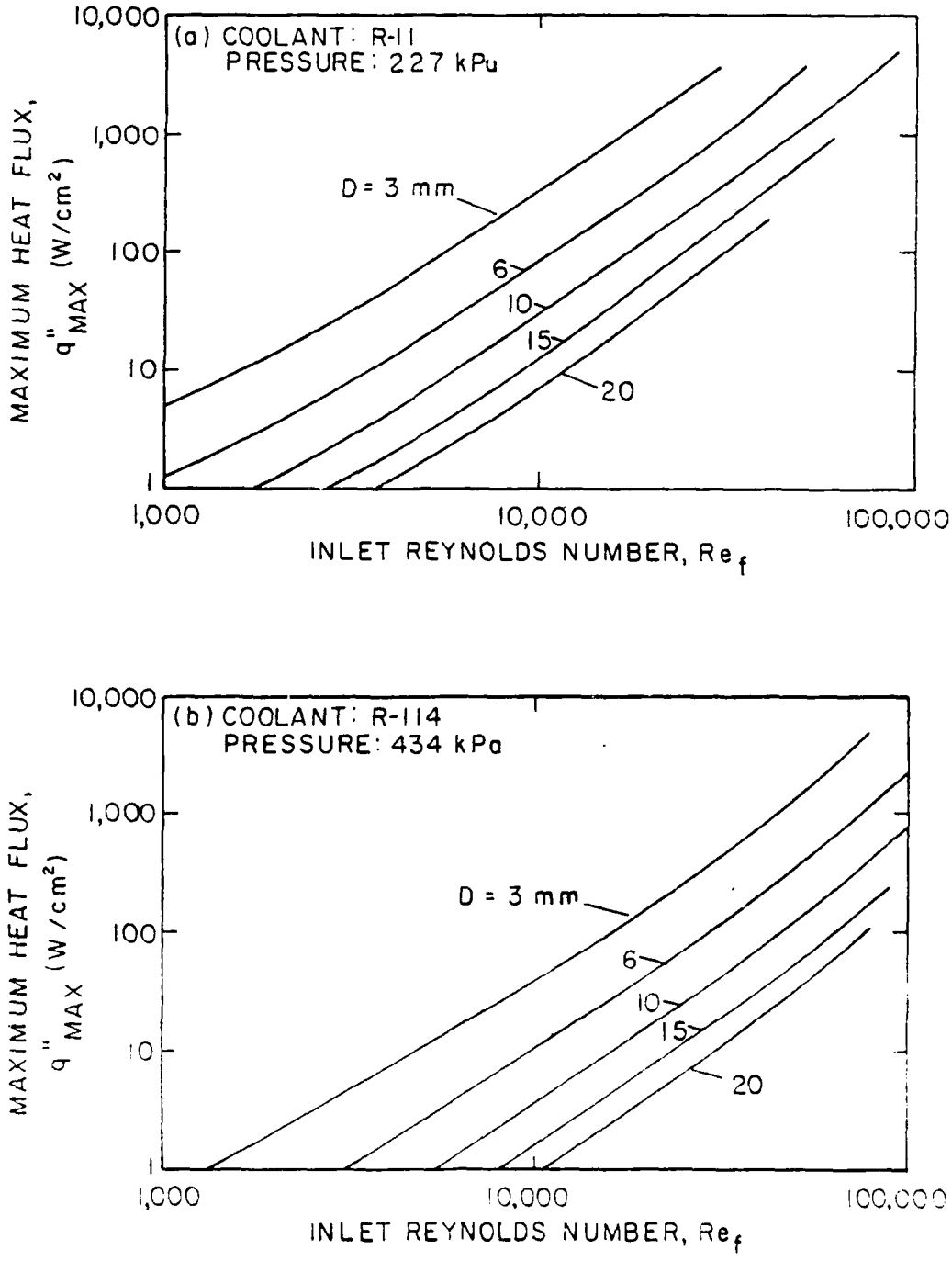

Figure 2.12. MAXIMUM HEAT FLUX FOR OPERATION IN MICROGRAVITY

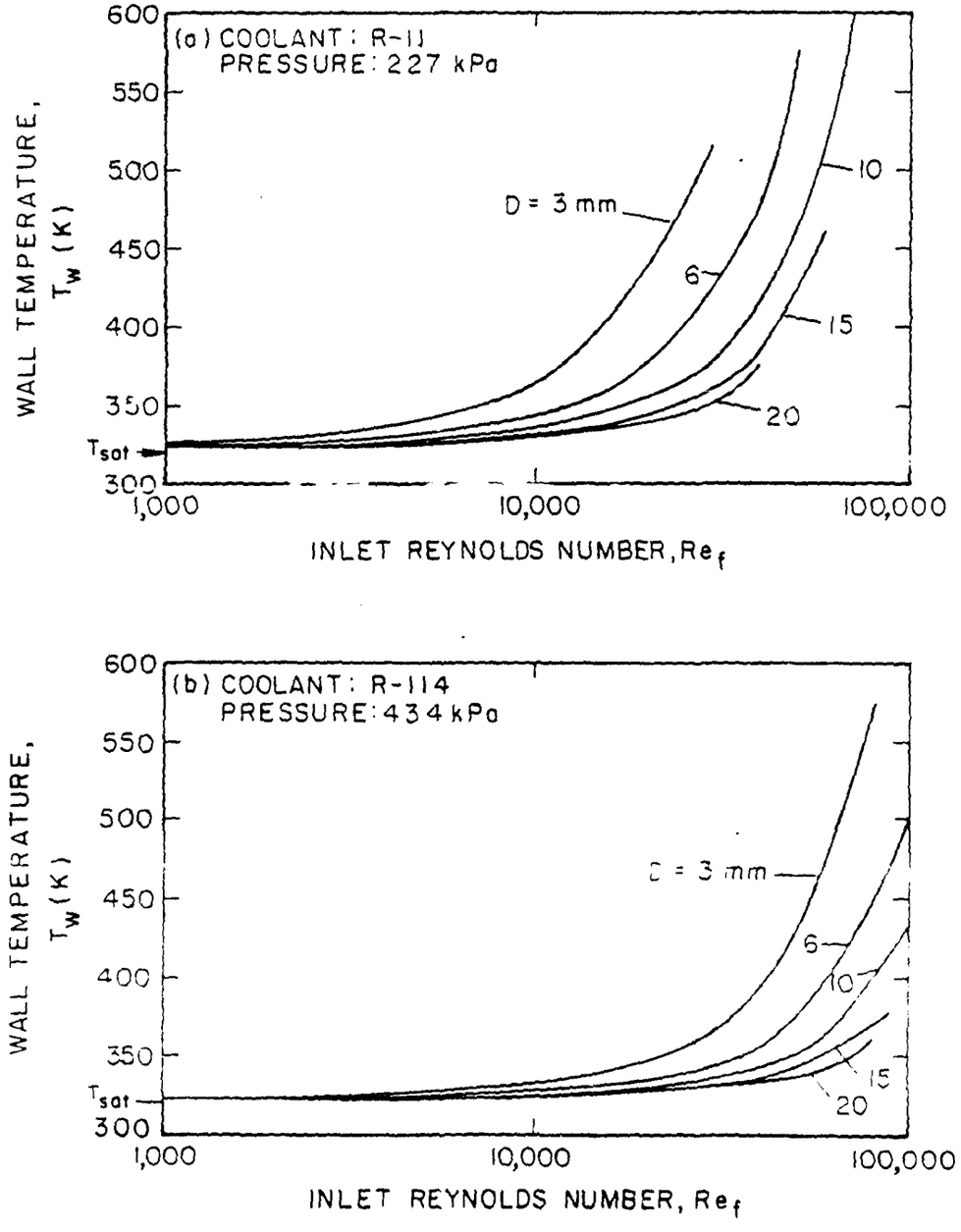

Figure 2.13. WALL TEMPERATURE AT MAXIMUM HEAT FLUX

Uncertainty. The main uncertainty in the heat transfer calculation is the effect of microgravity on nucleate–boiling heat transfer. The only models for forced–convection heat transfer have been developed based on experiments conducted under normal Earth gravity. The recommended approach is to design the evaporator so that the controlling phenomenon is forced–convection heat transfer. The designer should address this uncertainty by requiring a high fraction of the evaporator heat transfer (e.g. 90%) to be due to forced convection. Ongoing microgravity experiments will provide data so that more specific guidelines can be used in the future.

2.1.3 Equations for Heat Transfer

To first order, an evaporator tube can be designed assuming only one heat transfer regime: two–phase forced convection. However, for final design calculations more precision is often needed, and the detailed behavior of the coolant must be considered. These calculations should consider all the possible heat transfer regimes and calculate the transition from one regime to the next.

This section presents detailed design relations. Procedures are given to generate design maps for additional cases of interest or to program computerized calculations for forced convection evaporators. The usual way to use these design relations is to first divide the evaporator tube into a number of segments within which the fluid properties are approximately constant. In each segment there are three basic calculations:

- Determine the fluid state at the segment exit,
- Calculate the wall temperature, and
- Check for heat transfer regime transition.

Table 2.1 summarizes the equations for these calculations in each of the heat transfer regimes. Figure 2.14 shows schematically the sequence for performing these calculations. The sections which follow provide more detail.

One hundred or so segments are usually sufficient for the evaporator calculation. Conditions in the first segment are known from the evaporator inlet conditions and will usually be single–phase liquid at a known pressure and subcooling. Exit conditions calculated for one segment become the inlet conditions for the next. The following sections show how to calculate the fluid state, wall temperature and regime transitions in each of the heat transfer regimes experienced by the fluid as it travels through the evaporator: single–phase liquid, partial and fully developed nucleate boiling, and two–phase forced convection.

Single Phase Liquid Regime. In this regime, vapor bubbles are not present at all.

Fluid State. In the single–phase regime all of the heat is absorbed by the liquid as sensible heat. Therefore the temperature rise, ΔT_f, in a segment of length Δz is calculated from a simple energy balance:

$$\Delta T_f = \frac{4\ q''\ \Delta z}{G\ c_{pl}\ D_h} \qquad (2\text{–}22)$$

Table 2.1. HEAT TRANSFER CALCULATIONS FOR AN EVAPORATOR TUBE

REGIME	FLUID STATE	WALL TEMPERATURE	REGIME TRANSITION
SINGLE PHASE LIQUID	$\Delta T_l = \dfrac{4\,q''\,\Delta z}{G\,c_{pl}\,D_h}$	$T_w = T_f + \dfrac{q''}{h_{fc}}$	$\dfrac{k_l(T_w - T_{sat})_{ONB}}{q''\,r_{crit}} = \left[1 + \dfrac{2v_{fg}T_{sat}\sigma}{h_{fg}r_{crit}} \times \dfrac{1}{q''r_{crit}}\right]$
PARTIALLY DEVELOPED NUCLEATE BOILING	$\Delta T_l = \dfrac{4\,q''\,\Delta z}{G\,c_{pl}\,D_h}$	$T_w = T_{sat} + [q'' - h_{fc}(T_{sat} - T_f)]^{\frac{1}{2}}/22.65\exp(-0.014P)]$	$St = \dfrac{455}{Re_f Pr_l}$ $Re_f Pr_l < 70{,}000$ $St = 6.5\times10^{-3}$ $Re_f Pr_l > 70{,}000$
FULLY DEVELOPED NUCLEATE BOILING	$\Delta T_l = \dfrac{4\,\Delta z\,q''}{G\,c_{pl}\,D_h} \times \left[1 + 0.1(\rho_l/\rho_g)^{0.75}c_{pl}(T_{sat} - T_f)/h_{fg}\right]^{-1}$	$T_w = T_{sat} + 22.65(q'')^{\frac{1}{2}}\exp(-0.014P)$	$T_f = T_{sat}$
TWO PHASE FORCED CONVECTION	$\Delta x = \dfrac{4\,q''\,\Delta z}{G\,h_{fg}\,D_h}$	$T_w = T_{sat} + \left[\left(\dfrac{h_{fc}}{2h_{nb}}\right)^2 + \dfrac{q''}{h_{nb}}\right]^{\frac{1}{2}} - \dfrac{h_{fc}}{2h_{nb}}$	(NOT ADDRESSED IN DESIGN MANUAL)

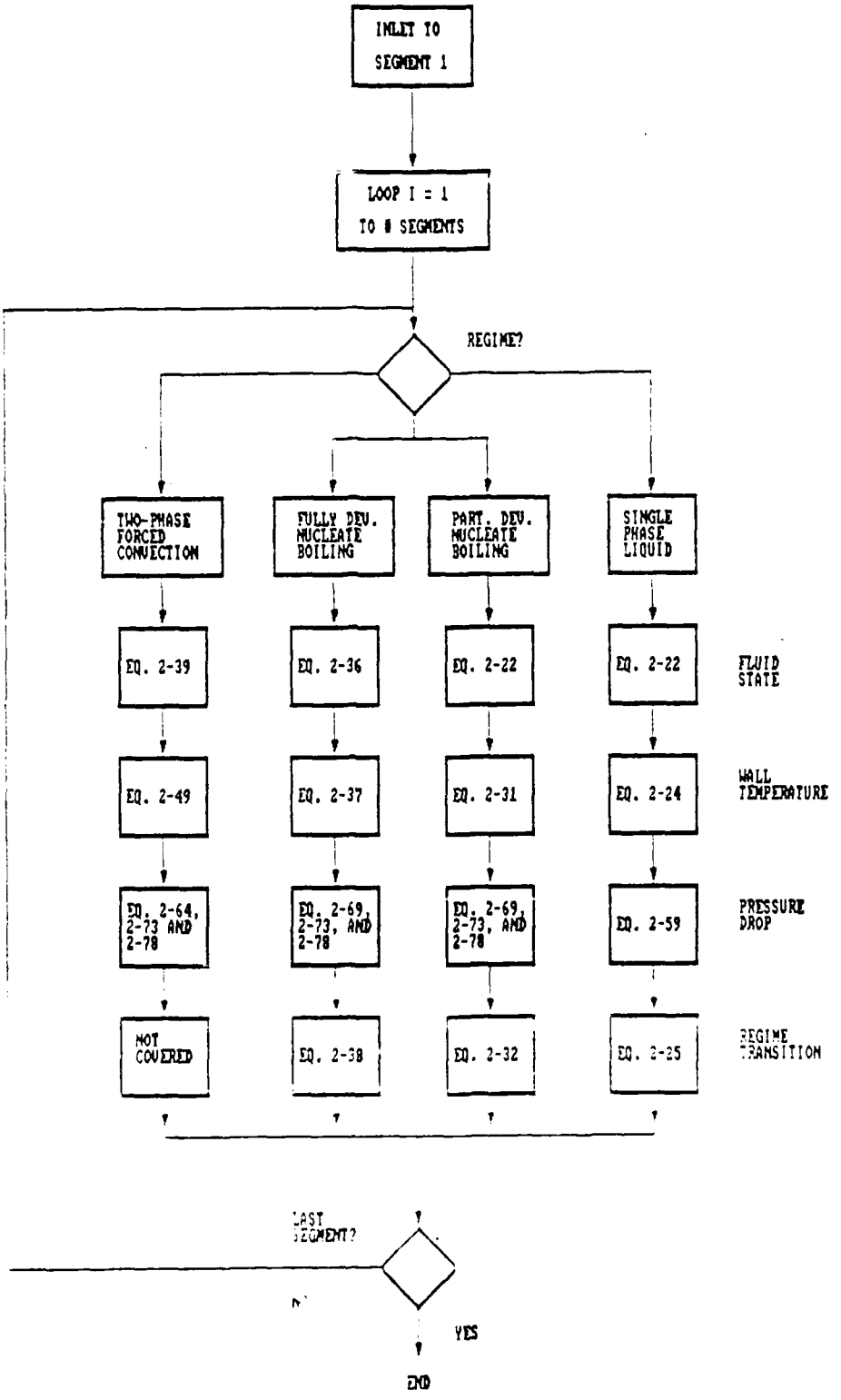

Figure 2.14. FLOWCHART FOR DETAILED EVAPORATOR CALCULATIONS

Wall Temperature. The evaporator wall temperature in the single–phase regime depends on the heat flux and the single–phase heat transfer coefficient, h_{fc}:

$$T_w = T_f + q''/h_{fc} \tag{2–23}$$

For turbulent flow, the Dittus–Boelter equation (Collier, 1986) yields the heat transfer coefficient:

$$h_{fc} = 0.023\,(k_l/D_h)\,(GD_h/\mu_l)^{0.8}\,(Pr_l)^{0.4} \tag{2–24}$$

where

k_l = thermal conductivity of the liquid (W/m–K), and
Pr_l = Prandtl number of the liquid ($Pr_l = \mu_l c_{pl}/k_l$).

Transition to nucleate boiling. The single–phase heat transfer regime ends when the wall temperature reaches a critical value, T_{wonb}, at which vapor bubble nucleation and subcooled nucleate boiling begins. The correlation of Davis and Anderson (1966):

$$T_{wonb} = T_{sat} + \left[\frac{8\,\sigma\,q''T_{sat}}{h_{fg}k_l\rho_g}\right]^{1/2} \tag{2–25}$$

is recommended, or that of Frost and Dzakowic (1967), which is identical except that the second term is multiplied by $Pr_l^{1/3}$.

This transition criterion can be expressed in dimensionless form as indicated in Table 2.1. The dimensionless criterion is:

$$\frac{k_l(T_w - T_{sat})_{onb}}{q''\,r_{crit}} = \left[1 + \frac{2v_{fg}T_{sat}\sigma k_l}{h_{fg}r_{crit}^2 q''}\right] \tag{2–26}$$

where r_{crit} is a critical bubble radius:

$$r_{crit} = \frac{2v_{fg}T_{sat}\sigma k_l}{h_{fg}q''} \tag{2–27}$$

and $v_{fg} = (1/\rho_g) - (1/\rho_l)$.

Partially Developed Nucleate Boiling Regime. The partially developed nucleate boiling regime is the first to occur following the single–phase liquid regime. It is characterized by incomplete activation of nucleation sites on the evaporator so that some fraction of the heat transfer occurs by normal single–phase convection between patches of bubbles. Vapor bubbles appear at the wall surface but do not detach and enter the flow.

Fluid State. In this regime there is no net vapor generation, so that fluid heating is the same as single–phase, Equation 2–22.

Wall Temperature. The recommended analytical approach is to treat the heat flux in this regime as the superposition of a subcooled boiling heat flux and a single–phase forced convection heat flux. Bowring (1962) suggests a simple additive approach:

$$q'' = q''_{sub} + q''_{fc} \tag{2–28}$$

$$= q''_{sub} + h_{fc}(T_{sat}-T_f) \tag{2–29}$$

The subcooled boiling heat flux is calculated using the correlation of Thom (1965):

$$q''_{sub} = 1.95\times10^{-3}\,(T_w-T_{sat})^2 \exp(0.023P) \tag{2–30}$$

(where T and P *must* be expressed in SI units – temperature in K and pressure in bars). The single–phase heat flux is calculated using the Dittus–Boelter relation (Equation 2–24). Combining Equations 2–24, 2–29, and 2–30 and solving for the wall temperature gives:

$$T_w = T_{sat} + [q'' - h_{fc}(T_{sat}-T_f)]^{\frac{1}{2}}\,[22.65\exp(-0.014P)] \tag{2–31}$$

With T_w known, the subcooled boiling and forced convection heat fluxes are calculated using Equations 2–30 and 2–28, respectively.

Transition from partially to fully developed subcooled boiling. Saha and Zuber (1974) recommend a model for the transition from partially to fully developed subcooled boiling (FDB). This model expresses the fluid subcooling at the transition as a function of the heat flux:

$$(T_{sat}-T_f)_{fdb} = (0.0022)\, q''\, D_h/k_l \tag{2–32a}$$

(when $Re_f Pr_l < 70{,}000$), or

$$(T_{sat}-T_f)_{fdb} = (153.8)\,\frac{q''}{Gc_{pl}} \tag{2–32b}$$

(when $Re_f Pr_l \geq 70{,}000$)

The transition criterion can also be written in dimensionless form:

$$St = \frac{455}{Re_f Pr_l} \qquad Re_f Pr_l < 70{,}000 \tag{2–33a}$$

$$St = 6.5\times10^{-3} \qquad Re_f Pr_l \geq 70{,}000 \tag{2–33b}$$

where St is the Stanton number:

$$St = \frac{Nu}{Re_f Pr_l} \tag{2–34}$$

Fully Developed Nucleate Boiling Regime. In this regime there is net vapor generation. Bubbles detach from the wall and flow with subcooled liquid.

Fluid State. In this regime there is no division of the heat flux between different heat transfer mechanisms since the entire surface of the tube is covered with bubbles. Nevertheless the liquid may still be subcooled and, if so, a fraction of the heat addition will increase the liquid temperature. This occurs by condensation of vapor bubbles in the subcooled liquid away from the wall.

Ivey and Morris (1962) suggest that the fraction of the heat flux, E_f, which goes to heating the fluid is:

$$E_f = 1 - \left[1 + 0.1(\rho_l/\rho_g)^{0.75} c_{pl}(T_{sat}-T_f)/h_{fg}\right]^{-1} \qquad (2\text{–}35)$$

In this case the fluid temperature rise in a segment is:

$$\Delta T_f = \frac{4\ \Delta z}{G\ c_{pl}\ D_h} E_f q'' \qquad (2\text{–}36)$$

Note that the bulk fluid temperature will not exceed the saturation temperature, T_{sat}. Once the liquid reaches T_{sat}, the heat transfer regime changes to two–phase forced convection, as discussed below.

Wall Temperature. Thom (1965) recommends this correlation for the wall superheat in fully developed boiling:

$$(T_w - T_{sat}) = 22.65\ (q'')^{0.5} \exp(-0.014P) \qquad (2\text{–}37)$$

(where T and P must be expressed in SI units – temperature in K and pressure in bar).

Transition from subcooled to saturated boiling. The nucleate boiling regime ends when the two–phase forced convection regime begins. To be precise, one could calculate a transition to annular flow based on the local void fraction, and this would represent the transition to two–phase forced convection heat transfer. However the transition void fraction is exceeded almost immediately as soon as the two–phase fluid achieves a positive quality. So it is acceptably accurate and simpler to assume that the nucleate boiling regime ends when the liquid reaches its saturation temperature:

$$T_f = T_{sat} \qquad (2\text{–}38)$$

Two–Phase Forced Convection Regime. Typically most of the evaporator will operate in this regime. This section will first give procedures for calculating the fluid state and wall temperature. The generation of design maps for forced convection fraction, maximum heat flux and maximum wall temperature (such as Figures 2.6 through 2.11) will also be described.

Fluid State. In this regime, all of the heat flux is used to generate vapor and increase the quality of the two–phase mixture. The change in quality, Δx, in a segment of length of Δz is:

$$\Delta x = \frac{4\ q''\ \Delta z}{G\ h_{fg}\ D_h} \qquad (2\text{–}39)$$

To calculate the pressure drop in the evaporator tube (Section 2.2) it will be useful to have an expression for dz/dx. Rearranging Equation 2–39 and taking the limit as Δz approaches zero gives:

$$\frac{dz}{dx} = \frac{G h_{fg} D_h}{4\ q''} \tag{2–40}$$

Wall Temperature. The wall temperature is calculated using the correlation developed by Chen (1963). There are eight steps described below.

1. Calculate the Martinelli parameter, X_{tt}:

$$X_{tt} = \left[\frac{1-x}{x}\right]^{0.9} \left[\frac{\rho_g}{\rho_l}\right]^{0.5} \left[\frac{\mu_l}{\mu_g}\right]^{0.1} \tag{2–41}$$

2. Calculate the Reynolds number factor, F. F can be determined either by examination of Figure 2.6, which shows F as a function of $1/X_{tt}$, or by using the following approximate equations:

$$F \begin{cases} = 1.0 & (\text{for } 1/X_{tt} \le 0.1) \\ = 2.35\ (0.213 + 1/X_{tt})^{0.736} & (\text{for } 1/X_{tt} > 0.1) \end{cases} \tag{2–42}$$

3. Calculate the effective two–phase Reynolds number, Re_{tp}.

$$Re_{tp} = \frac{G(1-x)D_h}{\mu_l} F^{1.25} \tag{2–43}$$

4. Calculate the forced convection heat transfer coefficient, h_{fc}:

$$h_{fc} = (0.023)(k_l/D_h)(Re_{tp})^{0.8}(Pr_l)^{0.33}\ F \tag{2–44}$$

5. Calculate the suppression factor, S. S can be read directly from Figure 2.8, where it is shown as a function of the two–phase Reynolds number. Or S may be calculated from these approximate equations:

$$S = \begin{cases} 0.90 & Re_{tp} \le 1.5\times10^4 \\ 3.09 - 0.234 \ln(Re_{tp}) & 1.5\times10^4 < Re_{tp} < 3.5\times10^5 \\ 0.1 & 3.5\times10^5 \le Re_{tp} \end{cases} \tag{2–45}$$

6. Calculate the factor h_{nb}', which is equal to the nucleate boiling heat transfer coefficient divided by $\Delta T_{sat}^{0.99}$:

$$h_{nb}' = 0.00122 \frac{k_l^{0.79} c_{p_l}^{0.45} \rho_l^{0.49} h_{fg}^{0.51}}{T_{sat}^{0.75} \sigma^{0.5} \mu_l^{0.29} \rho_g^{0.24} v_{fg}^{0.75}} S \qquad (2\text{–}46)$$

(Note that this correlation by Chen suggests that the nucleate boiling component of heat transfer is independent of gravity. However, other workers such as Shah (1976) maintain that gravity effects are significant.)

7. Solve for ΔT_{sat}:

$$\Delta T_{sat}^{1.99} h_{nb}' + \Delta T_{sat} h_{fc} - q'' = 0 \qquad (2\text{–}47)$$

To be precise, Equation 2–47 needs to be solved numerically; however, it is usually accurate enough to approximate this equation as a quadratic in ΔT_{sat}, in which case the solution is:

$$\Delta T_{sat} = \left[(h_{fc}/2h_{nb}')^2 + (q''/h_{nb}') \right]^{0.5} - (h_{fc}/2h_{nb}') \qquad (2\text{–}48)$$

This approximation is accurate for the range of heat fluxes normally encountered in evaporators. If the value of ΔT_{sat} given by Equation 2–48 does not solve Equation 2–47 to an acceptable degree of accuracy, then a few iterations will be enough to converge on an accurate estimate.

8. Calculate the wall temperature, T_w:

$$T_w = T_{sat} + \Delta T_{sat} \qquad (2\text{–}49)$$

Limits to Evaporator Heat Transfer. In a well–designed evaporator, two–phase forced convection is the final heat transfer regime. Following two–phase forced convection comes a liquid deficient region with droplet flow and then a single–phase vapor regime. Both of these regimes are characterized by poor heat transfer coefficients and correspondingly high wall temperatures. A substantial body of literature is available on predicting the end of the two–phase forced convection regime, which is often termed "dryout." However, this analysis is beyond the scope of this design manual report. Interested readers should refer to Collier (1986) for a complete discussion of dryout. Below, simple limits to check are recommended.

Forced Convection Fraction A design criterion for microgravity evaporators is that the fraction of heat transferred by forced convection should be close to 1.0. This fraction can be calculated using the above correlation for heat transfer in the two–phase forced convection regime.

The dimensional design maps in Figures 2.10 and 2.11 apply for specific, constant fluid properties, tube diameter and heat flux. If these parameters are known, then the above procedure (Equations 2–41 through 2–46) shows how to calculate h_{fc} and h_{nb}' as a function of the fluid quality, x. It will always be acceptable to use the quadratic approximation of Equation 2–48 since high forced convection fractions correspond to low values of ΔT_{sat}. The fraction of heat transfer due to forced convection, E_{fc}, is then:

$$E_{fc}(x) = \frac{h_{fc}\Delta T_{sat}}{q''} = \left[1/2 + \left[(1/4)+(q''h_{nb}'/h_{fc}^2)\right]^{0.5}\right]^{-1} \qquad (2\text{–}50)$$

Maximum Heat Flux. The maximum heat flux design maps (Figure 2.12) give the maximum heat flux for microgravity operation. Higher heat fluxes than indicated by these maps require too high a fraction of heat transfer by nucleate boiling. The maps are generated by finding the heat flux which yields a forced convection fraction equal to the design limit (90% for Figure 2.12).

The maximum heat flux is found iteratively at each Reynolds number. First guess a heat flux assuming that all heat transfer is by forced convection alone. Then calculate $E_{fc}(x)$ for a range of qualities representing different positions along the evaporator tube. The average value of E_{fc} along the tube should equal the design limit (e.g. 90%) at the maximum heat flux. If the average forced convection fraction is less than the design limit, then modify the next guess for the heat flux by decreasing it, otherwise increase the heat flux. Recalculate the average E_{fc} until it is acceptably close to the design limit This yields the maximum heat flux.

Wall Temperature. The maximum wall temperature design maps (Figure 2.13) are simple to generate once the maximum heat transfer calculations are complete. These maps simply show the average wall temperature which corresponds to the maximum heat flux. The average wall temperature is simply the arithmetic average of the segment wall temperatures found in the above calculation.

2.1.4 Validation with Microgravity Data

The only experiments which have been performed using a forced–convection evaporator of this type in microgravity are those of Lee (1987). Unfortunately, there are few data from these tests which are useful for validating the microgravity evaporator models. These tests were performed on a KC–135 aircraft which flew parabolic trajectories to provide short periods (~30s) of reduced (but unsteady) gravity. The test loop could not achieve steady state under these conditions. Furthermore, the test conditions and results are not well documented.

Recently, Cuta and Krotiuk (1988) have studied heat transfer data from a few selected tests in an evaporator flown as part of this experiment. Code calculations of the evaporator temperatures are close to the measured data for two of three tests examined. Since the model for saturated boiling in the computer code used in the analysis (COBRA/TRAC) is the same as recommended here, there is preliminary evidence that the model is satisfactory. Additional experiments and analysis are needed for validation, however.

2.2 Pressure Losses

2.2.1 Introduction

The pressure drop through an evaporator determines the pumping power requirement. Generally, good heat transfer performance requires higher pressure drops, so system level tradeoffs are necessary to balance component size and pumping power. For example, the pressure drop through an evaporator tube varies as the mass flux cubed while the maximum heat flux varies as the mass flux squared. Thus, for an evaporator tube there will be a certain mass flux beyond which small increases in heat transfer are accompanied by much greater pressure losses.

This section presents dimensionless design maps to calculate pressure losses in evaporator tubes. The dimensionless design variables provide physical insight and the maps are suitable for scoping level design. These maps ignore the less important heat transfer regimes which contribute only a small fraction of the total pressure drop. More precise estimates of the pressure drop account for all the various heat transfer regimes, and design equations are provided which are suitable for detailed computer calculations.

Pressure losses in an evaporator tube are due to the phenomena illustrated in Figure 2.15, which shows the forces acting on elemental control volume in the evaporator tube. The forces are:

- Wall friction,
- Body forces, and
- Fluid acceleration.

The total pressure drop in the evaporator is the sum of the pressure drops due to these three components. Pressure drops due to wall friction and body forces are similar to the pressure losses in a transport line (Section 1.2). The difference is that the fluid changes phase in an evaporator so the effective fluid properties vary along the tube. The pressure drop due to fluid acceleration is also caused by vaporization of liquid. Since the vapor is less dense than the liquid, it must have a higher velocity. To accelerate the fluid into the vapor phase a force must be exerted on the liquid. This force is the acceleration pressure loss in the evaporator tube.

The components of the pressure drop in one particular R–114 evaporator tube are illustrated in Figure 2.16. Note that almost all of the pressure drop occurs in the two–phase forced convection regime. The friction and fluid acceleration components of the pressure drop are roughly equal. The pressure loss due to body forces is negligible for this case, in which the gravity has magnitude 0.001g (directed opposite the flow vector). The acceleration pressure drop increases linearly along the tube because the heat flux is constant, which causes a constant rate of increase in quality with distance. Frictional pressure losses are roughly proportional to the square of the fluid velocity. The pressure gradient due to friction increases along the evaporator tube because the fluid velocity increases as its density is reduced by vaporization.

2.2.2 Design Maps

This section presents design maps to estimate pressure losses in an evaporator tube. These maps assume that the major pressure losses in the tube are due to the two–phase forced convection regime. If there is a very large subcooling at the entrance to the evaporator, then there may be a significant pressure loss in the single–phase liquid regime as well. Single–phase methods can be used if that is the case.

The basic procedure to estimate the evaporator pressure drop is:

1. Estimate the pressure drop due to friction in the two–phase region (Figure 2.17 and Equations 2–51 to 2–54),
2. Estimate the pressure drop due to body forces in the two–phase region (Figure 2.18 and Equation 2–55),
3. Estimate the pressure drop due to fluid acceleration in the two–phase region (Figure 2.19 and Equation 2–56),

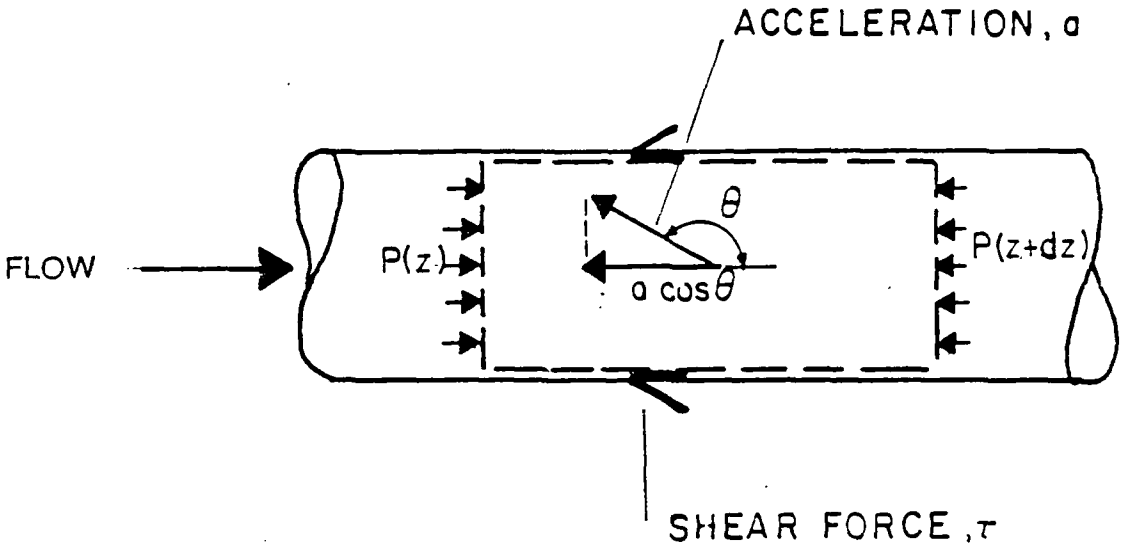

Figure 2.15. FORCES ON AN ELEMENTAL CONTROL VOLUME

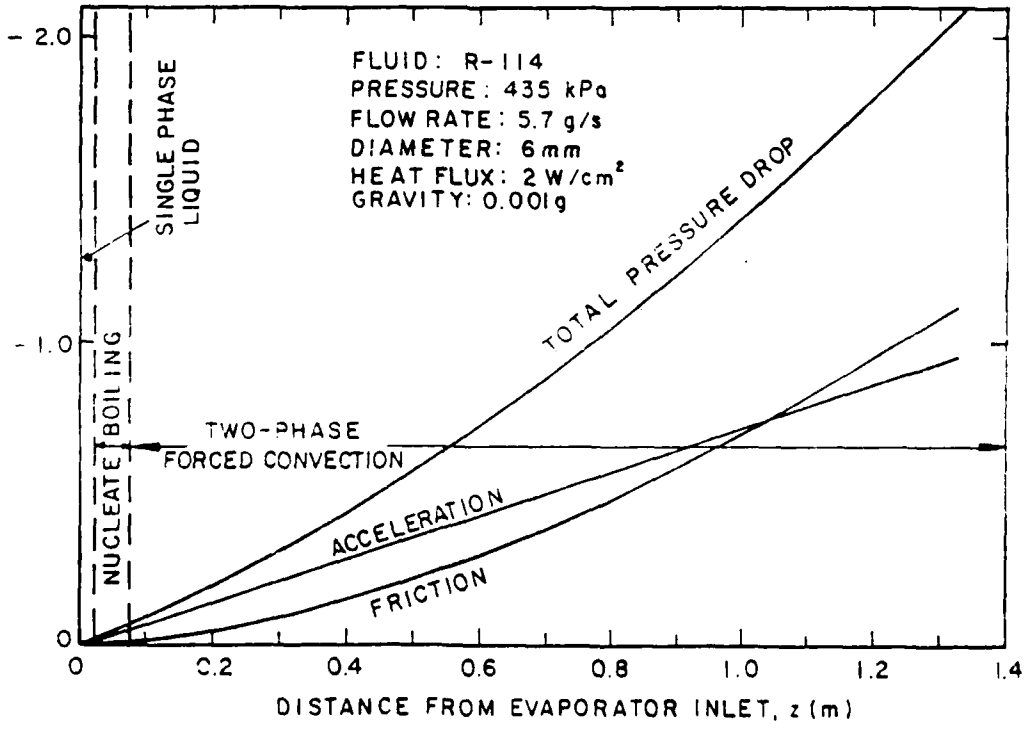

Figure 2.16. PRESSURE LOSSES IN A VERTICAL FORCED CONVECTION EVAPORATOR TUBE (0.001 g)

4. Calculate the total pressure drop in the two–phase region (Equation 2–57).
5. Estimate the pressure drop in the single–phase region (Equations 2–58 and 2–59).
6. Estimate the total pressure drop in the evaporator (Equation 2–60).

The following sections describe the procedure to obtain a best–estimate calculation for the pressure drop in the evaporator.

The main uncertainty in these calculations is the interfacial friction between the liquid and vapor phases in the two–phase forced convection region of the evaporator. The pressure drop can be bounded by choosing high or low values for the interfacial friction.

Calculating Pressure Losses. Most of the pressure drop typically occurs in the two–phase region. Procedures to calculate the three components of the pressure drop are given below. All of the dimensionless pressure drops are expressed as functions of the change in quality in the evaporator.

1) *Friction in the Two-Phase Region*. The procedure to calculate the frictional pressure drop is:

- Calculate the ratio of the liquid phase density to the vapor phase density, ρ_l/ρ_g.
- Locate the curve in Figure 2.17 which corresponds to this value of the density ratio and locate the point on the curve which corresponds to the evaporator outlet quality. Call the ordinate on the map at this point $\Delta P_{fe}^* / 4f_{wl}$.
- Calculate R_{ev}, the thermodynamic ratio of the evaporator:

$$R_{ev} = \frac{4\ q''}{G\ h_{fg}} \qquad (2\text{–}51)$$

- Calculate f_{wl}, the friction factor for liquid–only flow through the evaporator. This friction factor is a function of Re_f, the Reynolds number for liquid–only flow:

$$Re_f = \frac{GD_h}{\mu_l} \qquad (2\text{–}52)$$

The liquid–only friction factor is:

$$f_{wl} = \begin{cases} \dfrac{16}{Re_f} & \text{for } Re_f < 1500 \qquad (2\text{–}53a) \\ 0.046\ Re_f^{-0.2} & \text{for } Re_f \geq 1500 \qquad (2\text{–}53b) \end{cases}$$

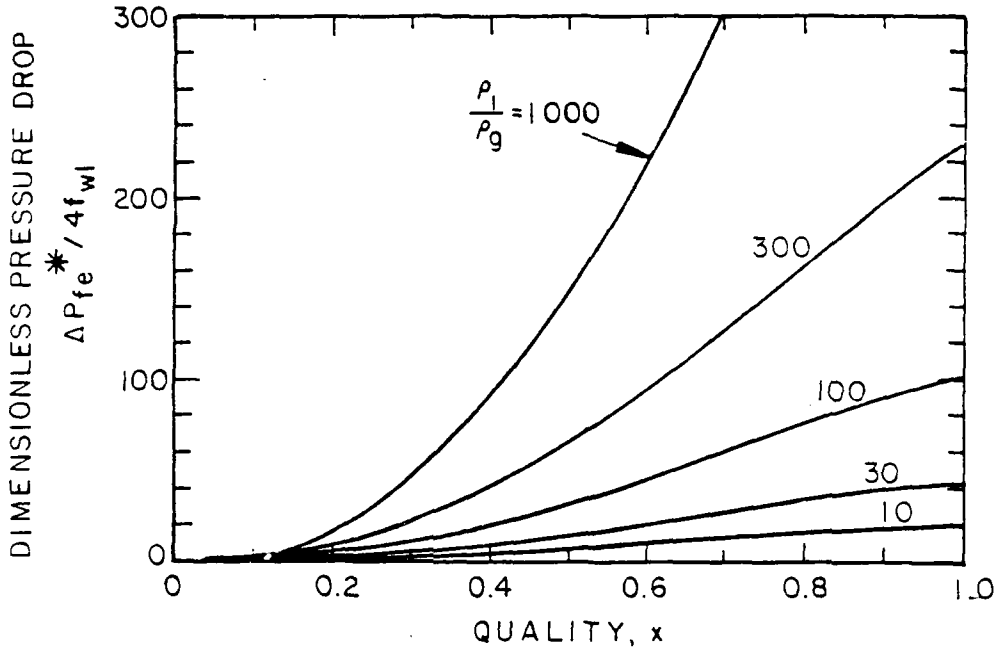

Figure 2.17. DIMENSIONLESS FRICTIONAL PRESSURE DROP IN THE EVAPORATOR

- Calculate ΔP_{fe}, the pressure drop in the two–phase section of the evaporator due to wall friction:

$$\Delta P_{fe} = 4f_{wl}\left[\frac{G^2/2\rho_l}{R_{ev}}\right]\left[\frac{\Delta P_{fe}^*}{4f_{wl}}\right] \qquad (2\text{–}54)$$

2) *Body Forces in the Two-Phase Region.* The procedure to calculate the pressure drop due to body forces is:

- Locate the curve in Figure 2.18 which corresponds to the liquid–to–vapor density ratio, ρ_l/ρ_g. Find the point on this curve which corresponds to the evaporator outlet quality. The ordinate of this plot is the dimensionless pressure drop ΔP_{ge}^*.

- Calculate the dimensional pressure drop, ΔP_{ge}:

$$\Delta P_{ge} = \left[\frac{\rho_l D_h \; a \cos\theta}{R_{ev}}\right]\left[\Delta P_{ge}^*\right] \qquad (2\text{–}55)$$

3) *Acceleration in the Two-Phase Region*. The procedure to calculate the pressure drop due to fluid acceleration in the evaporator is:

- Locate the curve in Figure 2–19 which corresponds to the ratio of liquid–to–vapor density, ρ_l/ρ_g. Find the point on this curve which corresponds to the evaporator outlet quality. The ordinate is the dimensionless pressure drop ΔP_a^*.

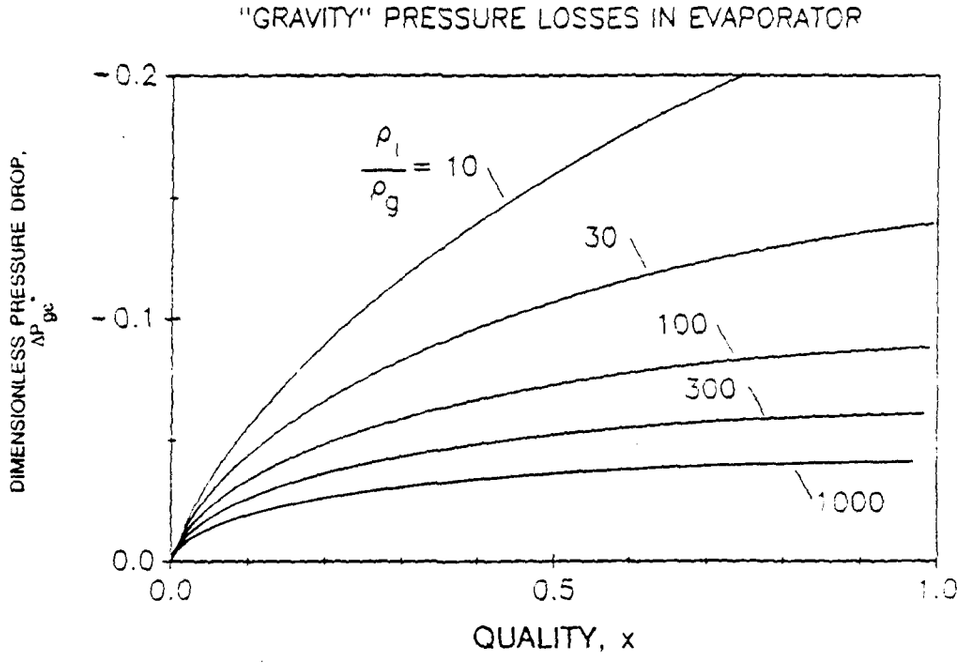

Figure 2.18. DIMENSIONLESS PRESSURE DROP DUE TO BODY FORCES IN THE EVAPORATOR

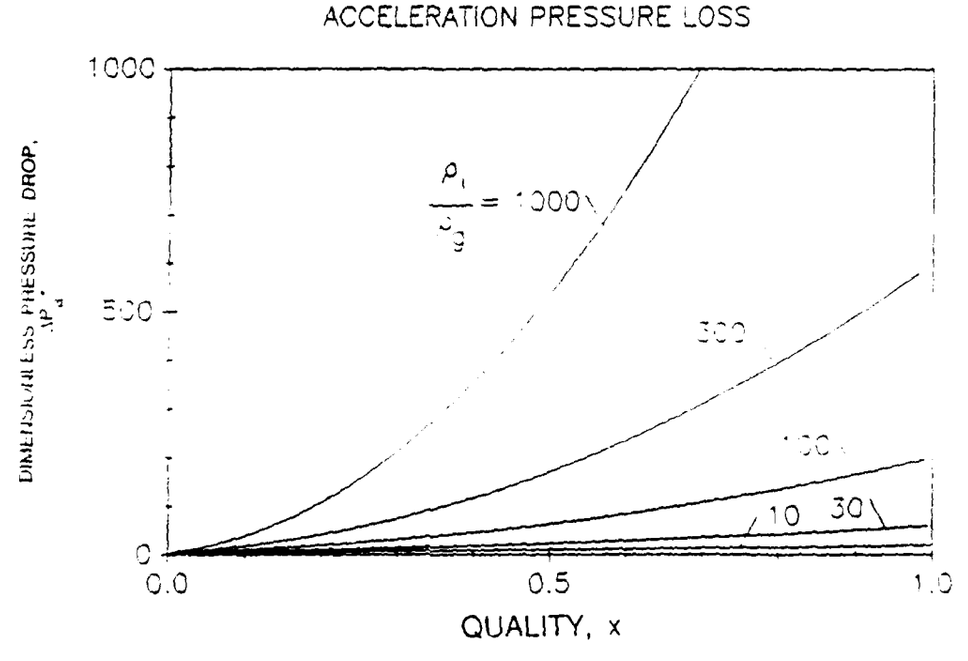

Figure 2.19. DIMENSIONLESS PRESSURE DROP DUE TO FLUID ACCELERATION IN THE EVAPORATOR

- Calculate the dimensional pressure drop, ΔP_a:

$$\Delta P_{ae} = \left[\frac{G^2}{2\rho_l}\right] (\Delta P_a^*) \qquad (2\text{–}56)$$

4) *Total Pressure Drop in Two-Phase Section*. The total pressure drop in the two–phase section of the evaporator, ΔP_{tp}, is the sum of the frictional, body force, and fluid acceleration components:

$$\Delta P_{tp} = \Delta P_{fe} + \Delta P_{ge} + \Delta P_{ae} \qquad (2\text{–}57)$$

5) *Pressure Drop in the Single-Phase Liquid Section*. This pressure drop will be insignificant unless the subcooling is very high. There are only two components of the pressure drop in the single–phase section: friction and body forces. The total pressure drop is easily estimated using parameters already calculated in the procedure for the two–phase section. The procedure is:

- Calculate L_{sc}, the length of the evaporator tube in which single–phase liquid flows. For these scoping calculations it is sufficient to estimate L_{sc} using this equation:

$$L_{sc} \simeq \left[\frac{G\ D_h c_{pl} \Delta T_{sub}}{4\ q''}\right] \qquad (2\text{–}58)$$

- Estimate ΔP_{sp}, the pressure drop in the single phase section:

$$\Delta P_{sp} = 4 f_{wl} \left[\frac{L_{sc}}{D_h} \frac{G^2}{2\rho_l}\right] - \rho_l L_{sc}\, a \cos\theta \qquad (2\text{–}59)$$

(Equation 2–59 can also be used for detailed calculations in which the evaporator is subdivided into many short segments. L_{sc} is simply the segment length (Δz) and ΔP_{sp} is the pressure drop in one single–phase segment.)

6) *Total Pressure Drop*. The total pressure drop in the evaporator tube is the sum of the pressure drops in the single–phase and two–phase sections:

$$\Delta P_{evap} = \Delta P_{tp} + \Delta P_{sp} \qquad (2\text{–}60)$$

where ΔP_{evap} represents the total pressure drop.

Bounding Calculations. The major components of the total pressure drop are friction and fluid acceleration in the two–phase forced convection region. (Figure 2.16 illustrates this dominance.) There is little uncertainty in the acceleration pressure drop, which depends only on the difference between inlet and outlet conditions. The primary uncertainty is the pressure drop calculation due to interfacial friction between the liquid and vapor phases in the annular heat transfer regime of two–phase forced convection.

The design map for friction pressure losses in Figure 2.17 uses the correlation of Wallis (1969) for the interfacial friction factor. This is probably a conservative estimate when applied to space thermal management systems, since it is based on air–water experiments in which the ratio of liquid to vapor phase densities is very large.

A lower bound estimate of the frictional pressure losses in the two–phase forced convection regime can be made using alternate models for the interfacial friction. A limiting case is when the interfacial friction factor is set equal to that for vapor flowing in a smooth pipe. Frictional pressure drops are roughly a factor of 3 lower than those calculated using the Wallis correlation. Alternate interfacial friction models are not presented in this Design Manual.

2.2.3 Detailed Equations for Pressure Losses

This section presents pressure drop equations which can be used in detailed computer calculations. The primary model is separated flow for the annular regime in two–phase forced convection. Homogeneous flow is assumed for the less important nucleate boiling regimes. Further information is available in Collier (1986) or Wallis (1969). Kakac (1988) has shown that this method works well for boiling systems on Earth. Table 2.2 summarizes the pressure drop calculations for all regimes in an evaporator tube. Figure 2.14 shows a scheme for calculating the pressure losses during the detailed heat transfer computation. Equations are provided for friction, body force and fluid acceleration pressure drops in the various heat transfer regimes of an evaporator tube. The following sections provide more detail, and the basis for the dimensionless design maps is also explained.

Friction. The basic equation for the pressure gradient due to wall friction is:

$$(dP/dz)_f = -f\,(4/D_h)\,(G^2/2\rho_l) \qquad (2\text{–}61)$$

in which f is a friction factor, $(4/D_h)$ is the perimeter to area ratio, and $(G^2/2\rho_l)$ is the kinetic energy per unit volume of the fluid. For two–phase flow this expression is modified as follows:

$$(dP/dz)_f = -f_{wl}\,\phi^2\,(1-x)^2\,(4/D_h)\,(G^2/2\rho_l) \qquad (2\text{–}62)$$

Now the friction factor and kinetic energy terms are calculated as if the flow were single–phase liquid. Two–phase effects are lumped into ϕ^2 which is the *two-phase multiplier*. The value of ϕ^2 depends on the fluid properties, the quality and the flow regime as described below.

Two-Phase Forced Convection Regime. This heat transfer regime is characterized by annular flow and the two–phase multiplier is (Collier, 1986):

$$\phi^2 = \frac{1}{(1-\alpha)^2} \qquad (2\text{–}63)$$

where α is the local void fraction. Then the pressure drop due to friction in a short tube segment of length Δz can be calculated using this expression:

$$\Delta P_{fc} = \frac{f_{wl}}{(1-\alpha)^2}\,(1-x)^2\,(4/D_h)\,(G^2/2\rho_l)\,\Delta z \qquad (2\text{–}64)$$

Table 2.2. DETAILED PRESSURE DROP CALCULATIONS FOR AN EVAPORATOR TUBE

HEAT TRANSFER REGIME	FRICTION PRESSURE DROP	BODY-FORCES PRESSURE DROP	ACCELERATION PRESSURE DROP	VOID FRACTION
TWO-PHASE FORCED CONVECTION	$\Delta P_{fc} = \frac{f_{wf}(1-x)^2}{(1-\alpha)^2}\left[\frac{4}{D_h}\right]\left[\frac{G^2}{2\rho_f}\right]\Delta z$	$\Delta P_{ge} = -[\alpha\rho_g+(1-\alpha)\rho_f]\cos\theta\Delta z$	$\Delta P_{ae} = G^2\Delta\left[\frac{x^2}{\alpha\rho_g}+\frac{(1-x)^2}{(1-\alpha)\rho_f}\right]$	$\left[\frac{1-x}{x}\right]^2 = \frac{\rho_f}{\rho_g}\frac{(1-\alpha)^2}{\alpha^{2.5}}\left[\frac{f_f}{f_{wg}}\right]^*$
PARTIALLY OR FULLY DEVELOPED NUCLEATE BOILING	$\Delta P_{fc} = f_{wf}\phi^2\left[\frac{4}{D_h}\right]\left[\frac{G^2}{2\rho_f}\right]\Delta z$ $\phi^2 = \left[1+x\left[\frac{\rho_f}{\rho_g}-1\right]\right]\left[1+x\left[\frac{\mu_f}{\mu_g}-1\right]\right]^{\frac{1}{4}}$	$\Delta P_{ge} = -[\alpha\rho_g+(1-\alpha)\rho_f]\cos\theta\Delta z$	$\Delta P_{ae} = G^2\Delta\left[\frac{x^2}{\alpha\rho_g}+\frac{(1-x)^2}{(1-\alpha)\rho_f}\right]$	$\alpha = \frac{x}{(1-x)(\rho_g/\rho_f)+x}$
SINGLE-PHASE REGION	$\Delta P_{sp} = f_{wf}\left[\frac{4}{D_h}\right]\left[\frac{G^2}{2\rho_f}\right]\Delta z$	$\Delta P_g = -\rho_f a\cos\theta\,\Delta z$	0	0

*$(f_f/f_{wg}) = [1 + 75(1-\alpha)]$ is recommended, although other models could be used.

where ΔP_{fe} is a pressure drop defined by:

$$\Delta P_{fe} = -\int_{z_i}^{z_{i+1}} (dP/dz)_f \, dz \qquad (2\text{–}65)$$

Thus, a positive value of ΔP represents a pressure loss, and a negative value implies a pressure recovery. The void fraction α is the only unknown. The void fraction depends on the local quality, the liquid to vapor density ratio, and f_i/f_{wg}. If the interfacial shear ratio is known, the void fraction is related to the quality by:

$$\left[\frac{1-x}{x}\right]^2 = \left[\frac{\rho_l}{\rho_g}\right] \left[\frac{(1-\alpha)^2}{\alpha^{2.5}}\right] (f_i/f_{wg}) \qquad (2\text{–}66)$$

This equation can be solved iteratively for the void fraction if an expression for f_i/f_{wg} is known. Wallis (1969) recommends the following expression for the shear ratio:

$$f_i/f_{wg} = [1 + 75(1-\alpha)] \qquad (2\text{–}67)$$

Other Heat Transfer Regimes. In the nucleate boiling heat transfer regimes, a homogeneous flow model is recommended to estimate the pressure drop. This model assumes that the liquid and vapor have the same velocity and that the two–phase fluid properties can be estimated by a quality–weighted average of the liquid and vapor properties.

McAdams (1942) recommends this value for the two–phase multiplier based upon a quality–weighted viscosity for the two–phase fluid:

$$\phi^2 = \left[1 + x\left[\frac{\rho_l}{\rho_g} - 1\right]\right]\left[1 + x\left[\frac{\mu_l}{\mu_g} - 1\right]\right]^{-1/4} \qquad (2\text{–}68)$$

The segment pressure drop is then:

$$\Delta P_{fe} = f_{wl} \phi^2 (1-x)^2 (4/D_h) (G^2/2\rho_l) \Delta z \qquad (2\text{–}69)$$

Dimensionless Formulation. The dimensionless formulation for frictional pressure losses assumes that the entire two–phase section of the evaporator can be treated as an annular flow. The rate of pressure decrease with fluid quality, dP/dx, can then be written as:

$$\frac{dP}{dx} = \frac{dP}{dz} \times \frac{dz}{dx} = -\frac{f_{wl}}{(1-\alpha)^2} (1-x)^2 (4/D_h) (G^2/2\rho_l) \frac{dz}{dx} \qquad (2\text{–}70a)$$

$$= -\frac{f_{wl}}{(1-\alpha)^2} (1-x)^2 (4/D_h) (G^2/2\rho_l) \frac{D_h}{R_{ev}} \qquad (2\text{–}70b)$$

$$= -\frac{4f_{wl}}{(1-\alpha)^2} (1-x)^2 (1/R_{ev}) (G^2/2\rho_l) \qquad (2\text{–}70c)$$

Using the dimensionless form of the pressure drop from Equation 2–54, Equation 2–70c is rearranged and integrated:

$$\Delta P_{fe}^{*} = 4 f_{wl} \int_{0}^{x_o} \frac{(1-x)^2 \, dx}{(1-\alpha)^2} \qquad (2-71)$$

For the design map, assume that the entire two–phase section of the evaporator is characterized by annular flow. Then the integral can be evaluated numerically using Equation 2–66 to relate α to x and Equation 2–67 for the interfacial shear ratio. Figure 2.17 plots the results.

Body Forces. The basic differential relation for the pressure gradient drop due to body forces is:

$$(dP/dz)_g = [\, \alpha \rho_g + (1-\alpha) \rho_l \,] \, a \cos\theta \qquad (2-72)$$

Evaluation of this pressure drop in an incremental pipe segment is thus:

$$\Delta P_{ge} = -[\, \alpha \rho_g + (1-\alpha) \rho_l \,] \, a \cos\theta \, \Delta z \qquad (2-73)$$

(The pressure drop is positive when the inlet pressure is greater than the outlet pressure.) The pressure drop depends on the void fraction, α, which in turn depends on the heat transfer regime as discussed below.

Two-Phase Forced Convection Regime. In this regime the void fraction should be evaluated using the same procedure as described above for the case of the friction pressure drop. (See Equations 2–66 and 2–67.)

Other Heat Transfer Regimes. In nucleate boiling heat transfer the flow is assumed to be homogeneous and the void fraction is a simple function of the quality and phase densities:

$$\alpha = \frac{x}{(1-x)(\rho_g/\rho_l) + x} \qquad (2-74)$$

In the single–phase liquid regime the void fraction is zero.

Dimensionless Formulation. The dimensionless expression for the pressure drop due to body forces is obtained as follows:

$$\frac{dP}{dx} = \frac{dP}{dz} \times \frac{dz}{dx} = [\, \alpha \rho_g + (1-\alpha) \rho_l \,] \, a \cos\theta \, \frac{D_h}{R_{ev}} \qquad (2-75)$$

$$= \frac{\rho_l \, a \, D_h \cos\theta}{R_{ev}} [\alpha(\rho_g/\rho_l) + (1-\alpha)]$$

Using Equation 2–55, we can rearrange and integrate Equation 2–75 to obtain:

$$\Delta P_{ge}^{*} = -\int_{0}^{x_o} [\alpha(\rho_g/\rho_l) + (1-\alpha)]\, dx \qquad (2\text{–}76)$$

The dimensionless map for the pressure loss due to body forces (Figure 2.18) is obtained by again assuming that the entire evaporator can be characterized by the dominant heat transfer regime (two–phase forced convection) and using the void fraction/quality relationship for annular flow (Equations 2–66 and 2–67) to numerically evaluate the integral in Equation 2–76.

Acceleration. The basic equation for pressure gradient due to fluid acceleration is:

$$(dP/dz)_a = -G^2 \frac{d}{dz}\left[\frac{x^2}{\alpha}\frac{1}{\rho_g} + \frac{(1-x)^2}{(1-\alpha)}\frac{1}{\rho_l}\right] \qquad (2\text{–}77)$$

Thus the pressure drop in a pipe segment due to fluid acceleration is:

$$\Delta P_a = G^2 \Delta\left[\frac{x^2}{\alpha}\frac{1}{\rho_g} + \frac{(1-x)^2}{(1-\alpha)}\frac{1}{\rho_l}\right] \qquad (2\text{–}78)$$

where the symbol "Δ" is used to represent the value of the bracketed quantity at the tube exit minus the value at the inlet. (Once again, the pressure drop is positive when the pressure gradient is negative.) The pressure drop is independent of the segment length and depends only on the fluid quality and void fraction at the inlet and outlet of the segment. This pressure drop is evaluated using the same void fraction/quality relations described above (Equations 2–66 and 2–67) for the pressure losses due to friction and body forces. The dimensionless form is obtained by dividing Equation 2–78 by $(G^2/2\rho_l)$, as in Equation 2–56, to obtain:

$$\Delta P_a^{*} = \Delta\left[\frac{x^2}{\alpha}\frac{\rho_l}{\rho_g} + \frac{(1-x)^2}{(1-\alpha)}\right] \qquad (2\text{–}79)$$

Figure 2–19 plots this dimensionless result. The curves on the plot can be generated by subtracting the values of the expression inside the brackets of Equation 2–79 when it is evaluated at the evaporator inlet and outlet conditions.

2.2.4 Validation with Microgravity Data

Lee (1988) measured pressure drops in a straight–tube, forced–convection evaporator under simulated microgravity conditions. Unfortunately, the pressure drop data vary greatly with the variable acceleration on the experimental package. Cuta and Krotiuk (1988) show that code calculations (using COBRA/TRAC) are poor compared with the data. Analysis of these data is beyond the scope of this Design Manual.

2.3 References

Bowring, R.W.; *Physical Model Based on Bubble Detachment and Calculation of Steam Voidage in the Subcooled Region of a Heated Channel*; OECD Halden Reactor Project Report HPR–10, 1962.

Chen, J.; *A Correlation for Boiling Heat Transfer to Saturated Fluids in Convective Flow*; ASME Paper 63–HT–34, 1963.

Collier, J.G.; Convective Boiling and Condensation; McGraw–Hill Book Company, 2nd Edition, 1986.

Cuta, J.M. and Krotiuk, W.J.; *Reduced Gravity Boiling and Condensing Experiments Simulated with the COBRA/TRAC Code*; 1st Nat'l. Fluid Dynamics Congress, Part 3, AIAA/SIAM/APS, Cincinnati, Ohio, July 25–28, 1988, pp. 1563–1571.

Davis, E.J. and Anderson, G.H.; *The Incipience of Nucleate Boiling in Forced Convection Flow*; AIChE J., V12, 1966, pp. 774–780.

Eastman, R.E.; *Spacecraft Straight-Tube Evaporator Design*; AFWAL–TR–85–3024, 1985.

Frost, W. and Dzakowic, G.S.; *An Extension of the Method for Predicting Incipient Boiling on Commercially Finished Surfaces*; ASME Paper 67–HT–61, 1967.

Ivey, H.J. and Morris, D.J.; *On the Relevance of the Vapor-Liquid Exchange Mechanism for Subcooled Boiling Heat Transfer at High Pressure*; AEEW–R137, U.K. Atomic Energy Agency, 1962.

Kakac, S., *Two-Phase Flow Thermal Instabilities in a Vertical Boiling Channel*; Fundamentals of Gas–Liquid Flows, E. E. Michaelides and M. P. Sharm, eds., FED Vol 72, ASME, 1988, pp. 49–56.

Lee, D.; *Thermohydraulic and Flow Regime Analysis for Condensing Two-Phase Flow in a Microgravity Environment*; Ph.D. Thesis, Nuclear Engineering, Texas A&M University, December, 1987.

McAdams, W.H. et al; *Vaporization Inside Horizontal Tubes - II - Benzene-Oil Mixtures*; Trans. ASME, 64, 1942, p. 193.

Saha, P. and Zuber, N.; *Point of Net Vapour and Vapour Void Fraction in Subcooled Boiling*; Proc. of 5th International Heat Transfer Conf., Tokyo, Paper B4.7, 1974.

Shah, M.; *A New Correlation for Heat Transfer During Boiling Flow Through Pipes*; ASHRAE Trans., 82(2), 66–8b, 1976.

Thom, J.R.S., et al; *Boiling in Subcooled Water During Flow Up Heated Tubes or Annuli*; Paper 6 presented at the Symposium on Boiling Heat Transfer in Steam Generating Units and Heat Exchangers, Inst. Mech. Engrs., Manchester, England, 1965.

Wallis, G.B.; One–Dimensional Two–Phase Flow; McGraw–Hill Book Company, 1969.

3 CONDENSERS: High Vapor Shear Condensers

Condensers transfer heat between two–phase heat transport systems and spacecraft heat rejection systems such as radiators. The condenser allows for controlled condensation of the two–phase working fluid so that heat can be efficiently and reliably removed from the two–phase loop. Overall design goals are similar to those of the evaporator. The condenser should be small and lightweight, have small pressure losses, and operate regardless of the spacecraft's acceleration. Small component size requires high heat fluxes during condensation. Since condensate films are typically the main heat transfer resistance, condensers require thin films or large temperature differences. For spacecraft thermal management systems, thin films and small temperature differences are preferred in order to minimize radiator area.

The absence of large body forces in microgravity makes phase control an important design issue. Gravity is often used on Earth to drain condensate from the heat transfer surface, but in space the condensate tends to accumulate and impede heat transfer. A number of different schemes have been devised for condensate control with two main approaches: high vapor shear (friction) forces and capillary forces.

Vapor shear is a simple way to control the thickness of the condensate layer and is the focus of this Design Manual. In a high vapor shear condenser, the vapor moves at high speed and exerts a high drag force on the condensate film. The film is thus propelled at high velocity and its thickness and resistance to heat transfer are reduced. This section presents recommended design methods for high vapor shear condensers where the flow geometry is a straight tube with uniform cross–section. An alternate concept, not covered in this Design Manual, is a tapered flow channel which maintains high vapor velocity as condensation occurs and the vapor mass flow rate decreases. Thin films are maintained over a longer distance than for channels with uniform cross–section. The design trade–off for the tapered geometry is increased heat transfer (and condensation rate) at the expense of increased pressure drop. (Furthermore, a condenser with a tapered tube operates best at only one flow condition.) Other proposed concepts involve suction of liquid through the condenser wall to maintain thin liquid films. The condenser models presented here cover basic phenomena which are similar in these alternate designs.

The capillary approach uses the surface tension of the liquid to separate the phases. No models for this type of condenser are addressed in this design manual.

Control of non–condensible gases is another important design issue. If these gases accumulate within the condenser, they can impede heat transfer. Thus condensers must provide for continuous removal of non–condensible gases from heat transfer surfaces. In high vapor shear condensers, the high velocity vapor continuously purges non–condensible gases from the condenser tube.

This section reviews the important phenomena during condensation heat transfer and presents two types of design tools for high vapor shear condensers. Design maps have been developed for scoping design, and equations are presented for detailed computer calculations of condenser performance.

This section focuses on the high vapor shear approach to condenser design. Shear condensers are used in the Boeing/Sundstrand and OAO thermal management systems being developed. This section specifically addresses condensation inside a circular tube with a constant diameter. Understanding this basic case is also the first step in designing more complex components, such as the tapered condensers with decreasing cross–sections which maintain high vapor velocity.

The discussion is divided into two major sections: heat transfer (Section 3.1) and pressure drop (Section 3.2). The heat transfer section instructs the designer in selecting tube length, temperature differences, mass flux, and other thermodynamic design variables. The pressure drop section shows the designer how to estimate pressure losses so that the pumping power can be calculated.

3.1 Heat Transfer

The condenser has heat transfer regimes which are analogous to those in the straight–tube evaporator. The dominant regimes are annular condensation and single–phase liquid cooling as described in Section 3.1.1. Section 3.1.2 presents design maps which enable the designer to quickly estimate the required tube length in both of these regimes. Section 3.1.3 presents detailed models for all heat transfer regimes which can be used in computerized calculations for final design or optimization. Finally, Section 3.1.4 reviews the available data from microgravity condenser experiments.

3.1.1 Introduction

In general, there are several possible boundary conditions for a condenser tube. This section focuses on the case of a fixed temperature on the outer wall of the condenser. The input variables for design in this case are illustrated schematically in Figure 3.1. They are the mass flux, tube diameter, inlet and outlet fluid conditions, and the temperature difference between the condensing fluid and the condenser secondary coolant. This is the most common situation for condensers, approximating such physical situations as radiators and heat exchangers with a high heat capacity in the flow on the secondary (coolant) side. This case is of particular interest for space thermal management systems because heat pipes (which are

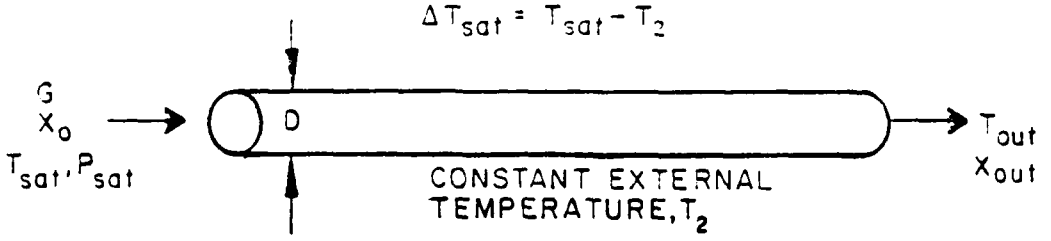

Figure 3.1. DESIGN INPUTS FOR A HIGH VAPOR SHEAR CONDENSER TUBE

constant temperature devices) may be used to reject heat. The basic differential relations presented in Section 3.1.3 are generally applicable regardless of the actual boundary conditions and can be used as the building blocks of customized design tools for any specific application.

Heat Transfer Regimes. As vapor becomes liquid within the condenser tube, the void fraction and quality decrease, leading to a succession of flow and heat transfer regimes. Figure 3.2 illustrates the general sequence of flow and heat transfer regimes in a high vapor shear condenser. In general the sequence from the condenser inlet to the outlet will be:

1. Annular condensation,
2. Slug condensation,
3. Bubbly condensation, and
4. Single–phase liquid cooling.

Most of the condensation heat transfer occurs in the annular regime, so high vapor shear condensers can be characterized as operating mainly in annular flow. The lengths of the slug and bubbly regimes are typically very short in relation to the overall tube length. The length of the single–phase liquid section depends on the degree of outlet subcooling which is desired. High subcooling requires a long single–phase section.

Annular Condensation. This is the first heat transfer regime in the condenser, characterized by high vapor velocity, high void fraction and high flow quality. Vapor flows in a cylindrical core and liquid condensate flows in an annular film on the tube wall. Heat transfer is limited by conduction across the liquid film, which is typically in laminar flow. As more vapor is condensed, the thickness of the liquid film increases which, in turn, reduces the heat flux. High gas velocity results in high vapor shear which improves heat transfer by reducing the film thickness.

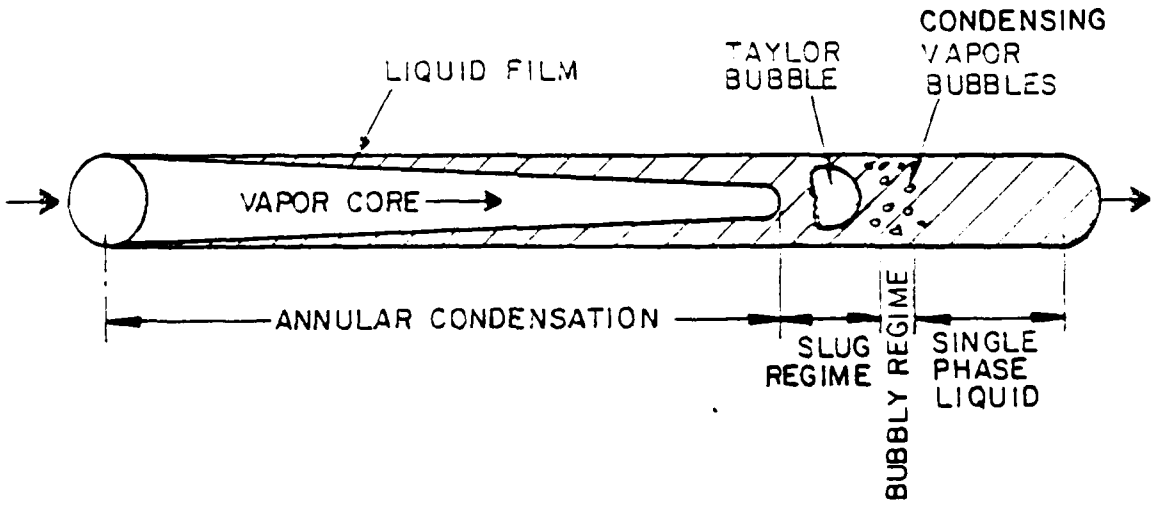

Figure 3.2. HEAT TRANSFER REGIMES IN A HIGH VAPOR SHEAR CONDENSER

The annular condensation regime ends when there is insufficient vapor left in the tube to support annular flow. Usually this occurs for void fractions of about 0.75, corresponding to a flow quality of about 0.10. Condensate bridges the tube, and the slug condensation regime begins.

Slug and Bubbly Regimes. Slug and bubbly regimes are low quality regimes intermediate between the annular condensation and single–phase liquid regimes. Typically these flow regimes are not present over very much of the tube length and can be neglected in first–order scoping calculations.

In the slug condensation regime, vapor flows in Taylor bubbles in the center of the tube, separated by liquid slugs. Heat transfer occurs by two mechanisms: conduction across the liquid film which surrounds the bubbles and single–phase convection into the liquid slugs. The heat flux in this regime can be quite high because the slugs move very quickly initially, leading to high convective heat transfer coefficients. As vapor condenses and the void fraction decreases, the slugs become bigger and the bubbles smaller. Eventually the large Taylor bubbles become unstable and break up into smaller bubbles, initiating the bubbly condensation regime.

In the bubbly condensation regime the vapor is present as small bubbles in a continuous liquid phase. The void fraction and quality are both low. Heat is transferred to liquid at the tube walls, then to the bubbles which condense.

One concern with this type of condenser is that the condensation process for vapor bubbles may be unsteady in the slug and bubbly flow regimes. The concern is that this would lead to unsteady behaviors similar to, but not as severe as, waterhammer phenomena. Preliminary analysis and experimental data indicate that this concern is unfounded.

Single-phase Liquid. After all the vapor has condensed, the liquid approaches the temperature of the secondary coolant. Heat transfer in this regime is simple forced convection to single–phase liquid. The degree of subcooling desired and the temperature of the secondary coolant determine the length of the "subcooler" portion of the condenser.

Typical Behavior. The calculated flow quality and void fraction in an R–114 condenser are illustrated in Figure 3.3. This condenser tube is 6 mm in diameter, and 2.8×10^{-3} kg/s of condensing fluid flows through at a saturation pressure of 435 kPa. The temperature difference driving condensation is 40 K.

The figure shows the dominance of annular condensation. In this regime, the void fraction remains high (over 80 percent) because the liquid is confined to a very thin film on the tube wall. The quality decreases steadily due to condensation. When the void fraction falls to a critical value (about 0.73 m into the tube) liquid slugs start to form. The quality at this point is roughly 15 percent and decreases rapidly due to high heat transfer in the slug regime. The large Taylor bubbles condense, and bubbly flow is present for a few centimeters. Single–phase liquid fills the final 15 cm of the tube. Only a small amount of subcooling (indicated by the small, negative quality at the tube exit) is achieved in this short length.

Figure 3.4 shows the predicted heat flux profile in this condenser. The total amount of heat transfer is proportional to the area under the heat flux curve. Approximately 85 percent of the heat transfer occurs in the annular regime, while the remaining 15 percent occurs in the slug, bubbly, and single–phase regimes combined. In the annular regime, the heat flux is inversely proportional to the thickness of the liquid film. Thus the heat flux is very high at the

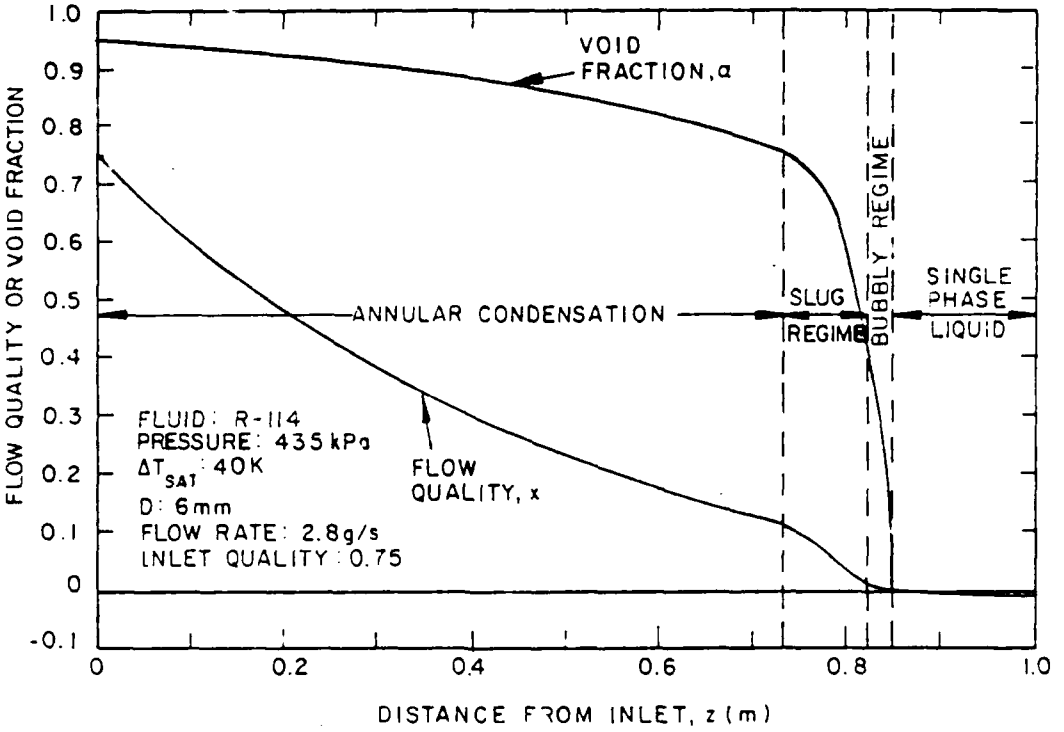

Figure 3.3. VOID FRACTION AND FLOW QUALITY IN A HIGH VAPOR SHEAR CONDENSER

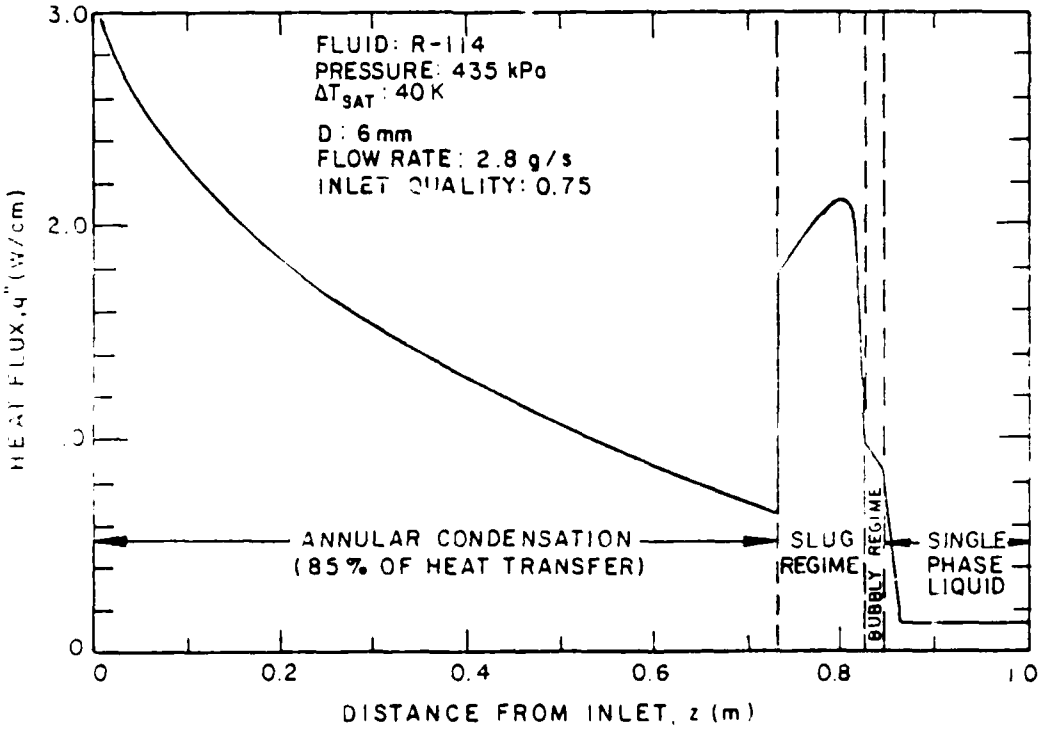

Figure 3.4. HEAT FLUX PROFILE IN A HIGH VAPOR SHEAR CONDENSER

tube entrance, where the film is quite thin, but decreases along the length of the tube as more vapor condenses and the film thickens. The heat flux increases in the slug regime because the high velocity liquid slugs have high convective heat transfer coefficients. The heat flux decreases sharply in the short bubbly regime and reaches its lowest value in the single–phase liquid.

3.1.2 Design Maps

The most common condenser design problem is to determine the tube length which is necessary to condense and cool the working fluid. This section presents dimensionless maps which enable the designer to estimate the length of the condenser given the major design parameters.

The quick design procedure is to:

- Check that the simple design maps will apply (Equation 3–1),
- Calculate the thermodynamic ratio for the condenser (Equation 3–2),
- Estimate the length of the two–phase region of the condenser (Figure 3.5 or 3.7 and Equation 3–4),
- Estimate the length of the single–phase region of the condenser (Figure 3.6 and Equation 3–8), and
- Calculate the total length of the condenser (Equation 3–9).

To perform the calculations presented in this section, the following design parameters are needed:

Fluid Properties

ρ_l	Liquid phase density (kg/m^3)
ρ_g	Vapor phase density (kg/m^3)
μ_l	Liquid phase viscosity (kg/m–s)
μ_g	Vapor phase viscosity (kg/m–s)
k_l	Liquid phase thermal conductivity (W/m- K)
h_{fg}	Latent heat of vaporization (J/kg)
σ	Surface tension (N/m)

Condenser Tube Properties

t_w	Condenser wall thickness (m)
k_w	Wall thermal conductivity (W/m–K)

Geometry

D	Condenser tube diameter (m)

Flow Rates

G	Mass flux of condensing fluid (kg/m^2–s)
x_0	Inlet quality of condensing fluid (–)

Temperatures

T_{sat} Saturation temperature of condensing fluid (K)
T_2 Temperature of the secondary condenser coolant (K)
T_{sub} The condensing fluid's outlet temperature (K)

Check Tube Thermal Resistance. The design maps presented here will apply if the thermal resistance of the condenser tube itself is less than that of the condensate film:

$$\frac{D}{t_w} > 200 \frac{k_l}{k_w} \tag{3–1}$$

If this condition is not satisfied then the detailed thermal models presented in section 3.1.3 should be used to design the condenser.

Condenser Thermodynamic Ratio. In order to use the design maps presented below, the value of the condenser thermodynamic ratio, R_c must be calculated. The thermodynamic ratio is defined as:

$$R_c \equiv \frac{4\ k_l\ \Delta T_{sat}}{G\ D\ h_{fg}} = \frac{4\ Ja}{Re_f\ Pr_l} \tag{3–2}$$

where $\Delta T_{sat} = T_{sat} - T_2$,
Ja = the Jakob number $(c_{pl}\Delta T_{sat}/h_{fg})$,
Re_f = the Reynolds number based only on the liquid flow (GD/μ_l), and
Pr_l = the Prandtl number of the liquid $(\mu_l c_{pl}/k_l)$.

The thermodynamic ratio is proportional to the ratio of the condensing mass flux to the inlet mass flux. The design maps below only apply for values of R_c less than a critical value:

$$R_c < 10^{-4} \tag{3–3}$$

Basically, this is the range for which the design curves are not themselves functions of R_c. For thermodynamic ratios greater than 10^{-4}, the detailed design models presented in Section 3.1.3 are recommended.

Dimensionless design maps can be made for thermodynamic ratios larger than 10^{-4}, however in this case the maps themselves become a function of R_c.

Length of Two–Phase Condenser Region. Figure 3.5 shows the dimensionless condenser length required to completely condense the fluid from the quality at the inlet of the condenser (i.e., from $x = x_o$ to $x = 0$). The procedure to calculate the two–phase condenser length is:

1) Calculate the ratio of the liquid to vapor density, ρ_l / ρ_g.

2) Locate the curve in Figure 3.5 which corresponds to this density ratio.

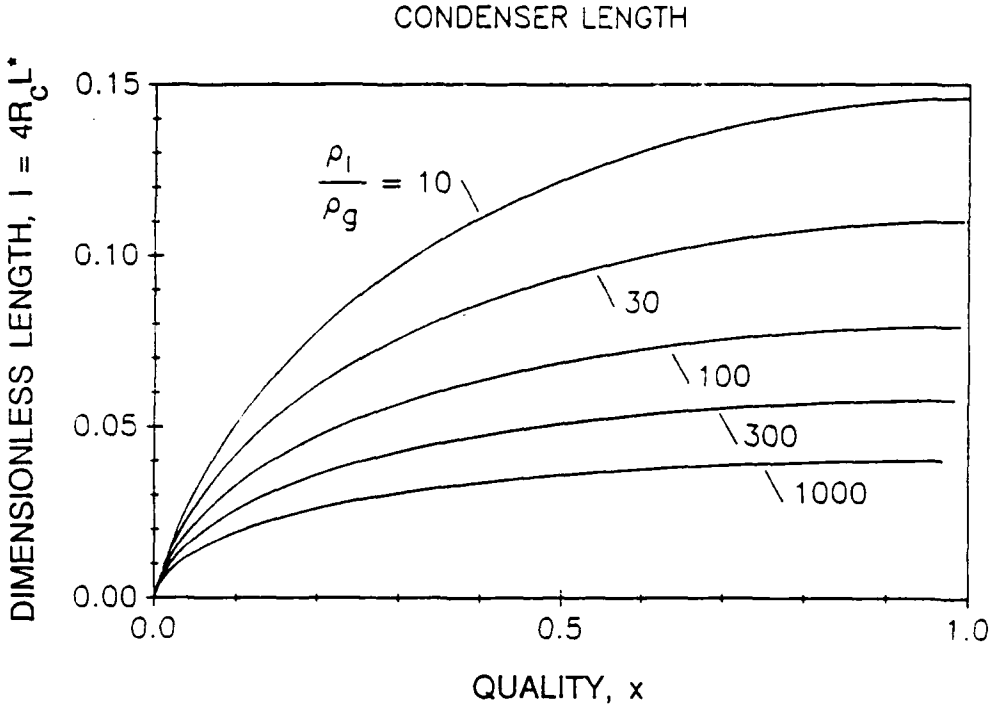

Figure 3.5. DESIGN MAP FOR THE LENGTH OF THE TWO–PHASE (ANNULAR) REGION OF THE HIGH VAPOR SHEAR CONDENSER ($f_i/f_{wg} = [1 + 75\ (1-\alpha)]$)

3) Find the point on that curve which corresponds to the required reduction in fluid quality. Determine the value of the point on the y–axis which corresponds to this point. This is the dimensionless length. The dimensionless length is determined by evaluating an integral (see Section 3.1.3), and is called the dimensionless integral I.

4) Calculate L_{tp}, the two–phase length required to condense the fluid:

$$L_{tp} = l \frac{D}{4R_c} \qquad (3-4)$$

Using Equation 3–2 in Equation 3–4 shows that the two–phase condenser length depends on the key design variables as follows:

$$L_{tp} \sim \frac{G\ D^2\ h_{fg}}{k_l \Delta T_{sat}} \qquad (3-5)$$

For example, the condensing length can be halved by doubling the temperature difference between the two–phase and secondary coolants or by decreasing the tube diameter by 30 percent. The length of the condenser is doubled if the mass flux is doubled.

Length of Single–Phase Heat Transfer Region. The length of the single–phase portion of the condenser depends upon the secondary coolant temperature and the degree of exit subcooling which is required. ("Subcooling" is the amount by which the fluid exit temperature is less than the saturation temperature.) If only a small amount of subcooling is required, then the single–phase portion of the condenser does not need to be very long. However, in two–phase loops using mechanical pumps the subcooling may need to be relatively high in order to provide the pump with adequate net positive suction head (NPSH). In these cases the single–phase length can be a significant fraction of the total condenser length because the heat transfer in this regime is much less efficient than in the condensing section. (Actual thermal management systems may have a separate, single–phase "subcooler" to cool the condensate more efficiently than the condenser tube.)

The length of the single–phase section depends upon the liquid Reynolds number, the liquid Prandtl number, the secondary coolant temperature and the liquid outlet temperature. The procedure to calculate the single–phase length is:

1) Calculate the liquid Prandtl number, Pr_l:

$$Pr_l = \frac{\mu_l c_{pl}}{k_l} \qquad (3–6)$$

2) Calculate the liquid Reynolds number, Re_f:

$$Re_f = GD/\mu_l \qquad (3–7)$$

3) Find the curve in Figure 3.6 which corresponds to the liquid Prandtl number and locate the point on the curve which corresponds to the liquid Reynolds number. This dimensionless length is called I_{sp}.

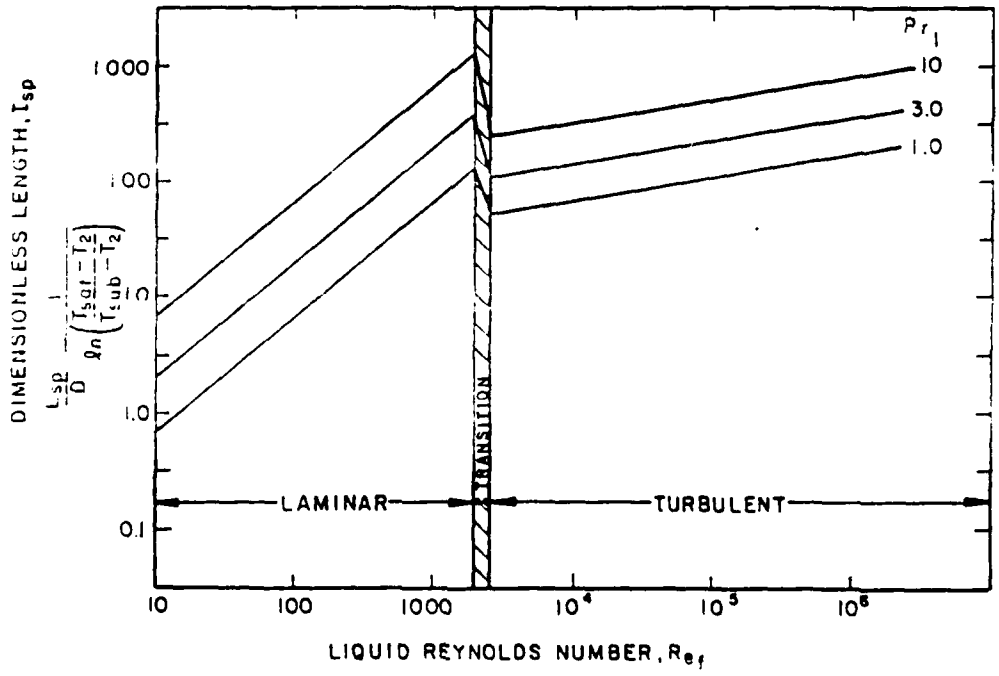

Figure 3.6. DESIGN MAP FOR THE LENGTH OF THE SINGLE–PHASE REGION OF THE CONDENSER

4) Calculate L_{sp}, the required length of the single–phase portion of the condenser:

$$L_{sp} = I_{sp} D \ln\left[\frac{T_{sat}-T_2}{T_{sub}-T_2}\right] \qquad (3\text{–}8)$$

The dependence of the single–phase tube length on the design variables is somewhat counter–intuitive because condenser tubes with larger Reynolds numbers require *longer* tubes to achieve the same subcooling. This is particularly true in the laminar flow regime. The reason is that increased flow through the condenser tube acts primarily to reduce the length of time that each element of fluid can be cooled. There is a compensating effect due to increased heat transfer coefficients for higher flow rates (in the turbulent flow regime), but this is not enough to reduce the required tube length.

Total Condenser Length. The total length of the condenser, L_{tot}, is the sum of the two–phase and single–phase lengths:

$$L_{tot} = L_{tp} + L_{sp} \qquad (3\text{–}9)$$

Uncertainty. The major uncertainty in this design calculation is in the value of the "interfacial friction factor". This parameter quantifies the drag between the vapor core and the liquid film in the annular condensation regime. The design map which has been presented (Figure 3.5) gives a best–estimate of the condenser length using Wallis's correlation for interfacial friction (Wallis, 1969). This correlation represents data from horizontal and vertical tubes at earth gravity.

If the tube length is a critical parameter, an upper bound can be obtained using the alternate design map shown in Figure 3.7. This figure shows the same design information as the best–estimate design map, except that the vapor/liquid interface is assumed to be perfectly smooth in the alternate case (i.e. the interfacial friction factor is the same as if the gas were flowing alone in a smooth pipe). The procedure to use this alternate design map is the same as for the best–estimate map.

Lengths calculated from the alternate map are typically twice the lengths calculated using the best–estimate map. These conservative estimates of the condensing length are greater than the best–estimate values because lower interfacial friction maximizes the liquid film thickness and thus reduces the rate of condensation. The alternate design map uses the minimum possible interfacial friction and thus yields the maximum possible condensing length.

One reason for considering this bounding case for interfacial friction and condensation heat transfer is to bound the range of uncertainty due to the effects of gravity. Preliminary data from microgravity experiments (Chen et al., 1988) indicate that interfacial friction may be less than at earth gravity.

Another reason for considering the bounding model is the effect of gravity on the liquid distribution around the perimeter of the tube in the two–phase region. For this low gravity application, the condensate is assumed to be distributed uniformly around the perimeter of the tube. On earth, or under acceleration, the liquid may be distributed asymmetrically. A detailed analysis by Keshock and Sadeghipour (1981) concludes that heat transfer may be slightly worse under microgravity conditions than at earth gravity due to the non–uniform

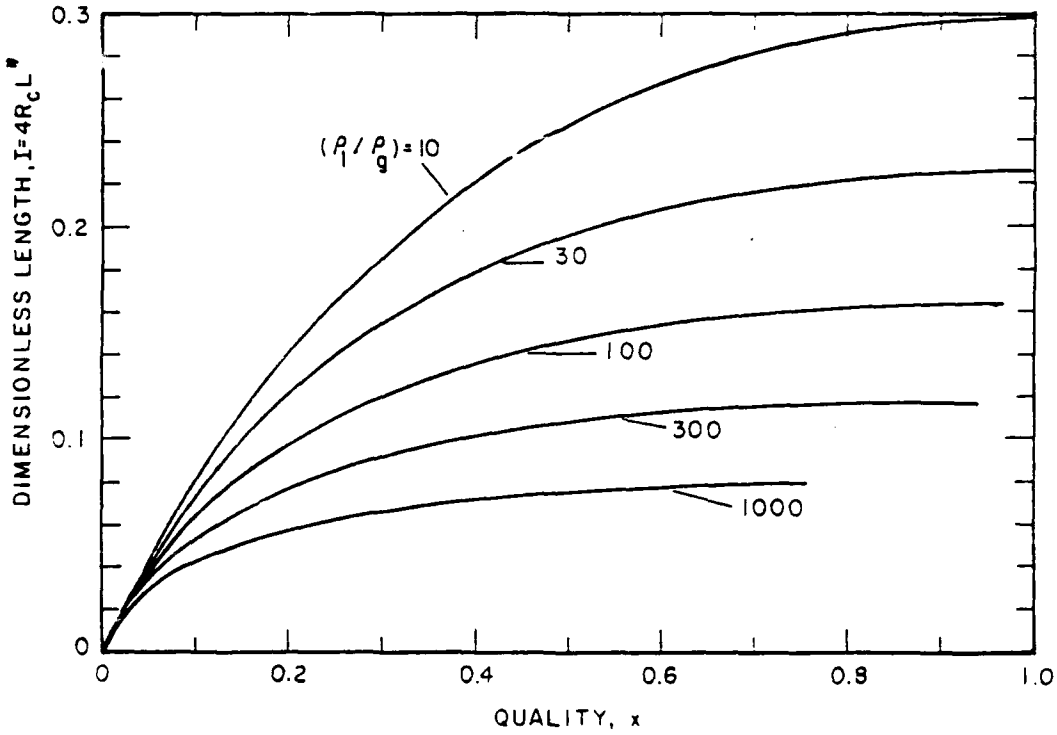

Figure 3.7. DESIGN LIMIT FOR THE LENGTH OF THE TWO-PHASE (ANNULAR) CONDENSER REGION ($f_i / f_{wg} = 1.0$)

distribution of the liquid film (because the average film thickness will be slightly thicker under microgravity conditions). Microgravity experiments aboard an aircraft, however, led Keshock (1974) to conclude that the average heat transfer rates were about the same under microgravity and earth gravity. So the simple assumption of a uniform liquid film may be sufficient, based upon preliminary data.

Laminar flow of liquid in the liquid film has been assumed so that thermal conduction controls the heat transfer. If the Reynolds number in the liquid film is large ($Re_f = (1 - x)GD/\rho_l > 4000$), then turbulence in the liquid film can increase the heat transfer in the liquid film. The condition with a turbulent liquid film is not treated in this Design Manual, although the approach to include the effect is outlined in the Section 3.1.3.

Another modelling uncertainty is the effect of liquid entrainment on heat transfer in the condenser. Entrainment of liquid will reduce the thickness of the liquid film and improve heat transfer. (The effect on the pressure drop will be small.) This effect is not accounted for in this Design Manaual.

3.1.3 Equations for Heat Transfer

To first order, a high-vapor shear condenser can be sized assuming only one or two heat transfer regimes (annular condensation and single-phase liquid, as shown in Section 3.1.2). For final design or optimization, however, the detailed behavior of the condensing fluid in all heat transfer regimes should be considered.

This section presents detailed design relationships for each heat transfer regime. Procedures are given to generate design plots for specific cases or to program computerized calculations for high vapor shear condensers. The usual way to use these equations is to divide the evaporator tube into a number of segments and to assume that the fluid properties are constant within each segment. In each segment there are three basic calculations:

- Calculate the heat flux,
- Determine the conditions at the segment exit, and
- Check for regime transition.

Table 3.1 summarizes the equations for these calculations in each of the heat transfer regimes. Figure 3.8 shows schematically the sequence for performing these calculations. The following sections provide more detail.

About one hundred segments are usually sufficient. The quality and flow rate entering the first segment are known from the condenser inlet conditions. Exit conditions calculated for one segment become the inlet conditions for the next. The following sections show how to calculate the fluid state, heat flux and regime transitions in each of the heat transfer regimes experienced by the fluid as it travels through the condenser: annular, slug and bubbly condensation followed by single–phase liquid cooling.

Annular Condensation Regime. The major phenomena which govern heat and mass transfer in this regime are conduction of heat across the liquid film and interfacial shear. Figure 3.9 shows the major variables used to analyze this regime. A similar analysis has been developed by Chow (1986), and Collier (1986) also discusses film condensation with vapor shear.

The procedure requires three main inlet conditions for each segment to be calculated: liquid velocity u_f, vapor velocity u_g, and film thickness δ. The procedure below shows how to calculate these three parameters at the segment exit as a function of the inlet values. The exit values from one segment can be the inlet values for the next. Or a more complex iterative scheme is possible in which the inlet and exit values of velocity and film thickness for each segment are used to estimate the average values in that segment. The procedure which follows can be adapted for either method.

Inlet Conditions. To begin calculations in the annular regime, the following parameters must be known:

- Fluid properties – ρ_l, ρ_g, μ_l, μ_g, h_{fg}, k_l, σ,
- Temperatures – T_{sat}, T_2,
- Flow rates – G, x_o (inlet quality),
- Velocities – u_{go}, u_{fo} (gas and vapor inlet velocities), and
- Inlet film thickness – δ_o.

Table 3.1. HEAT TRANSFER CALCULATIONS FOR A HIGH-VAPOR SHEAR CONDENSER

REGIME	HEAT FLUX	FLUID STATE AT SEGMENT EXIT	SIMPLE REGIME CRITERION
ANNULAR CONDENSATION	$q'' = \dfrac{\Delta T_{sat}}{\left(\dfrac{\delta}{k_l} + \dfrac{t_w}{k_w}\right)}$	$\delta_k = \left[\delta_{k-1}^3 + \dfrac{3\,\Delta z_k u_{fk}^2\, Ja}{\tau_{ik}\rho_l Pr_l}\right]^{1/3}$ $u_{fk} = u_{fk-1}\left(\dfrac{\delta_{k-1}}{\delta_k}\right) + \dfrac{G_c \Delta z_k}{\rho_l \delta_k}$ $u_{gk} = u_{gk-1} - \dfrac{4G_c \Delta z_k}{\rho_g D}$	$0.80 \le \alpha \le 1.0$
SLUG CONDENSATION	$q'' = \dfrac{\Delta T_{sat}}{\left(\dfrac{1}{h_{av}} + \dfrac{t_w}{k_w}\right)}$ $h_{av} = \left(\dfrac{L_b}{L_t}\right) h_f + \left(1 - \dfrac{L_b}{L_t}\right) h_{fc}$	$x_k = x_{k-1} - \dfrac{4q''\Delta z_k}{G\, Dh_{fg}}$ $j_k = G\left(\dfrac{x_k}{\rho_g} + \dfrac{1-x_k}{\rho_l}\right)$ $U_{bk} = j_k \left\{1 + 1.27\left[1 - \exp\left[-.38\left(\dfrac{\mu_l j_k}{\sigma}\right)^{0.8}\right]\right]\right\}$ $m_k \simeq \min\left[0.16, 0.56\left\{1 - \exp\left[-2.64\left(\dfrac{\mu_l u_{bk}}{\sigma}\right)^{0.567}\right]\right\}\right]$ $\alpha_k = \dfrac{x_k(1-m_k)}{x_k + (\rho_g/\rho_l)(1-x_k)}$	$0.45 \le \alpha \le 0.80$
BUBBLY CONDENSATION	$q'' = \left[\dfrac{\Delta T_{sat}}{\dfrac{1}{h_{tp}} + \dfrac{t_w}{k_w}}\right]$	$x_k = x_{k-1} - \dfrac{4q''\Delta z_k}{GDh_{fg}}$	$0 \le \alpha \le 0.45$
SINGLE-PHASE LIQUID	$q''(z_{sp}) = U\Delta T_{sat} \exp\left[-\dfrac{4Uz_{sp}}{GDc_{pl}}\right]$	$T_f(z_{sp}) = T_{sat} - \Delta T_{sat}\left\{1 - \exp\left[-\dfrac{4Uz_{sp}}{GDc_{pl}}\right]\right\}$	$\alpha = 0$

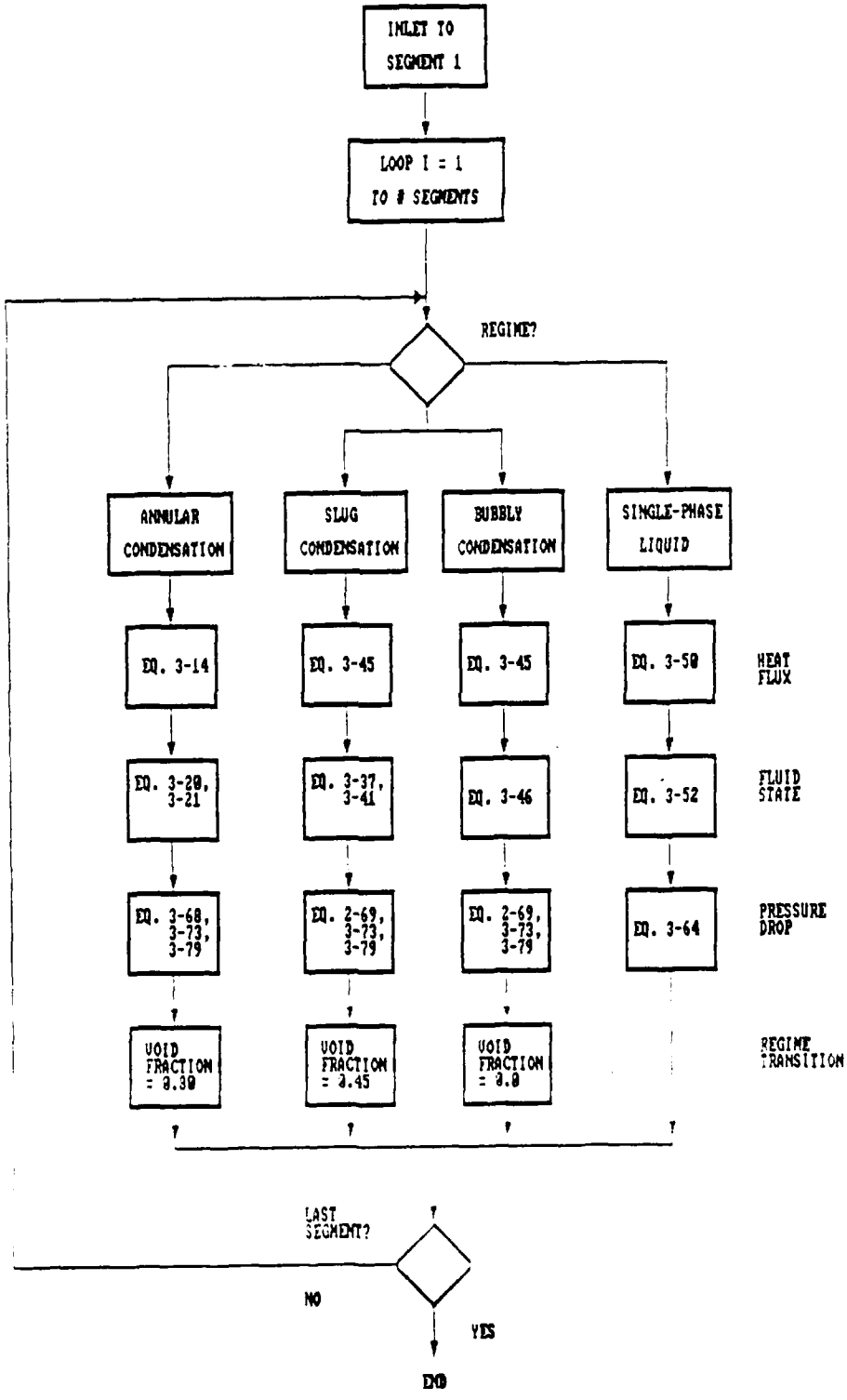

Figure 3.8. FLOWCHART FOR DETAILED CONDENSER CALCULATIONS

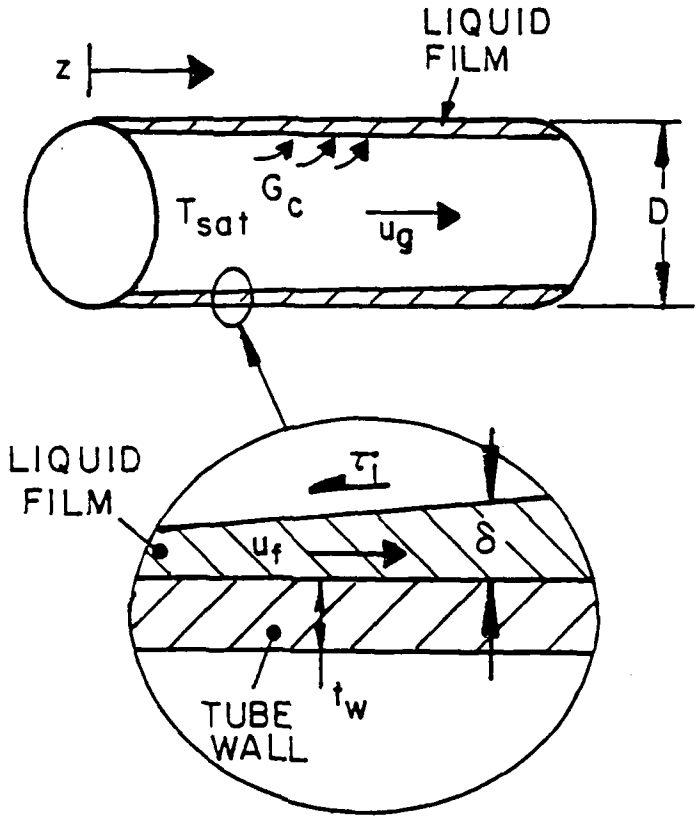

Figure 3.9. ANALYSIS VARIABLES FOR FLOW IN THE ANNULAR CONDENSATION REGIME

The fluid properties, temperatures and flow rates should all be known independently of the condenser design. The inlet velocities and film thickness must be calculated. The procedure is:

1) Calculate u_{go}, the gas inlet velocity, assuming homogeneous flow:

$$u_{go} = G\left[\frac{x_o}{\rho_g} + \frac{1-x_o}{\rho_l}\right] \tag{3-10}$$

2) Calculate the gas/wall friction factor, f_{wg}:

$$f_{wg} = 0.046\left[\frac{\rho_g u_{go} D}{\mu_g}\right]^{-0.2} \tag{3-11}$$

3) Solve for δ_o, the inlet film thickness:

$$\delta_o^2\left[1 + 300\left[\frac{\delta_o}{D}\right]\right] = \frac{GD(1-x_o)\mu_l}{f_{wg}\rho_l\rho_g u_{go}^2} \tag{3-12}$$

(This equation equates the shear stress at the film surface with the interfacial shear using Wallis's (1969) correlation for f_i/f_{wg}.)

4) Calculate the inlet liquid velocity, u_{fo}:

$$u_{fo} = \frac{GD(1-x_o)}{4\rho_l \delta_o} \tag{3–13}$$

Heat Flux. The heat flux in each segment depends on the film thickness and possibly the condenser tube thickness:

$$q'' = \frac{\Delta T_{sat}}{\left[\frac{\delta}{k_l} + \frac{t_w}{k_w}\right]} \tag{3–14}$$

In many cases it is reasonable to neglect the tube wall thermal resistance (t_w/k_w) compared to that of the liquid film (δ/k_l), especially if the tube wall is metal. Since the flow is often observed through a glass tube in experiments, the wall resistance could be significant in this case and should then be included.

For turbulent liquid films, the term δ/k_l for thermal conduction in the liquid film should be replaced or modified by $1/h$, where h is a convective heat transfer coefficient for condensation on liquid films. Collier (1986) presents a correlation by Soliman et al. which has been found to agree well with experimental results.

A word about notation: In the stepwise process of analyzing successive segments in the condenser, the inlet quantities (subscript o) are used to determine the values at the exit of the first segment (subscript k for the current segment, where k = 1 for the first segment). From that point on, values at the exit of the preceding segment (subscript k–1) become the inlet values for the current segment being analyzed.

Fluid State. In each segment the quality and film thickness (or void fraction) at the segment exit must be calculated as functions of the inlet parameters and the segment heat flux. The procedure is:

1) Calculate G_c, the condensation mass flux:

$$G_c = q''/h_{fg} \tag{3–15}$$

2) Calculate τ_i, the interfacial shear, using this expression:

$$\tau_i = f_{wg}\,(f_i/f_{wg})\,\frac{\rho_g(u_g-u_f)^2}{2} + G_c(u_g-u_f) \tag{3–16}$$

where

$$f_{wg} = 0.046\left[\frac{\rho_g u_g D}{\mu_g}\right]^{-0.2} \tag{3–17}$$

$$f_i/f_{wg} = [1 + 300(\delta/D)] \tag{3–18}$$

and δ is the inlet (or average, see below) film thickness in the segment.

3) Calculate the film thickness at the segment exit. Assuming constant interfacial shear in the segment, the film thickness at the exit can be calculated using this equation:

$$\delta_k = \left\{(\delta_{k-1})^3 + \left[\frac{3\Delta z_k \mu_l^2 \ Ja}{\tau_{ik} \quad \rho_l \ Pr_l}\right]\right\}^{1/3} \tag{3–19}$$

where the subscript "k" refers to the segment exit and

τ_{ik} = interfacial shear in the segment (N/m^2),
Ja = $c_{pl}\Delta T_{sat}/h_{fg}$, and
Pr_l = $\mu_l c_{pl}/k_l$.

4) Calculate the average velocity in the liquid film at the segment exit:

$$u_{fk} = u_{fk-1}\left[\frac{\delta_{k-1}}{\delta_k}\right] + \frac{G_c \Delta z_k}{\rho_l \delta_k} \tag{3–20}$$

where u_{fk-1} is the film velocity at the exit of the previous segment, and Δz_k is the length of segment "k".

5) Calculate the vapor velocity at the exit of the segment:

$$u_{gk} = u_{gk-1} - \frac{4G_c \Delta z_k}{\rho_g D} \tag{3–21}$$

Initially this procedure can be used in a "marching scheme", in which the interfacial shear and heat flux are calculated using the inlet conditions (film thickness and phase velocities) applied over the entire length of the segment. However, once the entire condenser has been calculated in this way the designer will have estimates for the film thickness at the inlet and exit of each segment. Averages for these parameters in the segments can be estimated by taking the mean of the inlet and exit values, then the interfacial shear and the heat flux can be recalculated based on segment average values (of δ, u_f and u_g). This procedure can be repeated until the results converge to any desired degree. This iterative procedure leads to more consistent results which are less sensitive to the size of the segments.

Dimensionless Design Map. All the heat transfer phenomena in the annular condensation regime can be summarized in a single design map, as shown in Figure 3.5. The curves on this map are derived from a dimensionless energy balance in which conduction heat transfer through the condensate film balances the energy removed by the vapor during condensation.

Figure 3.10 shows a control volume of length dz. Equating the change in fluid enthalpy with the heat flux across the tube walls:

$$G\,(\pi D^2/4)\,h_{fg}\,dx = -q''(\pi D)dz = \frac{-k_l \ \Delta T_{sat}}{\delta}(\pi D)dz \tag{3–22}$$

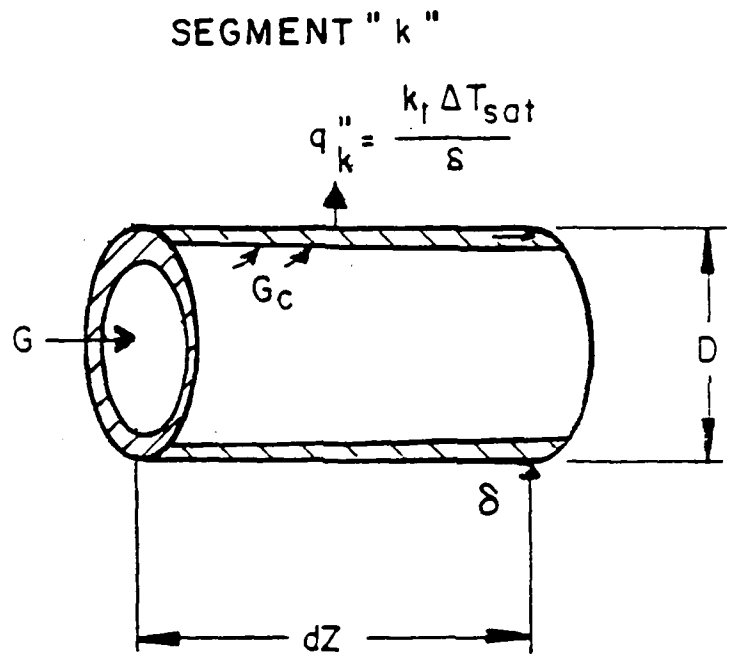

Figure 3.10. CONTROL VOLUME FOR HEAT TRANSFER ANALYSIS

Rearranging Equation 3–22 and using the approximation that $\delta = (1-\alpha)D/4$ gives:

$$(1-\alpha)\,dx = \frac{-16\ k_l\ \Delta T_{sat}}{G\ D^2\ h_{fg}}\,dz = -(4R_e/D)\,dz = -4\,R_e\,dz^* \qquad (3-23)$$

(where $z^* \equiv z/D$). An important result which we will use later to calculate pressure losses is:

$$\frac{dz}{dx} = -\frac{(1-\alpha)D}{4R_e} \qquad (3-24)$$

Integrating Equation 3–24 from quality x_0 at $z = 0$ to quality x at $z = L$ gives:

$$4\,R_e\,L^* = -\int_{x_0}^{x_s} (1-\alpha)\,dx = \int_{x_s}^{x_0} (1-\alpha)\,dx \qquad (3-25)$$

The final quality, x_s, can be taken as zero for a first approximation or set to 0.1, corresponding to the transition from annular to slug condensation. To evaluate the integral a relationship between the flow quality, x, and the void fraction, α, is necessary. An appropriate model has already been described for the annular flow regime in Equation 2–66:

$$\left[\frac{1-x}{x}\right]^2 = \frac{\rho_l}{\rho_g}\frac{(1-\alpha)^2}{\alpha^{2.5}}\left(f_i/f_{wg}\right) \qquad (3-26)$$

The integral in Equation 3–25 is evaluated numerically using Equation 3–26 for various constant values of (ρ_l/ρ_g). The results are presented in the design map of Figure 3.5.

A simple, closed–form solution can be derived if we assume that f_i/f_{wg} is constant and that $\alpha^{1.25} \approx 1.0$ over the range of the integral in Equation 3–25. The closed–form expression is:

$$I = 4R_cL^* = \frac{1}{4(\rho_l/\rho_g)^{\frac{1}{2}}\,(f_i/f_{wg})^{\frac{1}{2}}}\left[\ln\left[\frac{x_o}{x_s}\right] - (x_o - x_s)\right] \qquad (3–27)$$

where x_o = flow quality at the condenser inlet, and
x_s = 0.1, corresponding to the slug regime transition.

If we take f_i/f_{wg} to equal approximately 10.0, then the results of this simple equation are within 20% of the design map.

Transition to the slug regime. A convenient rule of thumb for microgravity condensers is to locate the end of the annular condensation region using a critical void fraction of 0.80. When the void fraction decreases below this value, assume that the slug condensation regime has begun.

This simple rule is an approximation to the more precise method for calculating the regime transition. The end of the annular regime can be found using the same methods described in Section 1.1 of this Design Manual. At the exit of each segment, calculate the Martinelli parameter, X. Figure 1.5 shows the value of X which corresponds to the annular/slug transition as a function of the dimensionless slope parameter, Y. When the transition value of X has been exceeded, the condenser has entered the slug condensation regime.

Slug Flow Regime. Heat transfer in the slug flow regime is calculated as a weighted average of film conduction into the vapor bubbles and single–phase convection into the liquid slugs. Figure 3.11 illustrates the analysis of this regime. The segment of interest is denoted by the subscript "k." Entrance conditions are denoted by the subscript "k–1" and exit conditions have the subscript "k."

The calculation procedure for the slug regime requires four inlet conditions for each segment. These are the quality, x_{k-1}, void fraction, α_{k-1}, total volumetric flux, j_{k-1}, and a parameter equal to the fraction of the pipe cross–section which is occupied by the liquid film which surrounds the Taylor bubbles, m_{k-1}. The heat flux in a segment is calculated based on these inlet conditions. The heat flux implies a certain rate of condensation in the segment which enables the designer to calculate the segment exit conditions.

Inlet Conditions. At the end of the annular regime the flow quality, x_o, is known. The designer must calculate the other three inlet conditions for the initial slug segment (α_o, j_o and m_o) using the following procedure.

1) The total volumetric flux, j_o, is:

$$j_o = G\left[\frac{x_o}{\rho_g} + \frac{1-x_o}{\rho_l}\right] \qquad (3–28)$$

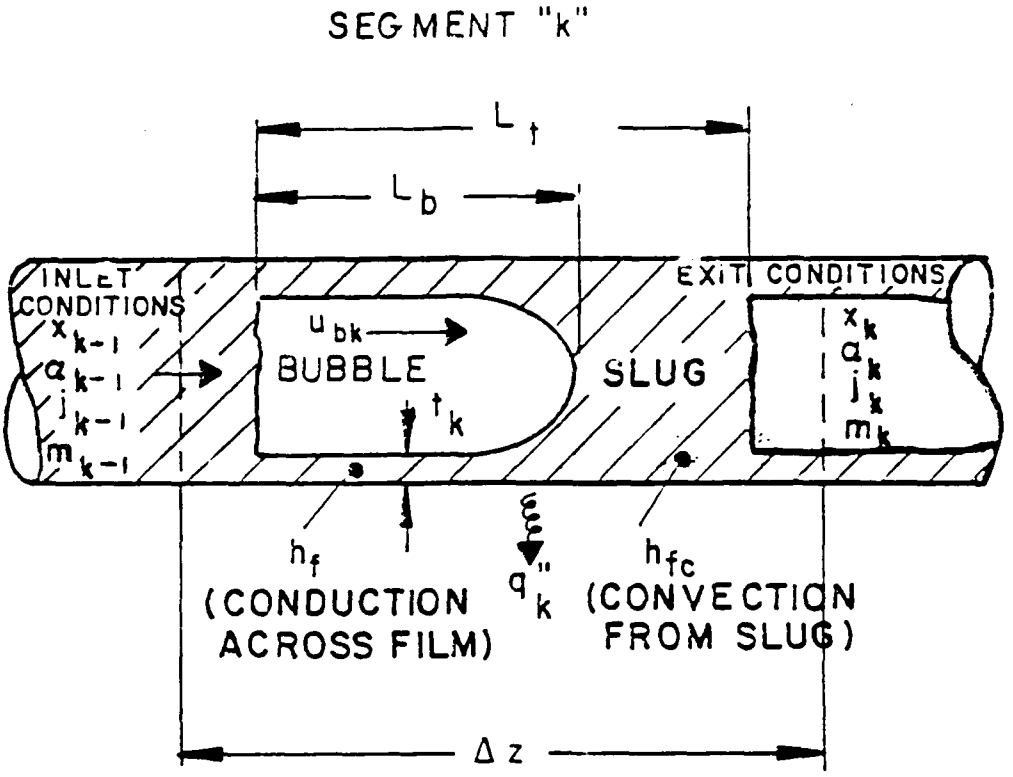

Figure 3.11. ANALYSIS OF SLUG CONDENSATION

2) To calculate m_o, first calculate the bubble velocity u_{bo} (Wallis, 1969):

$$u_{bo} = j_o\left[1 + 1.27\left[1 - \exp\left(-3.8\left[\frac{\mu_f j_o}{\sigma}\right]^{0.8}\right)\right]\right] \qquad (3-29)$$

The area ratio can then be read from Figure 3.12 or calculated by:

$$m_o = \min\left(0.16,\ 0.56\left[1 - \exp\left(-2.64\left[\frac{\mu_f u_{bo}}{\sigma}\right]^{0.567}\right)\right]\right) \qquad (3-30)$$

3) Calculate the initial void fraction, α_o (Wallis, 1969):

$$\alpha_o = \frac{x_o(1-m_o)}{x_o + (\rho_g/\rho_f)(1-x_o)} \qquad (3-31)$$

Heat Flux. The heat flux in segment "k" is calculated based on an average heat transfer coefficient which accounts for conduction from Taylor bubbles across the liquid film and forced convection from the liquid slugs. The procedure to calculate the heat flux is as follows:

1) Calculate the bubble length ratio, L_b/L_t. L_t is the length of a Taylor bubble plus its associated liquid slug, and L_b is the bubble length. The ratio is:

$$\frac{L_b}{L_t} = \left[\frac{\alpha}{1-m}\right] \tag{3-32}$$

2) Calculate the forced convection heat transfer coefficient, h_{fc}:

$$h_{fc} = \begin{cases} (0.023)\left[\frac{k_l}{D}\right]\left[\frac{\rho_l j D}{\mu_l}\right]^{0.8} Pr_l^{0.33} & \text{for } \frac{\rho_l j D}{\mu_l} \geq 1500 \text{ (turbulent)} \quad (3\text{-}33a) \\ (3.66)(k_l/D) & \text{for } \frac{\rho_l j D}{\mu_l} < 1500 \text{ (laminar)} \quad (3\text{-}33b) \end{cases}$$

3) Calculate h_f, the heat transfer coefficient representing conduction across the liquid film:

$$h_f = \frac{2k_l}{\left[D[1 - (1-m_k)^{0.5}\right]} \tag{3-34}$$

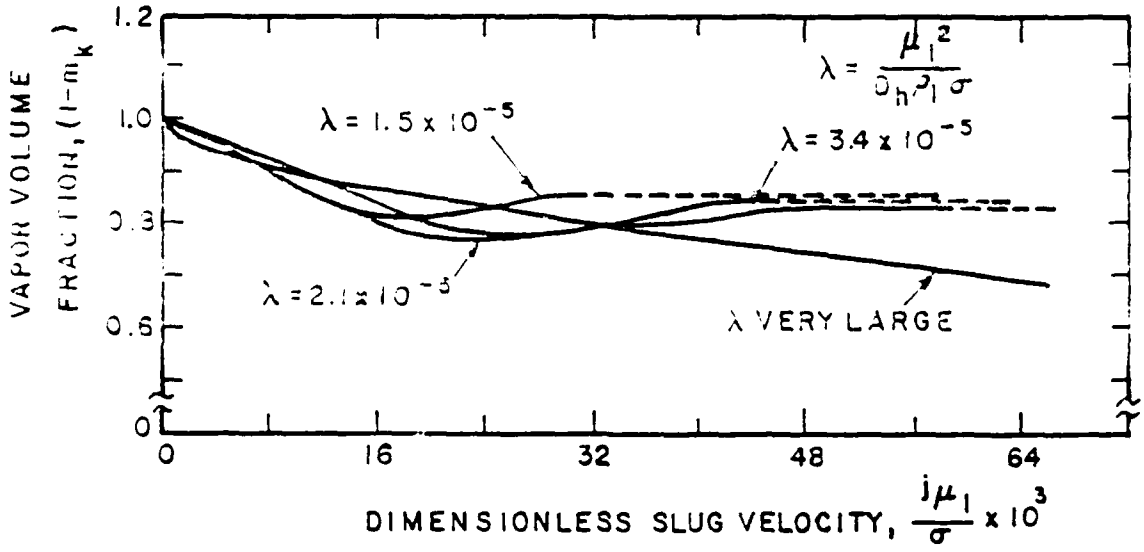

Figure 3.12. VELOCITY AS A FUNCTION OF $j\mu_l/\sigma$ (Suo and Griffith, 1963)

4) Calculate the average heat transfer coefficient, h_{av}:

$$h_{av} = \left[\frac{L_b}{L_t}\right] h_f + \left[1 - \frac{L_b}{L_t}\right] h_{fc} \qquad (3\text{–}35)$$

5) Calculate the heat flux:

$$q'' = \frac{\Delta T_{sat}}{\left[\frac{1}{h_{av}} + \frac{t_w}{k_w}\right]} \qquad (3\text{–}36)$$

Fluid State. The heat flux from the fluid results in decreasing quality along the tube length. The rate of condensation controls the segment outlet conditions. To calculate the outlet condition, use the following procedure:

1) Calculate the flow quality at the outlet of segment "k:"

$$x_k = x_{k-1} - \frac{4\ q''_k\ \Delta z_k}{G\ D\ h_{fg}} \qquad (3\text{–}37)$$

where Δz_k = the length of segment "k".

2) Calculate j_k, the total volumetric flux at the exit of the segment:

$$j_k = G\left[\frac{x_k}{\rho_g} + \frac{1-x_k}{\rho_l}\right] \qquad (3\text{–}38)$$

3) Calculate m_k, the film area ratio at the segment exit. First calculate the bubble velocity at the exit of the segment, u_{bk}:

$$u_{bk} = j_k \left\{1 + 1.27\left[1 - \exp\left[-3.8\left[\frac{\mu_l j_k}{\sigma}\right]^{0.8}\right]\right]\right\} \qquad (3\text{–}39)$$

Use this value of the bubble velocity to calculate m_k:

$$m_k \equiv \min\left[0.16, 0.56\left\{1 - \exp\left[-2.64\left[\frac{\mu_l u_{bk}}{\sigma}\right]^{0.567}\right]\right\}\right] \qquad (3\text{–}40)$$

4) Calculate $\alpha_k = \dfrac{x_k(1-m_k)}{x_k + (\rho_g/\rho_l)(1-x_k)}$ (3–41)

These steps (Equations 3–37 through 3–41) can be used initially in a marching method: the film thickness, bubble length ratio and liquid heat transfer coefficient are calculated from the inlet parameters only and assumed to apply over the entire length of the segment. A more

sophisticated scheme will use this marching calculation as the first step in an iterative procedure. Once the exit parameters for a segment have been estimated from the marching scheme, more precise estimates of the film thickness, bubble length ratio and liquid heat transfer coefficient can be made based on the segment average values of the quality and void fraction. The refined film thickness, bubble length ratio and heat transfer coefficient will, in turn, result in better estimates of the exit void fraction and quality. This procedure can be continued until the exit conditions converge, and the results will be less dependent on the length of the segments.

Transition to the bubbly regime. As more vapor condenses the Taylor bubbles will become shorter and shorter, and the volumetric flux will decrease. Slug condensation ends when the bubbles become unstable and break up into smaller bubbles.

This transition can be calculated using the procedure described in Section 1.1.3. A simple rule of thumb, accurate at acceleration levels below 10^{-2}g, is to assume that bubbly flow begins once the void fraction drops below 0.45.

Bubbly Flow Regime. In this regime the vapor phase consists of small bubbles dispersed through the liquid. A homogeneous model is recommended to analyze this section of the condenser. In this case only the flow quality at the segment inlet is required. The following procedure shows how to calculate the heat flux and exit quality.

Inlet Conditions. The flow quality at the inlet to the bubbly condensation region is simply the exit quality from the last segment of the slug region.

Heat Flux. The heat flux is calculated using standard methods for forced convection. The effect of two–phase flow is to increase the effective Reynolds number. The heat flux is estimated using this procedure:

1) Calculate $\bar{\mu}$, the average viscosity of the bubbly mixture:

$$\bar{\mu} = \left[\frac{x}{\mu_g} + \frac{1-x}{\mu_l}\right] \qquad (3-42)$$

2) Calculate the effective two-phase Reynolds number, Re_{tp}:

$$Re_{tp} = \frac{G\,D}{\bar{\mu}} \qquad (3-43)$$

3) Calculate the two–phase heat transfer coefficient, h_{tp}. The heat transfer coefficient depends on the two–phase Reynolds number as follows:

$$h_{tp} = \begin{cases} (0.023)\left[\frac{k_l}{D}\right](Re_{tp})^{0.8}(Pr_l)^{0.33} & Re_{tp} \geq 1500 \text{ (turbulent)} \quad (3\text{-}44a) \\ (3.66)(k_l/D) & Re_{tp} < 1500 \text{ (laminar)} \quad (3\text{-}44b) \end{cases}$$

4) Calculate the heat flux in the segment:

$$q''_k = \frac{\Delta T_{sat}}{\left[\frac{1}{h_{tp}} + \frac{t_w}{k_w}\right]} \quad (3\text{–}45)$$

Fluid State. Calculate the quality at the exit of the segment using this equation:

$$x_k = x_{k-i} - \frac{4\ q''\ \Delta z_k}{G\ D\ h_{fg}} \quad (3\text{–}46)$$

As in the previous flow regimes, this method can first be applied in a marching method in which the entire segment is characterized by the inlet quality. Subsequent iterations use the average quality in the segment to calculate the heat flux.

Transition to single-phase regime. The bubbly condensation regime ends when the void fraction and flow quality are zero. From this point to the condenser exit there is only single–phase liquid.

Single–Phase Liquid Regime. Single–phase flow is considerably simpler than two–phase flow because the fluid properties are constant, and heat transfer can be analyzed using standard methods. There is no need to divide the single–phase region into segments because the entire single–phase section can be modeled analytically. The single–phase regime is the final heat transfer regime in the condenser.

Inlet Conditions. The temperature at the inlet to the single–phase liquid region is the saturation temperature, T_{sat}.

Heat Flux. The heat flux in the single–phase region depends on the fluid properties, the flow rate, and the secondary coolant temperature. The heat flux can be calculated as a function of position with this procedure:

1) Calculate Re_f, which is the Reynolds number in the single–phase region:

$$Re_f = GD/\mu_l \quad (3\text{–}47)$$

2) Calculate the fluid heat transfer coefficient, h_{fc}. The equation for the heat transfer coefficient depends on whether the flow is laminar or turbulent, as indicated by the Reynolds number.

$$h_{fc} = \begin{cases} (0.023)\ \dfrac{k_l}{D} Re_f^{0.8} Pr_l^{0.33} & \text{for } Re_f \geq 1500 \text{ (turbulent)} \quad (3\text{-}48a) \\ (3.66)\ \dfrac{k_l}{D} & \text{for } Re_f < 1500 \text{ (laminar)} \quad (3\text{-}48b) \end{cases}$$

3) Calculate U, the overall heat transfer coefficient which accounts for the thermal resistance of the fluid boundary layer and the tube wall:

$$U = \left[\frac{1}{h_{fc}} + \frac{t_w}{k_w}\right]^{-1} \quad (3\text{–}49)$$

If the wall thermal resistance is negligible then $U \approx h_{fc}$.

4) The heat flux as a function of position in the single–phase section of the condenser tube can be calculated using this equation:

$$q''(z_{sp}) = U\,\Delta T_{sat} \exp\left[\frac{-4\ U\ z_{sp}}{G\ D\ c_{pl}}\right] \quad (3\text{–}50)$$

where z_{sp} is the position in the tube measured from the start of the single–phase liquid region.

The total heat transferred in the single–phase region, q_{sp}, can be calculated by:

$$q_{sp} = G\,c_{pl}\left[\frac{\pi D^2}{4}\right]\left\{1 - \exp\left[\frac{-4\ U\ L_{sp}}{G\ D\ c_{pl}}\right]\right\} \quad (3\text{–}51)$$

where L_{sp} is the total length of the single–phase region.

Fluid State. The fluid temperature as a function of position in the single–phase region is given by this equation:

$$T_f(z_{sp}) = T_{sat} - \Delta T_{sat}\left\{1 - \exp\left[\frac{-4\ U\ z_{sp}}{G\ D\ c_{pl}}\right]\right\} \quad (3\text{–}52)$$

The fluid temperature at the condenser exit is simply $T_f(L_{sp})$.

Dimensionless Map. A simple dimensionless design map can be constructed for the common situation in thermal management applications, in which the thermal resistance of the tube wall is negligible in comparison with the fluid boundary layer. In this case, the overall heat transfer coefficient, U, is approximately the fluid heat transfer coefficient, h_{fc}. The fluid temperature in the single–phase region is then given by:

$$T_f(z_{sp}) = T_{sat} - \Delta T_{sat}\left\{1 - \exp\left[\frac{-4\ h_{fc}\ z_{sp}}{G\ D\ c_{pl}}\right]\right\} \quad (3\text{–}53)$$

$$= T_{sat} - \Delta T_{sat}\left\{1 - \exp\left[\frac{-4\ Nu_{fc}\ z_{sp}}{Re_f\ Pr_l\ D}\right]\right\} \quad (3\text{–}54)$$

where Nu_{fc} is the Nusselt number for forced convection = $h_{fc}D/k_l$.

This equation can be rearranged into a form suitable to produce the universal design map:

$$I_{sp} = \frac{L_{sp}}{D} \frac{1}{\ln\left[\frac{T_{sat}-T_2}{T_{sub}-T_2}\right]} = \frac{Re_f \, Pr_l}{4 \, Nu_{fc}} \qquad (3\text{–}55)$$

where L_{sp} is used to represent the length of the single–phase section with an outlet temperature of T_{sub}.

The Nusselt number is actually a function of the Reynolds and Prandtl numbers, depending on whether the flow is laminar or turbulent:

$$Nu_{fc} = \begin{cases} (0.023)Re_f^{0.8}Pr_l^{0.33} & (Re_f \geq 2300)\ (turbulent) \qquad (3\text{-}56a) \\ 3.66 & (Re_f < 2300)\ (laminar) \qquad (3\text{-}56b) \end{cases}$$

Equations 3.55 and 3.56 are used to generate the design map (Figure 3.6) for the length of the single–phase section of the condenser.

3.1.4 Validation with Microgravity Data

No data are presently available to validate these models for condenser performance in microgravity. The key issue to be resolved is the possible effect of gravity on interfacial shear. Previous experiments by Keshock (1974) investigated a high vapor shear condenser under microgravity (aircraft) and earth gravity conditions. Insufficient data are available from these tests for quantitative comparison with the design models. Qualitatively, Keshock observed that the heat transfer behavior was not significantly different at both gravity levels. We have reviewed the data of Lee (1987) who operated a high–vapor shear condenser in simulated low gravity aboard a KC–135 aircraft. The condenser did not reach steady state in these tests, and consequently the data do not apply to the models developed here. Transient models are needed to predict these data. It is expected that new data to be obtained in experiments sponsored by the Weapons Laboratory will provide data needed for quantitative analysis.

3.2 Pressure Losses

3.2.1 Introduction

Pressure losses in the condenser occur primarily in the annular condensation regime. Just as in the case of the forced convection evaporator, there are three major components to the pressure drop:

- Friction,
- Body forces, and
- Fluid acceleration.

The total pressure drop is due to the sum of these component pressure drops. Because high vapor shear leads to improved heat transfer, the frictional component should be dominant. Note that for the case of a condenser the pressure drop due to fluid acceleration is *negative*. Deceleration of the fluid from the vapor to liquid phase acts to reduce the overall loss in pressure. If the frictional losses do not dominate the pressure recovery due to acceleration effects, then the condenser may cause instabilities in the two–phase system. So a design criterion for this type of condenser is that frictional pressure losses should dominate.

Pressure losses in an R–114 condenser tube are illustrated in Figure 3.13. The frictional and fluid acceleration pressure drops are shown as a function of tube length in all heat transfer regimes. Note that nearly all of the pressure losses occur in the annular regime where the velocities are high. The total pressure drop is only about half that due to friction alone because of the pressure recovery due to fluid deceleration. (The acceleration level for this calculation is 10^{-3}g and the pressure losses due to body forces are negligible).

3.2.2 Design Maps

Dimensionless design maps are provided for each component of the pressure drop in the two–phase annular condensation regime. The slug and bubbly condensation regimes contribute only small amounts to the total pressure drop and are addressed in detail only in Section 3.2.3. Pressure losses in the single–phase region are calculated by standard methods. The relevant equations are included here.

The overall procedure to estimate the condenser pressure losses is:

1. Estimate the frictional pressure loss in the two–phase region of the condenser (Figure 3.14 and Equation 3–60),
2. Estimate the pressure loss due to body forces in the two–phase region of the condenser (Figure 3.15 and Equation 3–61),
3. Estimate the pressure loss due to fluid acceleration (Figure 3.16 and Equation 3–62),
4. Add these components together to obtain ΔP_{tp}, the total pressure drop in the two–phase section of the condenser (Equation 3–63),
5. Calculate ΔP_{sp}, the pressure drop in the single–phase section (Equation 3–64), and
6. Add the pressure drops in the two–phase and single–phase sections to estimate the total pressure drop (Equation 3–65).

The following sections detail these calculations.

These design maps presented below are valid only for a certain set of conditions related to the thermal resistance of the condenser wall and the condenser thermodynamic ratio. Refer to Section 3.1.2 for procedures to check the validity of the dimensionless design maps for a specific application.

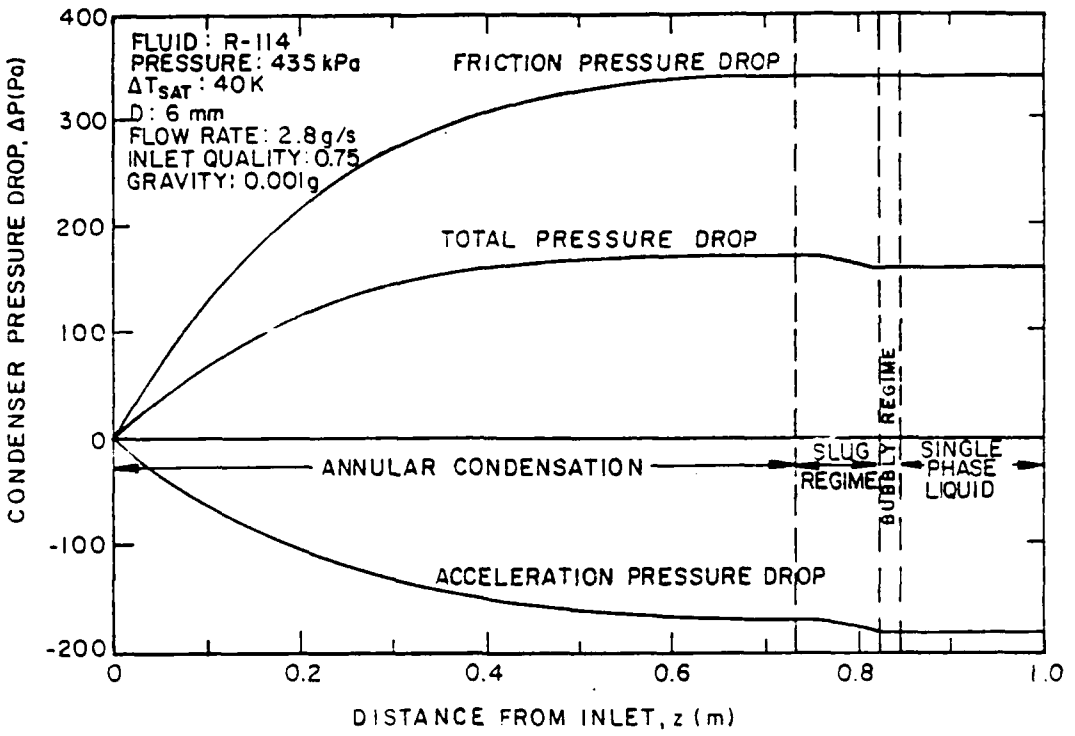

Figure 3.13. PRESSURE LOSSES IN A HIGH VAPOR SHEAR CONDENSER

The design parameters needed to estimate the pressure drop in the condenser include:

Fluid Properties

ρ_l	liquid density (kg/m^3)
μ_l	liquid viscosity (kg/m–s)
k_l	liquid thermal conductivity (W/m–K)
h_{fg}	latent heat of evaporation (J/kg)
ρ_g	vapor density (kg/m^3)

Geometry

D	condenser tube inner diameter (m)

Operating Conditions

G	condenser mass flux (kg/m^2 –s)
x_o	condenser inlet quality (–)
ΔT_{sat}	Temperature difference between condensing fluid and the secondary coolant (K)
a	magnitude of acceleration (m/s^2)
θ	angle between acceleration and flow vectors (°).

Calculating Pressure Losses. The total pressure drop in the annular condensation region is the sum of three component pressure drops due to friction, body forces and acceleration. Dimensionless design maps for these three pressure drop components are shown in Figures 3.14, 3.15 and 3.16, respectively. All of the dimensionless pressure drops are displayed as functions of quality, x. In most cases it is sufficiently accurate to approximate this quality by the condenser inlet quality. The following sections explain the use of the design maps.

1) Friction in the Two-Phase Region. Estimate the frictional pressure drop using Figure 3.14. The procedure is:

- Calculate R_c, the condenser thermodynamic ratio:

$$R_c = \frac{4\ k_l\ \Delta T_{sat}}{G\ D\ h_{fg}} \tag{3–57}$$

- Calculate the ratio of liquid to vapor densities, ρ_l/ρ_g.

- Calculate the Reynolds number due to liquid flow, Re_f:

$$Re_f = GD/\mu_l \tag{3–58}$$

- Calculate f_{wl}, the liquid–only friction factor:

$$f_{wl} = 0.046\ Re_f^{-0.2} \tag{3–59}$$

- Locate the curve in Figure 3.14 which corresponds to the liquid–to–vapor density ratio.

- Locate the point on this curve which corresponds to the condenser inlet quality, x_o. The ordinate of this plot is the dimensionless pressure drop $(\Delta P_{fc}^*/f_{wl})$.

- Calculate ΔP_{fc}, the frictional component of the pressure drop in the annular part of the condenser:

$$\Delta P_{fc} = 4\ f_{wl} \left[\frac{G^2/2\rho_l}{R_c}\right] \left[\frac{\Delta P_{fc}^*}{f_{wl}}\right] \tag{3–60}$$

2) Body Forces in the Two-Phase Region. Estimate the pressure drop due to body forces using Figure 3.15. The procedure is:

- Locate the curve in Figure 3.15 which corresponds to the liquid–to–vapor density ratio.

- Locate the point on this curve which corresponds to the condenser inlet quality, x_o. The abscissa of the plot gives the dimensionless pressure drop ΔP_{gc}^*.

- Calculate ΔP_{gc}, the pressure drop due to body forces by:

$$\Delta P_{gc} = \left[\frac{\rho_l\ D\ a\ \cos\theta}{R_c}\right] \Delta P_{gc}^* \tag{3–61}$$

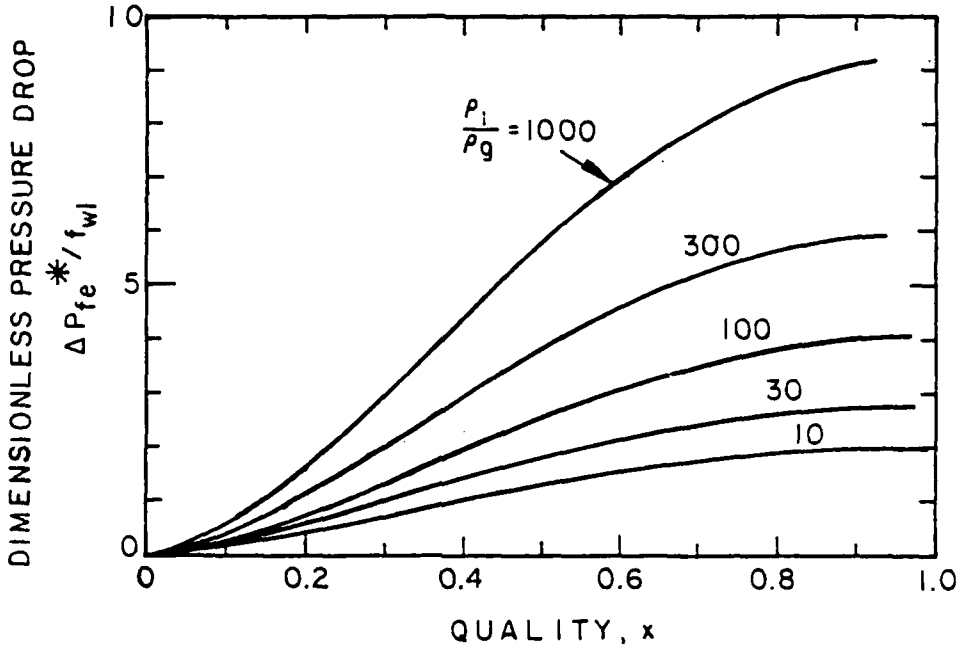

Figure 3.14. CONDENSER FRICTION PRESSURE DROP

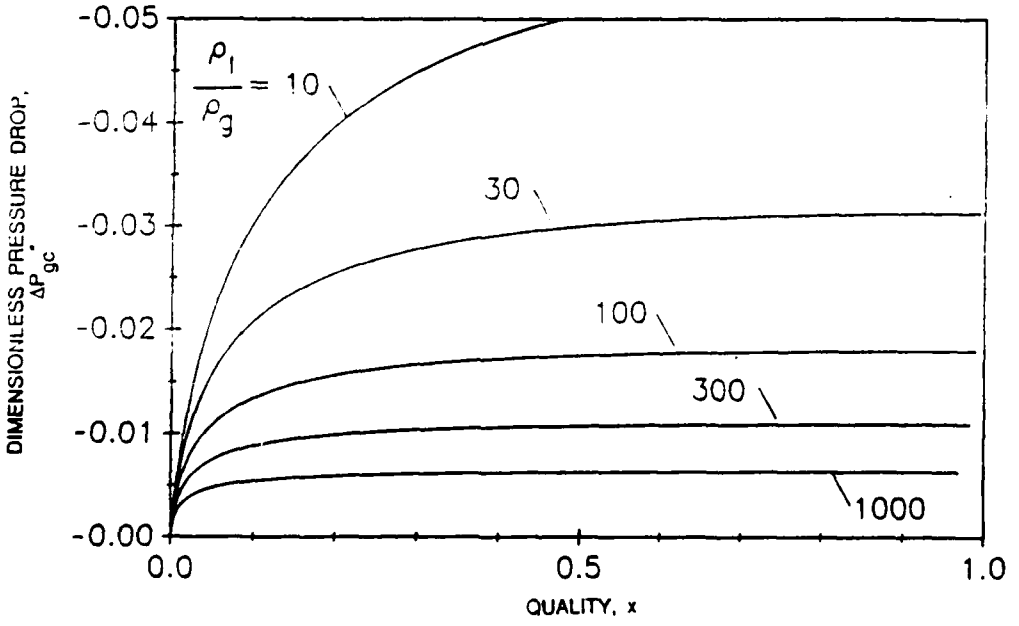

Figure 3.15. CONDENSER GRAVITY PRESSURE DROP

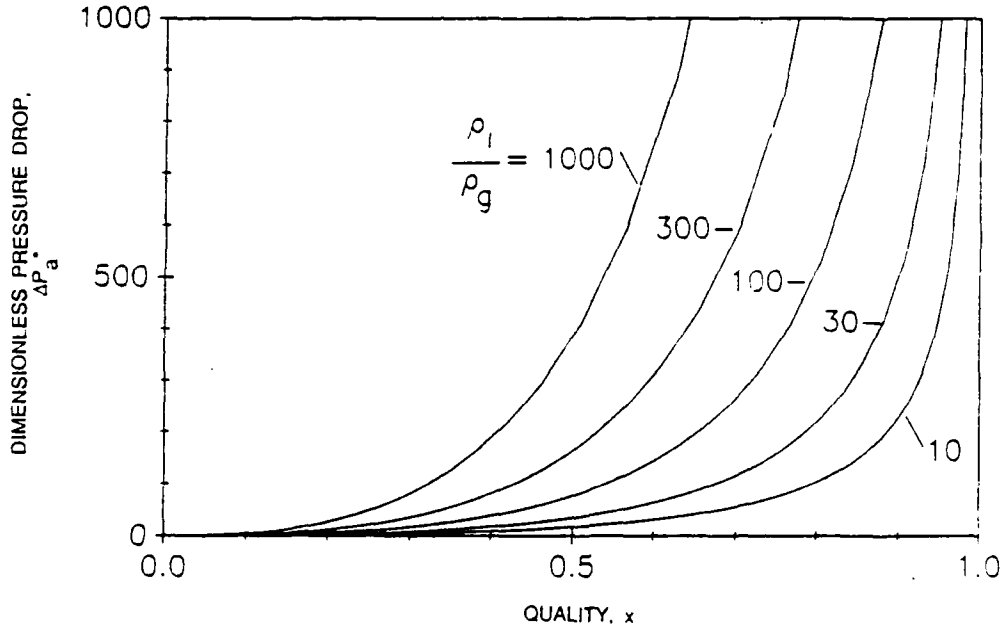

Figure 3.16. DESIGN MAP FOR CONDENSER ACCELERATION PRESSURE DROP

3) *Acceleration in the Two-Phase Region*. Estimate the pressure drop due to fluid acceleration using Figure 3.16. The procedure is:

- Locate the curve in Figure 3.16 which corresponds to the liquid–to–vapor density ratio.
- Locate the point on this curve which corresponds to the condenser inlet quality, x. The abscissa of the plot gives the dimensionless pressure drop ΔP_a^*.
- Calculate ΔP_{ac}, the pressure drop due to fluid acceleration:

$$\Delta P_{ac} = -[G^2/2\rho_l] \Delta P_a^* \qquad (3\text{–}62)$$

4) *Total Pressure Drop in the Two-Phase Section*. Now calculate ΔP_{tp}, the total pressure drop in the two–phase section of the condenser:

$$\Delta P_{tp} = \Delta P_{fc} + \Delta P_{gc} + \Delta P_{ac} \qquad (3\text{–}63)$$

5) *Pressure Drop in the Single-Phase Liquid Region*. Usually the pressure drop in the single–phase region will be very small due to low fluid velocity. It is easily estimated using parameters which have already been calculated to find the pressure drop in the annular condensation region. The pressure drop in the single–phase liquid region, ΔP_{sp}, can be estimated by:

$$\Delta P_{sp} = 4 f_{wl} (L_{sp}/D) (G^2/2\rho_l) - \rho_l L_{sp} a \cos\theta \qquad (3\text{–}64)$$

where f_{wl} = the liquid–only friction factor (Equation 3–59), and
L_{sp} = the length of the single–phase region (from Figure 3.6 and Equation 3–8).

6) Total Pressure Drop. The total pressure drop in the condenser is:

$$\Delta P_{cond} = \Delta P_{tp} + \Delta P_{sp} \qquad (3\text{–}65)$$

Uncertainty. The major uncertainty in the condenser pressure drop calculation is due to the interfacial friction between the vapor and liquid phases in the annular condensation regime. The design maps in Figures 3.14 through 3.16 assume that the interfacial friction factor is greater than the smooth–wall friction factor. Specifically, these curves use the friction factor correlation of Wallis (1969) which is presented in Section 1.2 in this manual. This is a conservative, high estimate for the interfacial friction.

A lower bound for the pressure drop can be estimated by assuming that the interfacial friction factor is the same as if the vapor were flowing in a smooth pipe. The friction pressure losses are roughly a factor of two less than would be calculated using the design map in Figure 3.14 with the higher interfacial friction. Design maps using interfacial friction relationships for microgravity conditions can be produced similarly when validated models become available.

3.2.3 Detailed Equations for Pressure Losses

This section presents pressure drop equations which can be used in detailed computer calculations and explains the basis for the dimensionless design maps. Table 3.2 summarizes the equations for friction, body force and fluid acceleration pressure drops in the four regimes of heat transfer within a condenser. The following sections present more detail.

Friction. The basic equation for the two–phase pressure gradient due to wall friction is the same as for the case of the evaporator tube:

$$(dP/dz)_f = -f_{wl} \phi^2 (1-x)^2 (4/D) (G^2/2\rho_l) \qquad (3\text{–}66)$$

All of these parameters are design inputs except for the single–phase friction factor, f_{wl}, and the two–phase multiplier, ϕ^2. The friction factor is calculated using Equation 3–59. The value of ϕ^2 depends on the fluid properties, the quality and the flow regime as described below.

Annular Condensation Regime. The two–phase multiplier for annular flow is (Collier, 1986):

$$\phi^2 = \frac{1}{(1-\alpha)^2} \qquad (3\text{–}67)$$

Table 3.2. PRESSURE DROP CALCULATIONS FOR A HIGH-VAPOR SHEAR CONDENSER

HEAT TRANSFER REGIME	FRICTION PRESSURE DROP	BODY-FORCES PRESSURE DROP	ACCELERATION PRESSURE DROP	VOID FRACTION
ANNULAR CONDENSATION	$\Delta P_f = \frac{f_{wl}(1-x)^2}{(1-\alpha)^2}\left[\frac{4}{D}\right]\left[\frac{G^2}{2\rho_l}\right]\Delta z$	$\Delta P_{gc} = -[\alpha\rho_g+(1-\alpha)\rho_l]\cos\theta\Delta z$	$\Delta P_a = -G^2\Delta\left[\frac{x^2}{\alpha\rho_g}+\frac{(1-x)^2}{(1-\alpha)\rho_l}\right]$	$\left[\frac{1-x}{x}\right]^2 = \left[\frac{\rho_l}{\rho_g}\right]\left[\frac{(1-\alpha)^2}{\alpha^{2.5}}\right]\left[\frac{f_i}{f_{wg}}\right]^*$
SLUG OR BUBBLY CONDENSATION	$\Delta P_{fc} = f_{wl}\phi^2\left[\frac{4}{D}\right]\left[\frac{G^2}{2\rho_l}\right]\Delta z$ $\phi^2 = \left[1+x\left[\frac{\rho_l}{\rho_g}-1\right]\right]\left[1+x\left[\frac{\mu_l}{\mu_g}-1\right]\right]^{\frac{1}{4}}$	$\Delta P_{gc} = -[\alpha\rho_g+(1-\alpha)\rho_l]\cos\theta\Delta z$	$\Delta P_a = -G^2\Delta\left[\frac{x^2}{\alpha\rho_g}+\frac{(1-x)^2}{(1-\alpha)\rho_l}\right]$	$\alpha = \frac{x}{(1-x)(\rho_g/\rho_l)+x}$
SINGLE-PHASE LIQUID	$\Delta P_{fc} = f_{wl}\left[\frac{4}{D}\right]\left[\frac{G^2}{2\rho_l}\right]\Delta z$	$\Delta P_{gc} = -\rho_l\, a\cos\theta\,\Delta z$	0	0

* $(f_i/f_{wg}) = [1 + 75\,(1-\alpha)]$ is recommended, although other models could be used.

where α is the local void fraction. Then the pressure drop due to friction in a short tube segment of length Δz can be calculated using this expression:

$$\Delta P_f = \frac{f_{w,l}}{(1-\alpha)^2} (1-x)^2 (4/D) (G^2/2\rho_l) \Delta z \qquad (3-68)$$

This is identical to the expression for an evaporator tube (Equation 2–64). See Section 2.2.3 for a procedure to evaluate the void fraction.

Note that the symbol "ΔP_f" is defined as a pressure drop:

$$\Delta P_f \equiv -\int (dP/dz)_f \, dz$$

A positive value therefore means a pressure loss and corresponds to a *negative* pressure gradient. (A negative pressure drop, which occurs with momentum changes due to phase change, indicates a pressure recovery.)

Other Condensation Regimes. In the slug and bubbly condensation regimes we recommend a homogeneous flow model to evaluate the pressure drop. The two–phase multiplier and segment pressure drop are calculated using the same expressions as for the nucleate boiling sections of an evaporator tube. Refer to Section 2.1.3 for this procedure.

Dimensionless Formulation. The dimensionless formulation assumes that the entire two–phase section of the condenser can be treated as an annular flow. The rate of pressure decrease with tube length is converted to a quality dependence using Equation 3–24 which relates the change in quality to distance along the condenser tube. The rate of pressure decrease with fluid quality, dP/dx, can be written as:

$$-\frac{dP}{dx} = -\frac{dP}{dz} \times \frac{dz}{dx} = \frac{f_{w,l}}{(1-\alpha)^2} (1-x)^2 (4/D) (G^2/2\rho_l) \left[\frac{dz}{dx}\right] \qquad (3-69a)$$

$$= -\frac{f_{w,l}}{(1-\alpha)^2} (1-x)^2 (4/D) (G^2/2\rho_l) \frac{(1-\alpha)D}{4R_c} \qquad (3-69b)$$

$$= -\frac{f_{w,l}}{(1-\alpha)} (1-x)^2 (1/R_c) (G^2/2\rho_l) \qquad (3-69c)$$

When Equation (3–69c) is rearranged and integrated, it becomes

$$\Delta P_{fc}^* = f_{w,l} \int_{x_s}^{x_o} \frac{(1-x)^2 \, dx}{(1-\alpha)} \qquad (3-70)$$

where x_s is the quality at the point of transition to slug flow, and ΔP^*_{fc} is the dimensionless pressure drop due to friction:

$$\Delta P^*_{fc} = \frac{\Delta P_{fc}}{4} \left[\frac{R_c}{G^2/2\rho_l}\right] \qquad (3-71)$$

The dimensionless map in Figure 3.14 has been created by using Equations 3–70 and 3–71, solving the integral with the void fraction/quality relationships shown in Table 3.2. To precisely calculate the pressure drop using Figure 3.14, the procedure is to take the difference in ordinates which correspond to qualities x_o and x_s. However, the ordinate corresponding to x_s is so close to zero that this correction makes no practical difference. It is accurate to approximate $(\Delta P_{fc}^*/f_{w\,l})$ as the ordinate in Figure 3.14 corresponding to the inlet quality, x_o.

Body Forces. The basic differential relation for the pressure drop due to body forces is:

$$(dP/dz)_g = [\,\alpha\,\rho_g + (1-\alpha)\,\rho_l\,]\,a\cos\theta \qquad (3-72)$$

Evaluation of the pressure drop in an incremental pipe segment is thus:

$$\Delta P_g = -[\,\alpha\,\rho_g + (1-\alpha)\,\rho_f\,]\,a\cos\theta\,\Delta z \qquad (3-73)$$

The void fraction, α, depends on the heat transfer regime as follows.

Two-Phase Forced Convection Regime. In this regime the void fraction should be evaluated using the same procedure as described above for the case of the friction pressure drop.

Other Heat Transfer Regimes. In the slug and bubbly regimes the flow is assumed to be homogeneous and the void fraction is:

$$\alpha = \frac{x}{(1-x)(\rho_g/\rho_l) + x} \qquad (3-74)$$

Dimensionless Formulation. The dimensionless expression for the pressure drop due to body forces is obtained as follows:

$$-\frac{dP}{dx} = -\frac{dP}{dz}\times\frac{dz}{dx} = [\,\alpha\,\rho_g + (1-\alpha)\,\rho_l\,]\,a\cos\theta\,\frac{(1-\alpha)D}{4R_c}$$

$$= \frac{\rho_l\,a\,D\cos\theta}{4R_c}\,[\alpha(\rho_g/\rho_l) + (1-\alpha)](1-\alpha) \qquad (3-75)$$

Rearrange and integrate to obtain:

$$\Delta P_{gc}^* = -\int_{x_s}^{x_o} [\alpha(\rho_g/\rho_l) + (1-\alpha)]\,(1-\alpha)dx \qquad (3-76)$$

where ΔP_{gc}^* is the dimensionless pressure drop due to body forces in the condenser:

$$\Delta P_{gc}^* = \Delta P_{gc}\,\frac{R_c}{\rho_l D a\cos\theta} \qquad (3-77)$$

The pressure drop due to body forces is negative because when the body force is in line with the flow ($\cos\theta > 0$) there is a pressure recovery in the condenser. The dimensionless map for the pressure loss due to body forces (Figure 3.15) is obtained by assuming that the entire condenser can be characterized by annular condensation. The design map is generated by using the void fraction/quality relationship for annular flow as given in Table 3.2.

Acceleration. The basic equation for pressure loss due to fluid acceleration is:

$$(dP/dz)_a = -G^2 \frac{d}{dz}\left[\frac{x^2}{\alpha}\frac{1}{\rho_g} + \frac{(1-x)^2}{(1-\alpha)}\frac{1}{\rho_l}\right] \qquad (3\text{–}78)$$

Thus the pressure loss in a pipe segment due to fluid acceleration is:

$$\Delta P_a = G^2 \Delta\left[\frac{x^2}{\alpha}\frac{1}{\rho_g} + \frac{(1-x)^2}{(1-\alpha)}\frac{1}{\rho_l}\right] \qquad (3\text{–}79)$$

Note that this expression is independent of the segment length and depends only on the fluid quality and void fraction at the inlet and outlet of the segment. This pressure drop is evaluated using the same void fraction/quality relationships described above for the pressure losses due to friction and body forces. The dimensionless form is obtained by dividing Equation (3–79) by $(G^2/2\rho_l)$ to obtain:

$$\Delta P_{ac}^* = \Delta\left[\frac{x^2}{\alpha}\frac{\rho_l}{\rho_g} + \frac{(1-x)^2}{(1-\alpha)}\right] \qquad (3\text{–}80)$$

where ΔP_{ac}^* is the dimensionless pressure drop due to fluid acceleration in the condenser:

$$\Delta P_{ac}^* = \Delta P_a \left[\frac{1}{G^2/2\rho_l}\right] = -\Delta P_a^* \qquad (3\text{–}81)$$

3.2.4 Validation with Microgravity Data

Only a few microgravity experiments for condensation behavior have been performed. These are discussed by Keshock (1974), Lee (1987), and Cuta and Krotiuk (1988). The early experiments by Keshock (1974) consider primarily heat transfer data and do not have pressure drop data for comparisons. In the experiments performed by Lee, which are the same experiments discussed by Cuta and Krotiuk, the data show that equilibrium conditions were not achieved in the condenser. Some unsteady behavior was observed, therefore the data are unsuitable to validate the design methods. Ongoing experiments by the Weapons Laboratory should provide the data necessary to validate the recommended models.

3.3 References

Chen, I.Y., Downing, R.S., Keshock, E. and Al–Shariff, M.M.; *An Experimental Study and Prediction of a Two-Phase Pressure Drop in Microgravity*; Presented at AIAA 27th Aerospace Science Meeting, Reno, Nevada, Paper No. 89–0074, January 9–12, 1989.

Chow, L.C.; *Condensation Heat Transfer in a Microgravity Environment*; Presented at 24th AIAA Aerospace Sciences Meeting, Reno, Nevada, January 6–9, 1986.

Collier, J.G.; Convective Boiling and Condensation; McGraw–Hill Book Company, 2nd ed., 1986.

Cuta, J.M. and Krotiuk, W.J.; *Reduced Gravity Boiling and Condensing Experiments Simulated with the COBRA/TRAC Code*; 1st Nat'l. Fluid Dynamics Congress, Part 3, AIAA/SIAM/APS, Cincinnati, Ohio, July 25–28, 1988, pp. 1563–1571.

Keshock, E.G.; *A Photographic Study of Flow Condensation in 1-g and Zero-Gravity Environments*; Presented at 5th International Heat Transfer Conference, Tokyo, Japan, September 3–7, 1974, Published in Proceedings Soc. of Heat Transfer Japan, A75–14226 03–34, Vol. 3, 1974, pp. 236–240.

Keshock, E.G. and Sadeghipour, M.S.; *Analytical Comparison of Condensing Flows Inside Tubes Under Earth Gravity and Space Environments*; Presented at International Astronautical Federation, 32nd International Astronautical Congress, Rome, Italy, September 6–12, 1981.

Lee, D.; *Thermohydraulic and Flow Regime Analysis for Condensing Two-Phase Flow in a Microgravity Environment*; Ph.D. Thesis, Nuclear Engineering, Texas A&M University, December 1987.

Suo, M. and Griffith, P.; Paper No. 63–WA–96, ASME, 1963.

Wallis, G.B.; One–Dimensional Two–Phase Flow; McGraw–Hill Book Company, 1969.

GLOSSARY

Annular. A two–phase flow regime in which liquid flows as a continuous film on the wall of a pipe (in an annular pattern) and the vapor flows as a continuous gas core in the center.

Bubbly. A two–phase flow regime in which vapor flows as discrete bubbles in a liquid.

Capillary Condenser. A condenser in which the heat transfer rate is governed by the thickness of a liquid film, which is in turn determined by capillary forces.

Critical Heat Flux (CHF). The point at which the heat transfer coefficient decreases and the wall temperature rises dramatically in boiling heat transfer. This is usually associated with dryout, or formation of a vapor film at the heated surface.

Drift–Flux. An approach to modelling two–phase flows in which the momentum equation is written similarly to the homogeneous modelling approach, but the velocities of each phase are related by a separate empirical relationship called the "drift–flux" relationship.

Flow Regime. A repeatable pattern by which liquid and vapor flow in a two–phase mixture.

Flow Regime Transition. A boundary defining the flow conditions for a change from one flow regime to another.

Fully Developed Subcooled Boiling. Boiling regime characterized by detachment of vapor bubbles from the wall surface. Vapor bubbles and subcooled liquid exist simultaneously in the heated flow channel.

High–Shear Condenser. A condenser approach in which the heat transfer is governed by the thickness of a liquid film whose dimension is set by friction between the vapor and liquid phases.

Homogeneous. An approach to modelling two–phase flows in which the momentum equation is written in a manner analogous to single–phase flow, except that the density, velocity, and friction factor are quantities based upon average fluid properties. This model assumes that the vapor and liquid phases travel at the same actual velocity.

Interfacial Shear or Interfacial Friction. The shear at a gas–liquid interface, given by empirical relationships in this Design Manual.

Mass Flux. The total mass flux (liquid plus vapor) per unit area of the flow cross–section.

Onset of Nucleate Boiling. The wall superheat (temperature difference between wall and fluid saturation temperature) at which vapor bubbles begin to nucleate in cavities of the wall surface. The phenomenon defines the transition from single–phase to subcooled boiling.

Partially Developed Subcooled Boiling. Boiling regime in which vapor bubbles form and condense at the heated wall surface, but remain attached to cavities in the wall surface.

Quality. The fraction of the total mass flow rate which is vapor in a vapor–liquid two–phase flow. Quality is obtained by taking the mass flow rate of the vapor and dividing by the total mass flow rate of the vapor plus the liquid.

Separated. An approach to modelling two–phase flows in which the conservation equations are written separately for each phase and interaction terms are defined to relate the shear (friction) between the phases. (See Interfacial Shear.)

Slug. A two–phase flow regime in which vapor flows as bullet–nosed bubbles surrounded by a thin liquid film. The bubbles are typically several pipe–diameters in length and separated by slugs of liquid.

Stratified. A two–phase flow regime in which vapor flows in the upper portion of a pipe and liquid flows in the lower portion of the pipe. Both phases are continuous in the flow direction.

Superficial Velocity. A superficial velocity is calculated for each of the liquid and vapor phases. The superficial velocity is the velocity that each phase would have if it flowed alone in the pipe, e.g. the superficial velocity for the liquid phase is $j_l = Q_l/A$ and the superficial velocity for the vapor phase is $j_g = Q_g/A$. Because these superficial velocities are based upon known input quantities, the phase flow rates and the cross–sectional flow area, two–phase flow models generally use these parameters and relate them to the actual flow velocities through the void fraction. For example, the actual velocity for the liquid phase $U_l = j_l/(1 - \alpha)$, and the actual velocity for the vapor phase is $U_g = j_g/\alpha$. Determining the void fraction, or the relationship between the velocities of each phase, is most of the problem in a two–phase flow.

Void Fraction. The volume of a vessel or the cross–sectional area of a pipe occupied by the vapor in a two–phase flow system.

Volumetric Flux. See Superficial Velocity. The superficial velocity is also know as the volumetric flux because it is the volumetric flow rate per unit area of the flow cross–section.